

# SANDIA REPORT

SAND2014-20146

Unlimited Release

Printed December 2014

## Development and Testing of an Integrated Sandia Cooler Thermoelectric Device (SCTD)

Program Manager: Thomas E. Felter

Authors:

Terry A. Johnson, Wayne L. Staats, Michael T. Leick, and Mark Zimmerman  
Energy Systems Engineering and Analysis Department 8366

Dr. Reinhard Radermacher, Dennis Nasuta, Cara Martin, Paul Kalinowski, and William Hoffman  
Optimized Thermal Systems, Inc.

Prepared by  
Sandia National Laboratories  
Albuquerque, New Mexico 87185 and Livermore, California 94550

Sandia National Laboratories is a multi-program laboratory managed and operated by Sandia Corporation, a wholly owned subsidiary of Lockheed Martin Corporation, for the U.S. Department of Energy's National Nuclear Security Administration under contract DE-AC04-94AL85000.

Approved for public release; further dissemination unlimited.



**Sandia National Laboratories**

Issued by Sandia National Laboratories, operated for the United States Department of Energy by Sandia Corporation.

**NOTICE:** This report was prepared as an account of work sponsored by an agency of the United States Government. Neither the United States Government, nor any agency thereof, nor any of their employees, nor any of their contractors, subcontractors, or their employees, make any warranty, express or implied, or assume any legal liability or responsibility for the accuracy, completeness, or usefulness of any information, apparatus, product, or process disclosed, or represent that its use would not infringe privately owned rights. Reference herein to any specific commercial product, process, or service by trade name, trademark, manufacturer, or otherwise, does not necessarily constitute or imply its endorsement, recommendation, or favoring by the United States Government, any agency thereof, or any of their contractors or subcontractors. The views and opinions expressed herein do not necessarily state or reflect those of the United States Government, any agency thereof, or any of their contractors.

Printed in the United States of America. This report has been reproduced directly from the best available copy.

Available to DOE and DOE contractors from

U.S. Department of Energy  
Office of Scientific and Technical Information  
P.O. Box 62  
Oak Ridge, TN 37831

Telephone: (865) 576-8401  
Facsimile: (865) 576-5728  
E-Mail: [reports@osti.gov](mailto:reports@osti.gov)  
Online ordering: <http://www.osti.gov/scitech>

Available to the public from

U.S. Department of Commerce  
National Technical Information Service  
5301 Shawnee Rd  
Alexandria, VA 22312

Telephone: (800) 553-6847  
Facsimile: (703) 605-6900  
E-Mail: [orders@ntis.gov](mailto:orders@ntis.gov)  
Online order: <http://www.ntis.gov/search>



SAND2014-20146  
Unlimited Release  
Printed December 2014

## **Development and Testing of an Integrated Sandia Cooler Thermoelectric Device (SCTD)**

T. A. Johnson, W. L. Staats, M. T. Leick, and M. D. Zimmerman  
Energy Systems Engineering & Analysis  
Sandia National Laboratories  
P.O. Box 969  
Livermore, California 94550

Dr. Reinhard Radermacher, Dennis Nasuta, Cara Martin, Paul Kalinowski, and William Hoffman  
Optimized Thermal Systems, Inc.  
5000 College Avenue, Suite 3105  
College Park, Maryland 20740

### **Abstract**

This report describes a FY14 effort to develop an integrated Sandia Cooler Thermoelectric Device (SCTD). The project included a review of feasible thermoelectric (TE) cooling applications, baseline performance testing of an existing TE device, analysis and design development of an integrated SCTD assembly, and performance measurement and validation of the integrated SCTD prototype.

## **ACKNOWLEDGMENTS**

The authors thank Imane Khalil and Daniel Matthew for their early significant contributions to this project.

# CONTENTS

Acknowledgments.....	4
Contents .....	5
Figures.....	6
Tables.....	8
Nomenclature.....	9
1. Executive Summary.....	11
1.1 Project Description.....	11
1.2 System Modeling .....	11
1.3 Prototype Development .....	12
1.4 Experimental Testing and Results Summary.....	12
2. Introduction.....	15
2.1 Motivation.....	16
2.2 Project Objectives .....	17
3. Thermoelectric application market study.....	18
3.1 Market Research Approach.....	18
3.2 Market Research Results.....	18
3.2.1 Portable Coolers .....	19
3.2.2 Compact Refrigerators .....	20
3.2.3 Wine Coolers.....	20
3.2.4 Air Conditioners .....	22
3.2.5 Dehumidifiers.....	22
3.2.6 Other.....	23
3.3 Selection of the Thermoelectric Application and Baseline Unit .....	23
4. Initial baseline testing .....	26
4.1 Experimental Setup and Approach .....	26
4.2 Results.....	28
4.3 Wine Cooler Testing.....	30
4.4 Heat Sink Thermal Resistance Testing.....	32
4.4.1 Analytical Approximation of Thermal Resistance .....	34
4.5 Recommendation to Move Forward with Sandia Prototype.....	34
5. Modeled Performance and preliminary prototyping.....	35
5.1 Model Description .....	35
5.2 Model Inputs .....	36
5.3 Model Results .....	39
6. Prototype design development.....	43
6.1 Conceptual Design .....	43
6.2 Impeller Design and Fabrication.....	44
6.2.1 Impeller Thermal Analysis .....	45
6.2.2 Impeller Fabrication.....	48
6.3 Motor and Controller .....	50
6.3.1 Motor Selection .....	50

6.3.2 Controller Selection.....	50
6.3.3 Control Module .....	51
6.4 System Design and Assembly.....	52
6.4.1 Frame and Shaft Assembly.....	52
6.4.2 Clamping Design.....	54
6.4.3 Shroud Design .....	56
6.4.4 Electrical Feed-Through.....	57
6.4.5 Final Assembly.....	57
7. Initial Prototype Testing .....	61
7.1 Experimental Set Up.....	61
7.2 Challenges Identified and Associated Modifications .....	61
7.2.1 Heat Source .....	61
7.2.2 Insulated Box Assembly.....	63
7.2.3 Motor Heat Contributions .....	63
7.2.4 Ambient Conditions .....	64
7.2.5 Heat Leak Through the Thermoelectric Modules .....	64
8. Final Testing .....	66
8.1 Experimental Set Up.....	66
8.1.1 Measurement Accuracy and Uncertainty Analysis .....	67
8.2 Results.....	68
8.3 Comparison with Model Predictions .....	72
9. Conclusions and recommendations.....	74
10. References.....	76
Appendix A: Detailed Market Research Results .....	77
Appendix B: Laird Thermoelectric Air Conditioner Specifications.....	82
Appendix C: Thermoelectric Module Specifications .....	84
Distribution .....	86

## FIGURES

Figure 1. The Sandia Cooler .....	15
Figure 2. Portable cooler price by volume and manufacturer.....	20
Figure 3. Wine cooler price by size (bottle count) and manufacturer .....	21
Figure 4. Wine cooler reported power consumption by size (bottle count) and manufacturer ...	22
Figure 5. Baseline Laird thermoelectric air conditioning test setup – exterior of insulated box.	26
Figure 6. Baseline Laird thermoelectric air conditioner test setup – interior of insulated box....	27
Figure 7. Preliminary baseline Laird capacity results.....	29
Figure 8. Pull-down time and temperatures for baseline Laird unit, maximum $\Delta T$ case .....	30
Figure 9. Pull-down time for baseline wine cooler, maximum $\Delta T$ case.....	31
Figure 10. Pull-down power for baseline wine cooler, maximum $\Delta T$ case.....	31
Figure 11. Heat sink experimental setup.....	32
Figure 12. Hot-side heat sink thermal resistance using area-weighted temperatures .....	33
Figure 13. Cold-side heat sink thermal resistance using area-weighted temperatures .....	33

Figure 14. Thermoelectric module modeling approach.....	35
Figure 15. Example Laird thermoelectric module used for model validation .....	37
Figure 16. Laird Thermoelectric module manufacturer specified area and model predicted performance .....	38
Figure 17. Model predicted a) capacity and b) COP of the Sandia Cooler Thermoelectric Device for a range of operating speeds with 5” impellers .....	39
Figure 18. a) Capacity and b) COP comparison between the Laird device and the modeled Sandia Cooler Thermoelectric Device with 5” impellers at 2000 rpm.....	40
Figure 19. a) Capacity and b) COP comparison between the Laird device and the modeled Sandia Cooler Thermoelectric Device with 5” impellers at 2000 rpm and the correct TE modules .....	40
Figure 20. a) Capacity and b) COP comparison between the Laird device and the modeled Sandia Cooler Thermoelectric Device with 5” impellers at 2000 rpm with optimized couples for multiple voltages.....	42
Figure 21. Cross-section of Sandia Cooler device concept .....	44
Figure 22. Comsol model of thermoelectric device showing geometry and boundary conditions (left) and example temperature distribution (right) .....	46
Figure 23. Temperature distribution for eight 20mm square thermoelectric modules .....	47
Figure 24. Hot side impeller assembly .....	49
Figure 25. Cold side impeller assembly.....	49
Figure 26. Motor/controller efficiency as a function of output torque .....	50
Figure 27. Control module includes power supply, controller, and diagnostics.....	52
Figure 28. Control module front panel .....	52
Figure 29. Motor stator and shaft.....	53
Figure 30. Frame and shaft subassembly.....	54
Figure 31. Structural model of frame.....	54
Figure 32. Pressure indicating film showing clamping pressure distribution for Laird device...	55
Figure 33. Pressure indicating film showing effect of screw torque on clamping pressure distribution for the Sandia Cooler Thermoelectric Device .....	56
Figure 34. Cold side subassembly with foam insulation .....	57
Figure 35. View of the cold side of the final assembly .....	58
Figure 36. View of the hot side of the final assembly .....	59
Figure 37. Isometric views of the final assembly .....	59
Figure 38. Bench top testing at Sandia prior to shipping to OTS .....	60
Figure 39. Sandia Cooler Thermoelectric Device preliminary prototype experimental setup ....	61
Figure 40. Capacity vs temperature difference for preliminary Sandia Cooler Thermoelectric Device prototype with and without covered light bulb.....	62
Figure 41. Uncovered heater assembly .....	62
Figure 42. Improved enclosure insulation .....	63
Figure 43. Cooling capacities calculated from erroneous heat leak test and corrected result for Laird.....	65
Figure 44. Enclosure heat leak for all systems/speeds.....	68
Figure 45. Apparent cooling capacity (excluding effect of motor heat) vs. temperature difference .....	69
Figure 46. Capacities including motor heat .....	70
Figure 47. COP vs temperature difference .....	71

Figure 48. COP for thermoelectric performance only (excludes fan and motor power) .....	72
Figure 49. Predicted SCTD cooling capacities .....	73

## TABLES

Table 1. Summary of market research results.....	19
Table 2. Wine cooler unit options for baseline testing and evaluation .....	24
Table 3. Air conditioner unit options for baseline testing and evaluation .....	24
Table 4. Baseline Laird unit tests conducted .....	28
Table 5. Manufacturer and measured operating power during preliminary baseline testing.....	29
Table 6. Example Laird thermoelectric module specified and calculated properties used for model validation.....	38
Table 7. Calculated properties for Laird ZT5 16F1,4040 module.....	41
Table 8. Thermal model results for various platen thicknesses and module configurations .....	48
Table 9. Motor power consumption for various impeller speeds .....	51
Table 10. Measurement Equipment and Uncertainties .....	67
Table 11. Absolute and Relative Uncertainties for Calculated Parameters .....	67
Table 12. Market Research Results for Portable Coolers .....	77
Table 13. Market research results for compact refrigerators .....	78
Table 14. Market research results for wine coolers – 1 .....	78
Table 15. Market research results for wine coolers – 2 .....	79
Table 16. Market research results for air conditioners .....	80
Table 17. Market research results for dehumidifiers .....	81
Table 18. Market research results for other thermoelectric applications.....	81

## NOMENCLATURE

<b>Symbol</b>	<b>Definition</b>
$\alpha_m$	Seebeck coefficient, thermoelectric module
$A_{hs}$	Area, heat sink
COP	Coefficient of performance
I	Current
$k_{hs}$	Thermal conductivity, heat sink
$\theta_c$	Cold side heat sink thermal resistance
$\theta_h$	Hot side heat sink thermal resistance
$\theta_{ic}$	Thermal interface resistance, cold side
$\theta_{ih}$	Thermal interface resistance, hot side
$\theta_m$	Thermal resistance, thermoelectric module
OTS	Optimized Thermal Systems, Inc.
PWM	Pulse Width Modulation
Q	Heat input
$q_a$	Cold side cooling capacity
$Q_{bulb}$	Capacity (power), light bulb (heater)
$Q_c$	Cooling capacity of unit
$q_e$	Hot side heat load
$Q_{heater}$	Capacity (power), electric resistance heater
$Q_{leak}$	Heat leak through the insulated box
$Q_{loss}$	Heat loss through insulation in heat sink test
$Q_{motor}$	Fan or motor heat transferred into enclosure
$Q_{TE}$	Capacity, thermoelectric module
$R_{eff}$	Effective thermal resistance
$R_{hs}$	Thermal resistance, heat sink
$R_m$	Electrical resistance, thermoelectric module
SCTD	Sandia Cooler Thermoelectric Device
SNL	Sandia National Laboratories
$\Delta T$	Temperature difference
$T_a$	Cold side temperature
$T_{ambient}$	Ambient temperature
$T_c$	Cold side heat sink temperature
TE	Thermoelectric

$T_e$	Hot side temperature, thermoelectric module
$T_h$	Hot side air temperature
$T_{heater}$	Heater temperature
$T_{in}$	Internal temperature
$T_{ins}$	Insulation temperature
$T_m$	Average surface temperature of the thermoelectric modules
$th_{ins}$	Insulation thickness
$\Delta T$	Heat leak value
$U_{max}$	Maximum voltage
V	Voltage
Z	Figure of merit

# 1. EXECUTIVE SUMMARY

Optimized Thermal Systems, Inc. (OTS) was contracted by Sandia National Laboratories (SNL) to investigate the potential for incorporating a modified version of the Sandia air-bearing heat exchanger in existing products already using thermoelectric (TE) technology, effectively creating a Sandia Cooler Thermoelectric Device (SCTD). OTS and SNL collaborated between August 2013 and October 2014 to evaluate concept potential, conduct baseline unit testing, design and construct a SCTD prototype, and test and compare prototype performance.

## 1.1 Project Description

The OTS/Sandia team initiated this project in order to evaluate the potential of the Sandia Cooler with TE modules for niche market applications using TE cooling. TE devices provide benefits such as long shelf life, minimal moving parts, compactness, and operation without a vapor compression system (refrigerants). When integrating TE modules by sandwiching them between two Sandia coolers, a very compact and simple air-to-air heat pumping device is created that consists of a single rotating part and has the potential for higher compactness and/or higher efficiency than traditional TE approaches. In addition, the use of the Sandia Cooler in this application brings to bear the advantages of inherent low noise, low fouling, and minimum of moving parts

A market study was conducted to understand existing TE cooling applications. Ultimately, small scale air conditioning systems typically used for electronics cooling was selected as the area of focus. This application was selected given that performance data is more readily available for TE air conditioners and specification sheets include detailed dimensions. These details enabled better up-front design of the SCTD for this application over several others considered.

The Sandia team was responsible for modeling the SCTD and estimated its performance as compared to the selected baseline TE cooler, produced by Laird. SNL was also responsible for designing and fabricating the SCTD prototype, once the team decided to pursue prototype construction and testing.

The OTS team was responsible for testing the baseline Laird unit and the SCTD prototype. Multiple rounds of testing were completed as new information was gathered and the experimental procedure was improved.

## 1.2 System Modeling

The Sandia team developed a thermal circuit model based on the model of Lineykin and Ben-Yaakov [9]. Modeling inputs included system boundary conditions, such as ambient air temperature; imposed conditions, such as the power supply voltage applied to the TE modules; and properties of the modules, interfaces and heat sinks.

Initial modeling of the SCTD assumed different TE modules than were used in the actual Laird unit used for baseline experimental testing. Initial modeling results using these alternate Laird modules suggested an improvement of the SCTD over the Laird cooler by 33% for capacity and

20% for the coefficient of performance (COP). Correcting the model for the correct Laird TE modules reduced the capacity improvement of the SCTD to around 17%, with minimal improvement of COP for the maximum capacity condition.

Modeling was also conducted for an optimal SCTD configuration with higher performance TE properties. In this scenario, the SCTD is predicted to provide nearly twice the capacity and almost double the COP as the Laird unit. To achieve such performance a custom TE module or modules would be required which would be matched to the footprint of the SCTD and designed to maximize for the specific cooling capacity and temperature difference desired.

### **1.3 Prototype Development**

The general concept for the SCTD was to sandwich one or more TE modules between two Sandia Cooler impellers; one to act as the hot side heat exchanger and the other the cold side heat exchanger. In this configuration, the entire device would rotate as a unit and there would be no air gap and no air bearing required. The result would be a fairly simple device that just required one motor, a frame to mount it on, and a method to provide electrical power to the rotating TE module(s).

The Sandia team evaluated each aspect of the prototype including the impeller design, motor selection, controller selection, frame and shaft assembly, clamping of the TE modules, shroud design, and electrical feed-through to power the TE modules and motor. One tradeoff was impeller size versus performance. A lower thermal resistance could be achieved with a larger impeller, which would improve the system performance. However, the device had to be no larger than the Laird unit for comparison purposes. Given the specific project constraints, a diameter of 5” was selected as a tradeoff between size and performance. A thermal analysis was also conducted for the impeller to evaluate the impact of TE module placement on the impeller surfaces. An optimal configuration of eight equally spaced TE modules was identified, however to match the baseline Laird unit assembly, only two TE modules were used. To minimize the effective thermal resistance given the use of the two TE modules, a platen thickness of 0.5” was chosen.

A DC hobby motor was used and a winding arrangement was selected to enable a top speed around 2000rpm, a speed identified during the modeling period of the project offering the best capacity and COP trade-off improvement over the baseline Laird system. The final motor assembly was found to have a higher power consumption than expected and this assembly may be one area for improvement in future SCTD prototype iterations.

The shaft and frame were designed for structural rigidity as well as to feed the electrical wires to the motor and TE modules. The Sandia team evaluated the clamping configuration of the baseline Laird assembly and strived to match clamping pressure to provide similar contact resistance between the TE modules and heat exchangers.

### **1.4 Experimental Testing and Results Summary**

The OTS team conducted several tests to evaluate the potential of the SCTD concept. Testing of an existing TE cooler assembly from Laird was initially conducted to develop a project baseline and inform the decision to pursue a SCTD prototype. To measure performance, the Laird unit was installed on the side of an insulated enclosure, approximately a 16" cube. Both pull down tests in which the Laird unit was operated to achieve the coldest internal conditions, and heat leak tests, where an internal heat source was turned on to create a reverse temperature gradient across the box, were conducted to evaluate the unit's capacity. A light bulb was used as the heat source for initial tests and ambient conditions were generally kept around 29 – 31°C.

Once the SCTD prototype was complete, the OTS team repeated the same test procedures as were employed for the Laird baseline. Initial results revealed several deficiencies in the testing approach:

- The light bulb heat source was found to negatively impact the results due to radiative effects, so it was replaced with a small electric resistance heater that was covered completely with aluminum foil.
- The box assembly was also improved to increase the level of insulation on all sides except the face of the box where the TE coolers were installed.
- While relatively minimal, the effect of ambient temperature was noted as another item inconsistent between tests. As such, all final testing was conducted inside an environmental chamber at an ambient temperature of 32°C (+/- 0.5°C); this temperature was selected based on performance data specifications provided by the manufacturer.
- The motor in the SCTD was found to contribute heat to the inside of the box assembly, skewing calculated cooling capacity results for the unit. Additional tests were added to the experimental procedure to account for this effect and provide more appropriate estimates of overall system capacity.
- During the reverse heat leak tests, a significant amount of heat leak was found to occur through the TE modules themselves since they were not powered during these tests. This resulted in inaccurate calculations of the heat leak through the insulated enclosure and consequently, inaccurate system capacities, particularly at higher temperature differentials. As with the motor heat leak, additional tests were conducted to account for this phenomenon and improve the accuracy of the overall calculated capacities.

Final experimental results revealed that at lower speed the SCTD provided the expected performance improvement over the Laird unit, but cooling capacity did not significantly increase with motor speed. Model predictions suggested an improvement of 11.5% of the SCTD at 1400rpm over the Laird baseline; experimental results confirmed this hypothesis, showing an improvement of 12%. At 2000rpm, the highest motor speed, model predictions suggested a capacity improvement by as much as 22%; experimental results only showed a 14% improvement of the SCTD over the Laird baseline. Experimental results for the SCTD showed an increase in COP for every motor speed, though the improvement over the Laird baseline is more significant at higher temperature differences.

The evaluation of the SCTD showed expected performance gains over the commercial device in a smaller package and good match between experimental results and modeling predictions. With this improved understanding, we have shown that an optimized configuration could provide

nearly twice the capacity and coefficient of performance compared to commercial devices. Several improvements to the existing SCTD prototype would enable such performance including an advanced impeller design, more efficient motor assembly and reduced motor heat leak, improved impeller-to-module thermal interface and custom TE modules that are matched to the footprint of the impeller.

## 2. INTRODUCTION

The Sandia Cooler [1-5], shown in Figure 1, is a novel, motor-driven, rotating, finned heat exchanger that consists of three main components: an impeller (a rotating, finned heat sink), a baseplate, and an integrated brushless DC motor. In its original configuration, the impeller is powered by the motor, allowing it to rotate on a thin hydrodynamic air bearing above the stationary baseplate. Originally developed for electronics cooling, the underside of the baseplate is mounted to a heat source. Heat flows through the baseplate, air bearing gap (0.01 mm), impeller base, and impeller fins and is ultimately transferred to surrounding airflow. The key to the Sandia Cooler is the heat-sink impeller, which consists of a disc-shaped impeller populated with fins on its top surface. The impeller functions like a hybrid of a conventional finned metal heat sink and a fan. Air is drawn in the downward direction into the central region having no fins, and expelled in the radial direction through the dense array of fins. Because the impeller fins rotate at up to several thousand rpm, the airflow experiences a continual radial acceleration that decreases the thickness of the boundary layer by as much as a factor of ten [6,7]. This thinning of the boundary layer significantly improves the air-side heat transfer coefficient of the heat exchanger compared with traditional fan and fin devices. Due to the rotation of the heat transfer surfaces, the Sandia Cooler is inherently resistant to fouling, condensate retention, and frost accumulation. Finally, by integrating the fan and the heat exchanger, each of which is a source of noise in a conventional heat exchanger, improvements in overall noise level can be expected. The concept is also very practical from the standpoint of cost, complexity, and ruggedness.

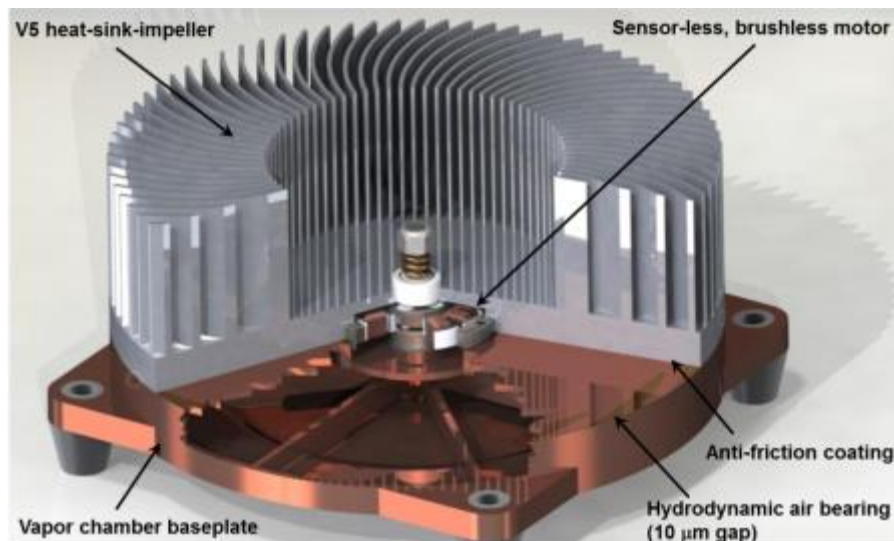


**Figure 1. The Sandia Cooler**

Sandia National Laboratories (SNL) has significantly advanced the Sandia Cooler technology over the last five years through funding from DOE's Building Technologies Office (BTO). All aspects of the heat exchange device have been improved for performance, ease of fabrication, assembly, and cost. BTO funding has enabled the advancement of the Sandia Cooler from a proof-of-concept device to technology readiness level of TRL5 for the electronics cooling application. Several other applications of the Sandia Cooler are currently funded by BTO,

including the development of a prototype refrigerator condenser and a heat exchanger for HVAC applications.

A recently published market assessment study of the Sandia Cooler commissioned by BTO identified thermoelectric devices as a high-potential market for commercialization of the technology [8]. The benefits cited for the Sandia Cooler over current technology were “Opportunity for either size reduction or performance enhancement, reduced fouling.” To address these claims, BTO provided funding during FY 2014 to SNL, in partnership with Optimized Thermal Systems, Inc. (OTS) to investigate the potential for incorporating a modified version of the Sandia air-bearing heat exchanger with thermoelectric (TE) technology, effectively creating a Sandia Cooler Thermoelectric Device (SCTD).

Work started in August 2013 by investigating suitable TE applications to which the Sandia Cooler heat exchanger concept could be applied. Once a TE cooling device was selected, OTS conducted baseline testing to establish the minimum cooling capacity and performance the SCTD prototype would need to meet and exceed. As a parallel effort, engineers at SNL developed a model of the proposed SCTD and conducted preliminary testing of an assembly using off-the-shelf components. In late January 2014, the OTS / Sandia team elected to move forward with prototype development and testing of a complete SCTD assembly. The prototype was completed in mid-May 2014 and the OTS team started testing it shortly thereafter. A number of challenges and issues arose during the test process over the summer and additional baseline testing was warranted. This report summarizes each step of the project and the overall success of the developed SCTD.

## **2.1 Motivation**

Thermoelectric cooling/heat pumping devices have increasingly poor performance as the temperature lift increases, which severely limits their applications. There are, however, significant niche markets for TE devices where characteristics such as long shelf life, the lack of moving parts, compactness and convenience are the drivers. Examples are hotel room refrigerators, car seat heating/cooling, picnic coolers, medical devices, and small electronics cooling air conditioners.

When integrating the TE device by sandwiching it between two Sandia coolers, a very compact and simple air-to-air heat pumping device is created that consists of a single rotating part and has the potential for higher compactness and/or higher efficiency than traditional TE approaches.

## **2.2 Project Objectives**

The project objective was to evaluate and quantify the potential of an integrated SCTD. Specifically, the project aimed to:

1. Understand the existing TE cooler applications and performance; and,
2. Assess the performance potential of the TE device integrated between two Sandia coolers.

### **3. THERMOELECTRIC APPLICATION MARKET STUDY**

As the first step of the project, OTS conducted a market research study in order to identify existing TE products, their intended functions, and their potential for improvement through integration with the Sandia cooler. The criteria for selecting a suitable application include the following:

1. A reasonable market for the product, showing a true consumer need, with opportunity for market competition; and,
2. A relatively low temperature difference ( $\Delta T$ ) in order to maximize COP for the overall unit.

Based on the results of the market study and further discussions with Sandia, two sample products were selected for further evaluation and experimentation. The market study effort and outcome are summarized in the subsections below.

#### **3.1 Market Research Approach**

Research was largely internet-based, focusing on major manufacturers currently selling products advertised as using TE technology for the given cooling application. Based on the search results produced, products were classified within one of the following six categories:

1. Portable Coolers (recreational and medical)
2. Compact Refrigerators
3. Wine Coolers
4. Air Conditioners
5. Dehumidifiers
6. Other

Information collected for a given product included manufacturer, model number, volume/size, advertised price, rated power and energy consumption (if listed), external dimensions, and cooling specifications. Detailed findings are provided in table format in Appendix A.

#### **3.2 Market Research Results**

The market research effort is summarized in Table 1 below. Additional details about each application are provided in the following subsections.

**Table 1. Summary of market research results**

<b>Application</b>	<b>Evaluated Market Size</b>	<b>Power Consumption</b>	<b>Ambient Conditions<sup>1</sup></b>	<b>Cooling Capabilities</b>	<b>Potential <math>\Delta T</math> Range</b>
Portable Coolers	26 units	48 – 72W	Variable, Indoors and Outdoors	40°F below ambient	15-40°F
Compact Refrigerators	5 units	Not Reported	Indoors, 68-78°F conditioned, 68-85°F unconditioned	40-50°F below ambient	30-50°F
Wine Coolers	45 units	60 – 200W	Indoors, 68-78°F	45-65°F	3-33°F
Air Conditioners	62 units	Not Reported	Variable, Indoors and Outdoors	Variable	70°F
Dehumidifiers	4 units	60 – 80 W	Indoors, 68-78°F	N/A	N/A
Other	5 units, 3 applications	Not Reported	Indoors, 68-78°F	Variable	Variable

### *3.2.1 Portable Coolers*

Information for a total of 26 portable coolers representing six different manufacturers was collected. The primary use for portable coolers is recreational, though several medical coolers were identified. Most units are equipped for use within a vehicle (12V DC), but have the option for interior home or hotel use with an 110V AC adapter. Most coolers advertise the capability to cool as low as 40°F below ambient conditions and some units have the ability to switch to a heating mode to temporarily keep foods warm during car travels.

From the information gathered, there are a number of comparable products representing a market need and good market competition. Coleman coolers appear to be popular, though there are a limited number of models from which to choose. Koolatron offers the most variety with greatest selection. Koolatron was also the only manufacturer found that sells precision control medical coolers using TE technology.

Pricing for the coolers varies based on manufacturer, size, function and features. Pricing information, as was available, is graphically shown in Figure 2. As can be seen in the figure, Coleman generally offers the lowest pricing and likely dictates market cost. The costs for two medical coolers, offered by Koolatron, are not depicted in Figure 2. Coolers with this type of precision control cost on the order of \$600 and were reported to be able to cool up to 45-50°F below ambient conditions.

Several manufacturers include rated power draw for the units. Most models have a rated power around 48W, with a few having rated powers as high as 60 or 72W.

---

<sup>1</sup> Assumed based on advertised product use.

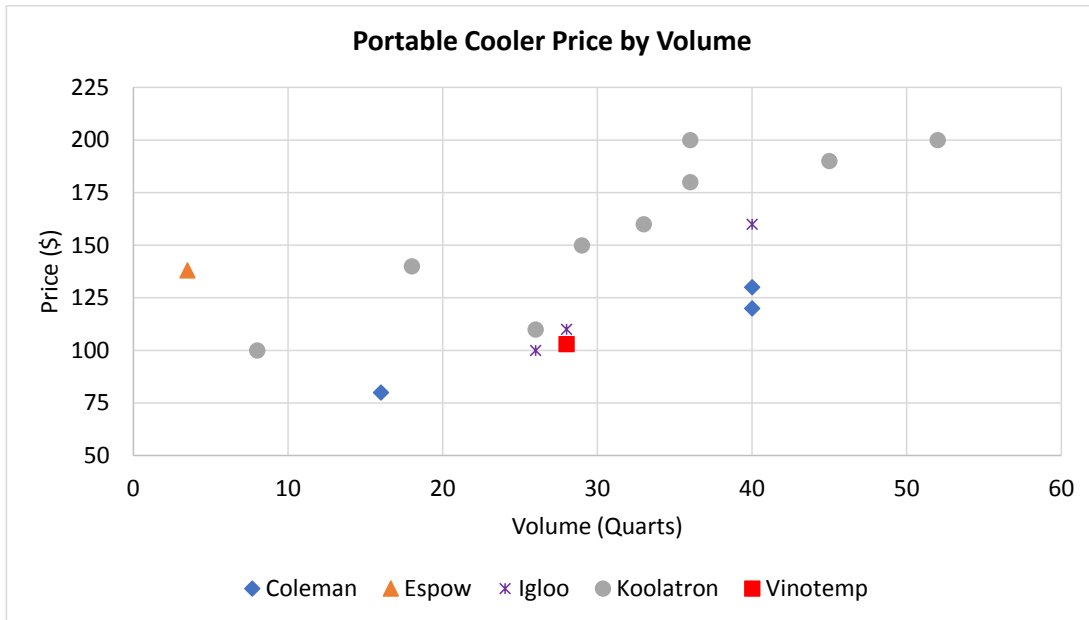


**Figure 2. Portable cooler price by volume and manufacturer**

### 3.2.2 Compact Refrigerators

Few compact refrigerators already utilizing TE cooling technology are available on the market. Only five units were identified (two from Koolatron, one from Avanti, one from Danby, and one from Haier). All units had a volume of 1.7 cubic feet and were marketed for personal use, such as in a private office space or dormitory room. Prices were generally on the order of \$120 - \$130. Cooling details were scarce. The Koolatron models reported similar cooling capabilities as their portable coolers, suggesting the compact refrigerators could cool 30-40°F below ambient conditions. Other identified models did not provide cooling capability details.

### 3.2.3 Wine Coolers

There are a relatively large number of wine coolers available on the market that are already using TE cooling technology. TE cooling is actually quite attractive in this application because of the reduced noise and vibration in comparison to a cooler using a compressor. Vibration can disturb sediment, which is meant to fall out of the wine; hence, cooling systems with lower potential for vibration are desirable. A 2013 report found on TopTenReviews.com showed that eight out of the top ten wine coolers selected use TE cooling<sup>2</sup>.

A total of 45 wine coolers were identified during the market study. Several more are also available through a few, less popular manufacturers. Sunpentown appears to provide the greatest variety, offering 14 different cooler configurations. Vinotemp and Edgestar (aka Koldfront) provide a comparable selection with 11 and 9 available models, respectively.

<sup>2</sup> <http://wine-cooler-review.toptenreviews.com/>

Coolers are generally categorized by the number of bottles they store. Unit price, based on manufacturer and size, is shown in Figure 3. Note that there may be multiple price points for the same unit size, even for a given manufacturer, because of unit features and exterior dimensions. Units with two cooling zones, heating capability and/or a slimmer design tend to be more expensive.

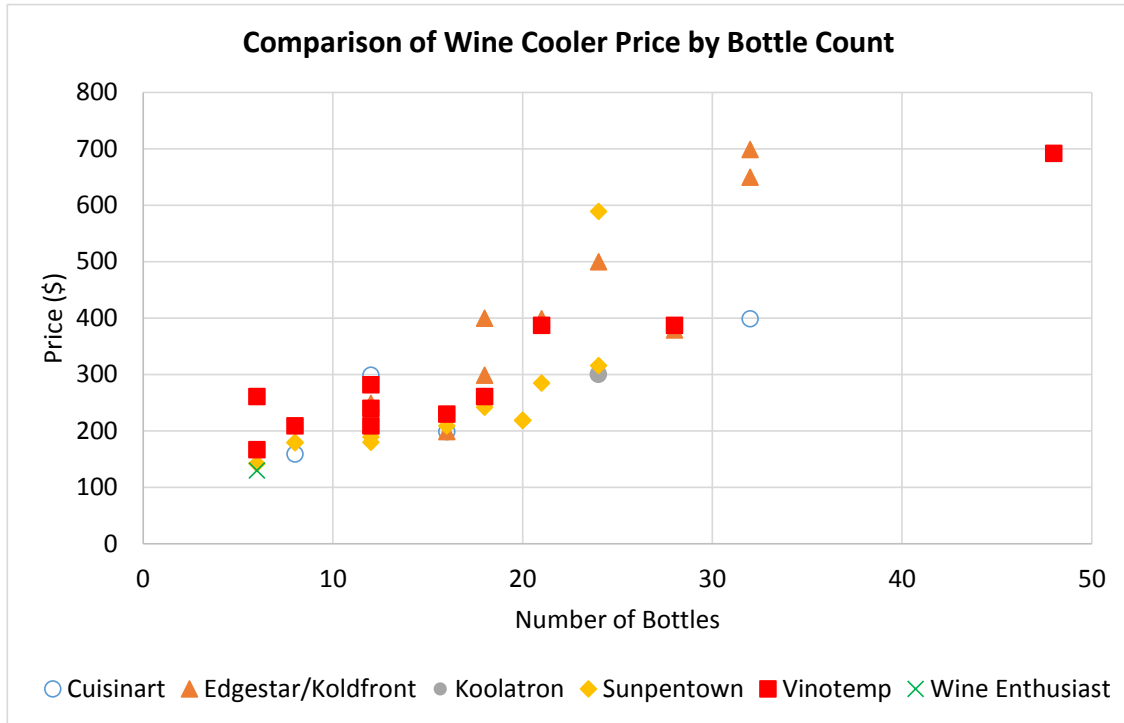


**Figure 3.** Wine cooler price by size (bottle count) and manufacturer

Temperature control is relatively consistent between coolers and manufacturers. Most wine coolers are reported to have cooling control capability between 45-65°F. Ambient conditions are generally recommended to be controlled between 68-77°F to optimize performance of the coolers and maintain wine temperatures.

Power draw for wine coolers is generally higher than that for portable coolers and has a much larger range given the larger variation in unit size. Power was reported anywhere between 60 and 200W, as shown in Figure 4.

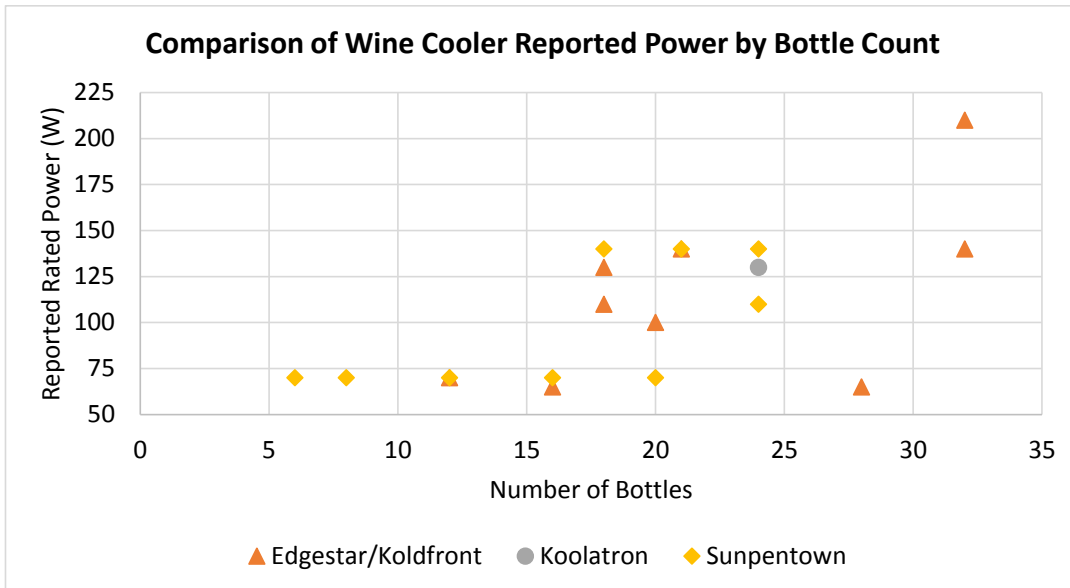


**Figure 4.** Wine cooler reported power consumption by size (bottle count) and manufacturer

### 3.2.4 Air Conditioners

Data was collected for a total of 62 small-scale air conditioners from six different manufacturers. These air conditioners are meant for electronics cooling, typically within a small enclosure. Units suitable for both indoor and outdoor operation were identified, though data collected focused on units meant for indoor use. Unit capacities are relatively small, typically less than 1,000 Btu/h, with only two manufacturers (EIC Solutions and TECA Corporation) offering larger units up to 6,000 – 18,000 Btu/h (0.5 – 1.5 tons). Most units are rated to provide cooling up to a maximum ambient temperature of 140-160°F, though cooling capacity decreases significantly at these high temperatures.

Power draw or energy consumption for these units is not generally available since it will depend heavily on the exact application, ambient conditions, and desired cooling temperature. TECA Corporation reports the COP for several of their units; it never exceeds 1.25. Pricing information is also generally scarce since most units are custom designed.

### 3.2.5 Dehumidifiers

There are a handful of dehumidifiers on the market using TE technology. Sunpentown appears to be the most available manufacturer, though one larger and more expensive unit was identified from Hoffman. These dehumidifiers are meant for use in a small, residential room and advertise quiet operation (since there is no compressor) as the main advantage over a traditional dehumidifier.

It is difficult to compare this application against the others included within this market study since the mini-dehumidifiers are not actually providing direct cooling and do not list cooling specifications.

### 3.2.6 Other

Several other small household cooling devices incorporating TE cooling technology were identified during the market research stage. These included two mini-beer keg coolers, two tabletop water coolers, and one yogurt maker. Because these applications did not have a wide-spread market, and limited details were generally available, further research on these applications was not conducted.

## 3.3 Selection of the Thermoelectric Application and Baseline Unit

Following completion of the market research study, OTS and Sandia collectively evaluated the potential applications for the SCTD. Several applications were immediately eliminated as potential candidates given their small market size and relatively high temperature difference ( $\Delta T$ ). These included compact refrigerators, dehumidifiers, and the other miscellaneous applications (beer keg, water cooler, and yogurt maker). Of the remaining application options, portable coolers were further eliminated as an option given that wine coolers and air conditioners both had lower potential temperature differences in addition to larger market potential.

Once the team decided to investigate wine cooler and air conditioners in more detail, additional research was conducted to identify suitable units for the baseline comparison and analysis stage of the project. A 60W cooling power range was selected as the reference point. OTS identified specific units suitable for baseline testing, outlined in Tables 2 and 3.

**Table 2. Wine cooler unit options for baseline testing and evaluation**

	<b>Option 1</b>	<b>Option 2</b>	<b>Option 3</b>
Manufacturer	Sunpentown	Sunpentown	Koldfront
Model	WC-06	WC-12	TWR160S
# Bottles	6	12	16
Price	\$142	\$180	\$199
Input Power	70W	70W	65W
Temperature Control Range	44-66°F	50-66°F	52-64°F
# Control Zones	1	1	1
Outside Dimensions	10" x 20" x 14.5"	14" x 21" x 19"	20.5" x 17.25" x 20.25"
Image			

**Table 3. Air conditioner unit options for baseline testing and evaluation**

	<b>Option 1</b>	<b>Option 2</b>	<b>Option 3</b>	<b>Option 4</b>
Manufacturer	EIC Solutions	TECA Corp.	Watronix, Inc.	Laird
Model	ThermoTEC 120	AHP-301FF	INB 180-12-AA	AA-060-12-22
Cooling Capacity (W)	58.6	64.4	52.7	58.0
Price	\$850	\$730	\$175	\$408
Ambient Range	Up to 140°F	Up to 70°C	Up to 85°C	Up to 51°C
Dimensions	7.25" x 5.125" x 7"	5.5" x 10" x 7"	5.1" x 6.2" x 5.9"	4.8" x 9" x 5.7"
Image				

The team decided to focus on an air conditioner system as the primary application for the SCTD. This decision was driven based on the following:

1. Performance data for air conditioner systems is more readily available, proving a manufacturer's reference point in addition to the baseline data collected; and,
2. Specification sheets for the units include detailed dimensions, better facilitating design efforts for the SCTD.

Of the identified models, the OTS / Sandia team selected the Laird AA-060-12-22 model to use as the baseline system. This model was mid-range in terms of cost and Sandia engineers had previously corresponded with Laird regarding the development of TE modules in general. Additional details about the Laird unit are provided in Appendix B. Specifications for the TE modules believed to be included in the Laird unit are provided in Appendix C.

While the Laird air conditioner was selected as the baseline system, OTS also purchased the mid-size 12-bottle wine cooler from Sunpentown. Given that this unit was relatively inexpensive, the team decided it would be worthwhile to purchase a unit and conduct some preliminary testing to gain additional information about the feasibility of a wine cooler application. Detailed testing with the wine cooler was ultimately not conducted, but rudimentary testing provided some additional insight about the unit assembly, as outlined in Section 4.3.

## 4. INITIAL BASELINE TESTING

With the Laird TE air conditioner selected for the baseline condition, OTS ordered a sample model and designed the experimental approach to measure the unit capacity and efficiency. The Laird unit was purchased in early October 2013. Shake down testing was complete by late November 2013. Modifications to the test set up and experimental approach were then discussed and implemented. Initial baseline testing was completed in late January 2014 and impacted the team's decision to pursue a full SCTD prototype.

Testing of the wine cooler and some additional testing of the baseline Laird TE air conditioner were also conducted during this phase of the project. The experimental set up, measurement approach, and results of the baseline and additional exploratory tests are outlined in the subsections below.

### 4.1 Experimental Setup and Approach

To enable testing of the capacity and calculation of the unit efficiency, the baseline Laird TE air conditioner was installed on the side of an insulated 16" x 16" x 15" box, as shown in Figure 5. Inside the box, a light bulb was used as a heat source, as shown in Figure 6. A total of eight thermocouples, with three on the exterior and five on the interior, were attached to the assembly to measure inside and outside temperatures. Aluminum tape was positioned around the internal thermocouples to help eliminate radiation effects from the light bulb.

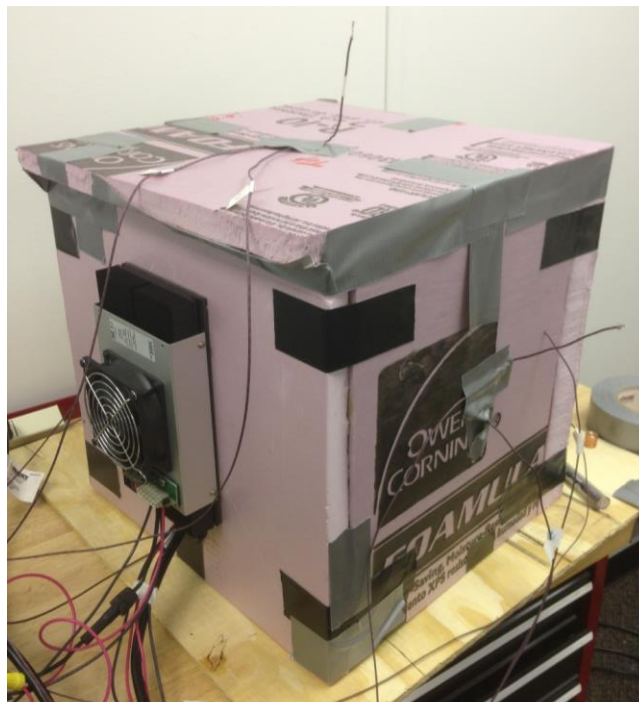


**Figure 5.** Baseline Laird thermoelectric air conditioning test setup – exterior of insulated box

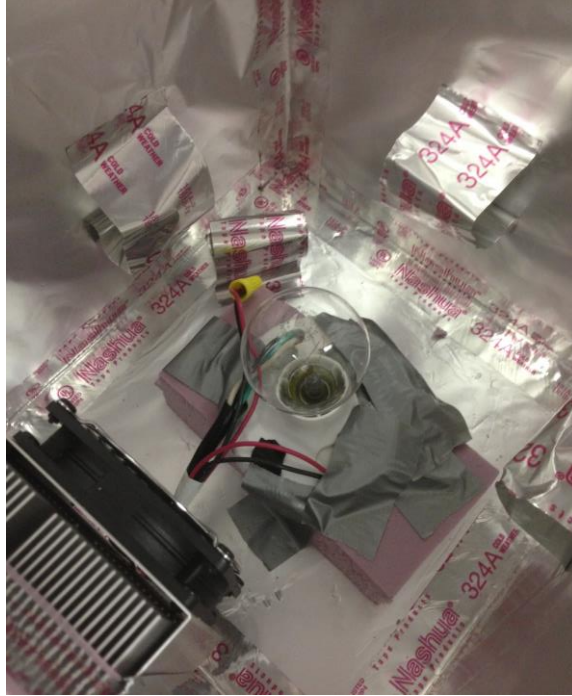


**Figure 6.** Baseline Laird thermoelectric air conditioner test setup – interior of insulated box

In addition to the internal and external temperatures, the power consumption of the light bulb and the voltage and current for the TE air conditioner were measured. Modifications were later made such that the power consumption of the TE modules and the unit fan could be individually measured.

Two types of baseline tests were conducted to evaluate the Laird unit performance:

1. Pull-Down Test: The Laird unit is operated as normal and cools the box as much as possible. The light bulb power is adjusted for each test such that the relationship between capacity and temperature difference between the inside and outside of the box can be determined. The test is conducted until steady state is achieved. Fifteen (15) minutes worth of steady state data is used to calculate capacity for the achieved temperature difference ( $\Delta T$ ).
2. Reverse Heat Leak Test: This test was conducted to determine the heat leak from the insulated box, or the “UA” value used to calculate the Laird unit capacity. For these tests, the Laird unit was turned off and the light bulb was turned on (at multiple power levels), creating a reverse temperature difference as compared to the pull-down tests. Once conditions were stable, 15 minutes worth of steady state data was used to calculate the UA value.

Using the data collected from each of the above outlined tests for multiple temperature differentials ( $\Delta T$  values), the capacity for the Laird unit could be calculated using Equations (1):

$$Q_{TE} = Q_{bulb} + Q_{leak} \quad \text{Eq. (1)}$$

Where  $Q_{TE}$  is the total cooling capacity of the TE air conditioner,  $Q_{bulb}$  is the power of the light bulb, and  $Q_{leak}$  is the capacity lost through the insulated box, as defined in Equation (2):

$$Q_{leak} = UA(T_{ambient} - T_{in}) \quad \text{Eq. (2)}$$

Where  $UA$  is the heat leak through the insulated box,  $T_{ambient}$  is the measured ambient temperature, and  $T_{in}$  is the average internal temperature.

With the test approach and set up finalized, OTS conducted a total of 12 different test configurations, as summarized in Table 4. Several tests were repeated to confirm the approach and show reproducibility of the methodology. Tests were conducted with a 12V power supply, as directed by the manufacturer.

**Table 4. Baseline Laird unit tests conducted**

No.	Test Type	Ambient Temperature (°C)	Light Bulb Power (W)
1	Heat Leak	25	5
2			10
3			15
4			20
5			147.5
6	Pull Down	28	0
7		30	10
8		31	20
9			30
10			40
11			50
12			60

## 4.2 Results

Initial baseline testing generated capacities lower than data reported by the manufacturer, as shown in Figure 7. Due to the testing methodology and set up, results could not be obtained at a temperature difference greater than approximately 27°F. The maximum capacity measured was approximately 17% lower than that specified by the manufacturer. Final testing showed performance of the Laird unit to be much closer to the manufacturer specified performance due to several improvements in the experimental setup including the inclusion of the fan heat gain in the calculation of cooling capacity, replacement of the light bulb heating element with a lower temperature heater (to minimize radiation), recalibration of the thermocouples, and the use of an environmental chamber to control ambient temperature more accurately. Average operating power conditions were generally in good agreement during the initial baseline tests, as shown in Table 5.

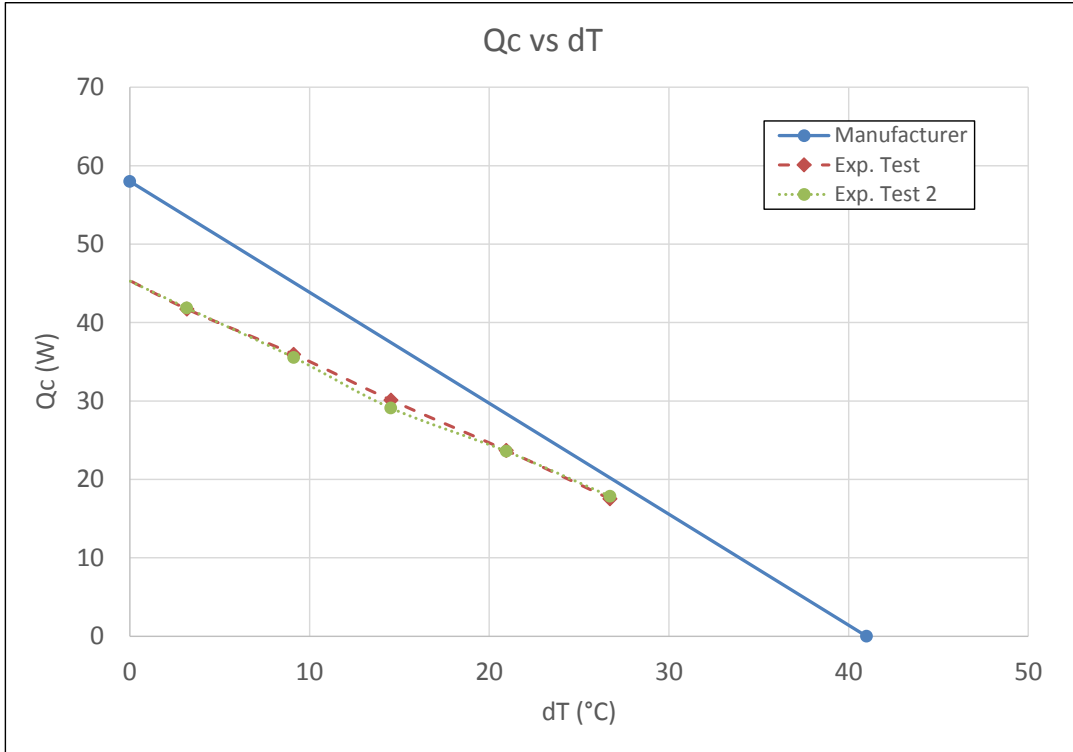


**Figure 7.** Preliminary baseline Laird capacity results

**Table 5. Manufacturer and measured operating power during preliminary baseline testing**

Parameter	Manufacturer Data (@ 32°C)	Test Data (@ 31°C)
Voltage (V)	12	12.1
Running Current (A)	6.2	6.1
Startup Current (A)	7.2	7.2
Power Input (W)	74	72

Pull-down/performance tests were typically conducted sequentially, starting with the maximum temperature difference (no light bulb power). Steady state conditions for this initial condition were generally achieved within an hour of starting the test, as shown in Figure 8.

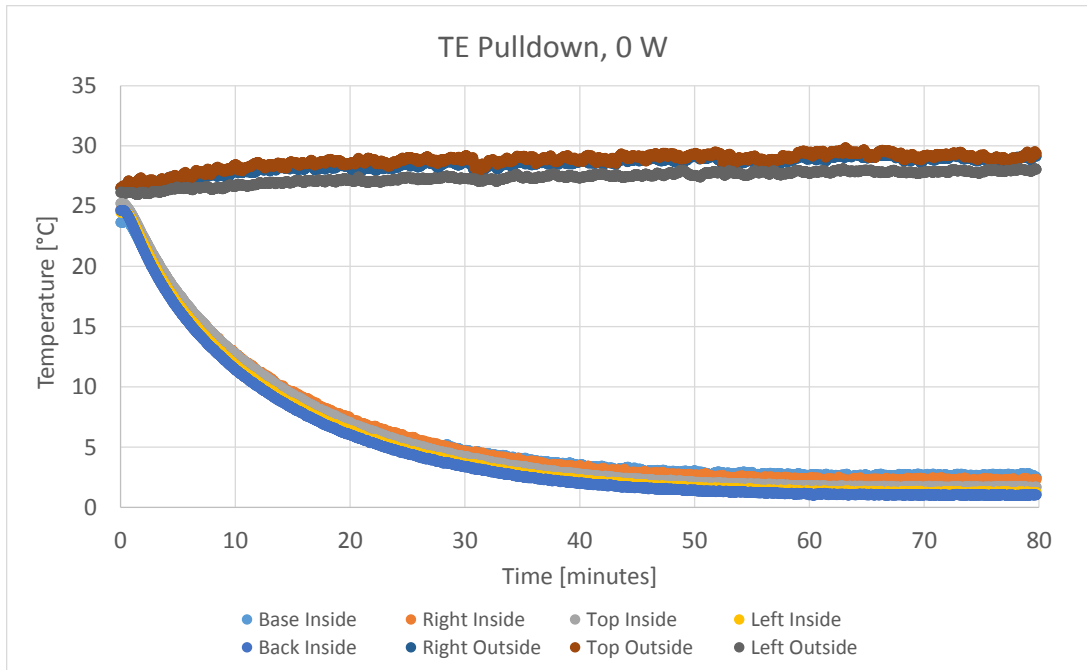


**Figure 8.** Pull-down time and temperatures for baseline Laird unit, maximum  $\Delta T$  case

Several issues were later identified with the initial baseline testing and results. These include:

- Some stratification inside and outside the insulated box assembly;
- An incomplete UA assessment that did not account for fan airflow and assumed a constant UA for all temperature differences; and,
- Ambient temperature fluctuations.

As outlined in the sections below, these deficiencies were corrected in later testing efforts to improve the reliability of the measured results.

### 4.3 Wine Cooler Testing

The same testing approach used for the Laird TE air conditioner was attempted for the wine cooler. Six thermocouples were used to measure unit temperatures, with three on the inside and three on the outside. An initial pull down test suggested a maximum achievable temperature difference of approximately  $10^{\circ}\text{C}$ , with an average internal temperature of  $10^{\circ}\text{C}$  (consistent with the lowest cooling setting per the manufacturer). Similar to the Laird unit, the wine cooler was able to achieve pull down within one hour, as seen in Figure 9. Power draw was initially high, around 55W, but averaged around 19W once steady state was achieved, as shown in Figure 10. The unit is rated for up to 70W, per the manufacturer's specifications.

A light bulb was again used as an internal heat source. Early heat leak tests, however, presented challenges in obtaining good results and adequately calculating unit capacity. Testing with the Laird air conditioning unit was determined to be a project priority and further investigation with the wine cooler was abandoned.



**Figure 9.** Pull-down time for baseline wine cooler, maximum  $\Delta T$  case

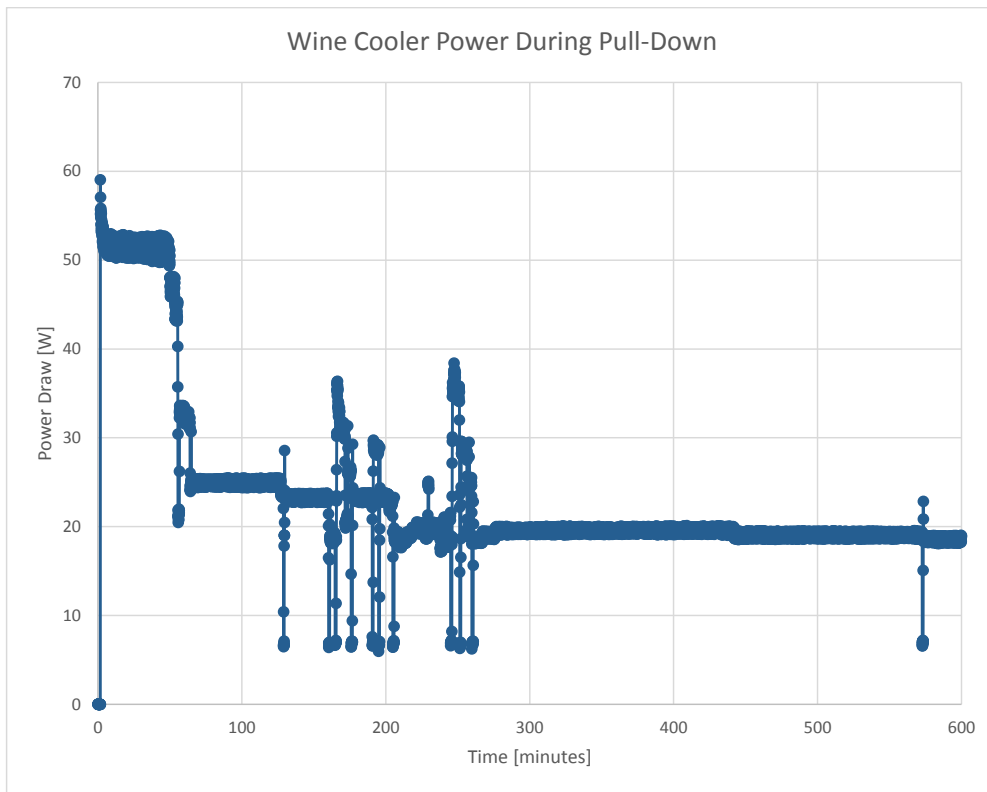


**Figure 10.** Pull-down power for baseline wine cooler, maximum  $\Delta T$  case

## 4.4 Heat Sink Thermal Resistance Testing

To better understand the thermal performance of the Laird TE air conditioner, a series of tests was conducted to approximate the thermal resistance of each of its heat sinks. Since the thermal resistance of the Sandia cooler has been thoroughly studied by Sandia, these tests allowed for analytical modeling that could compare the performance of the baseline and Sandia assemblies.

Tests were carried out by attaching a thin-film electric resistance heater and three thin film thermocouples to the back of the heat sink covering most of the area covered by the TE modules in the assembly, as shown in Figure 11. As heat is transferred to the setup, the inlet and outlet air stream temperatures are measured and collected data is used to calculate the effective thermal resistance of the heat sink using Equation (3).

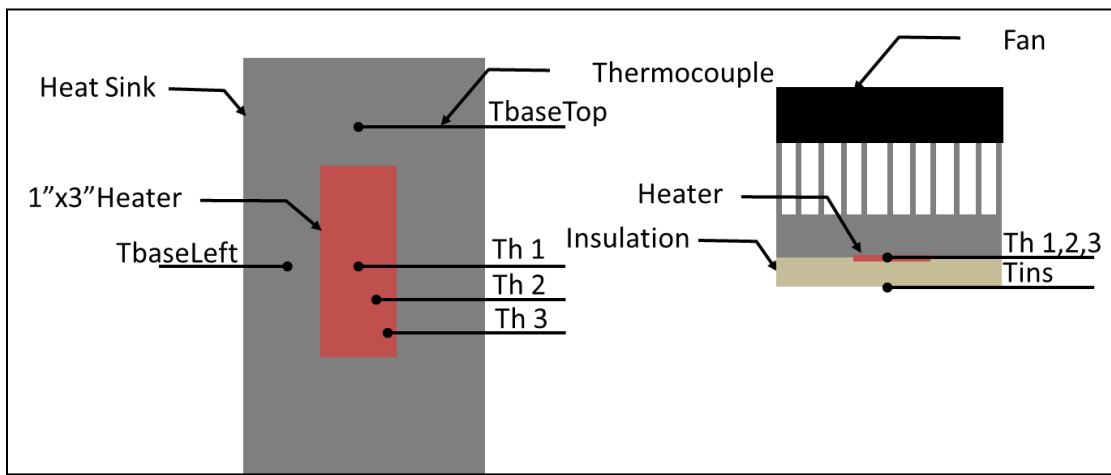


**Figure 11.** Heat sink experimental setup

$$R_{HS} = \frac{T_{heater} - T_{ambient}}{(Q_{heater} - Q_{loss})} \quad \text{Eq. (3)}$$

Where  $R_{HS}$  is the thermal resistance of the heat sink,  $T_{heater}$  is the area-weighted average temperature of the heater,  $T_{ambient}$  is the ambient temperature,  $Q_{heater}$  is the capacity of the heating elements,  $Q_{loss}$  is the capacity lost through the unit, as defined by Equation (4).

$$Q_{loss} = \frac{k_{ins} A_{hs}}{th_{ins}} (T_{heater} - T_{ins}) \quad \text{Eq. (4)}$$

Where  $k_{ins}$  is the thermal conductivity of the insulation,  $A_{hs}$  is the area of the heat sink,  $th_{ins}$  is the thickness of the insulation, and  $T_{ins}$  is the temperature under the heat sink insulation.

Several tests were performed with different heater power inputs and the results are presented in Figures 12 and 13. It is important to note the very large error bars stemming from the high degree of uncertainty in the measurement of small temperature differences. Also, the calculated thermal resistances are considerably different when the measured temperatures are arithmetically averaged versus averaged on a surface area basis; thus, it is reasonable to conclude that the

approach of area-weighting the surface temperature is not truly representative of the actual temperature profile.

Another unexpected result is the variation of thermal resistance with heater power input. This effect is due to the higher uncertainties at low power settings (smaller temperature differences). The conclusion of these tests was that the thermal resistances of both heat sinks for the Laird unit are roughly 0.3-0.34 K/W.

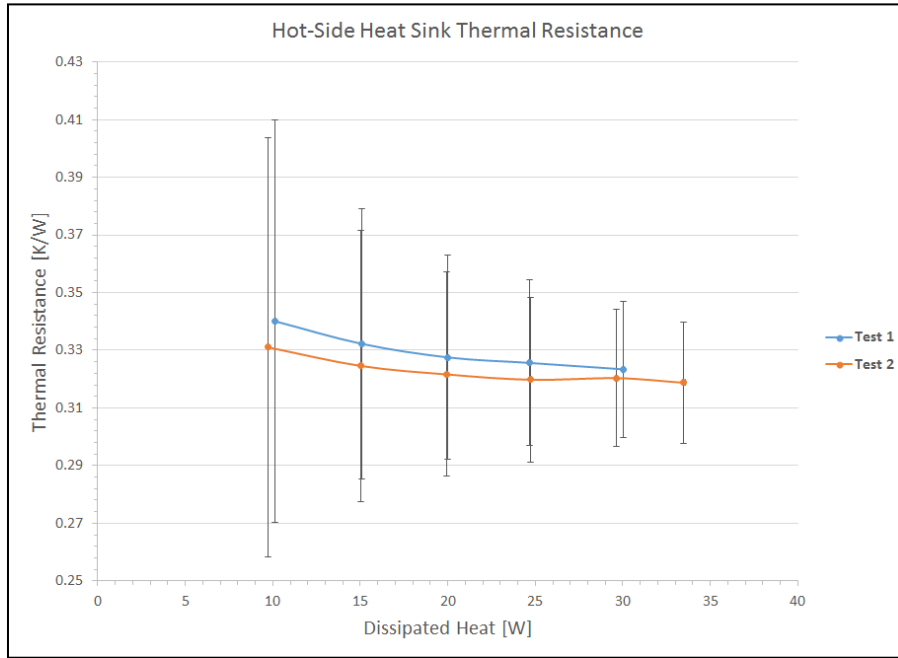


Figure 12. Hot-side heat sink thermal resistance using area-weighted temperatures

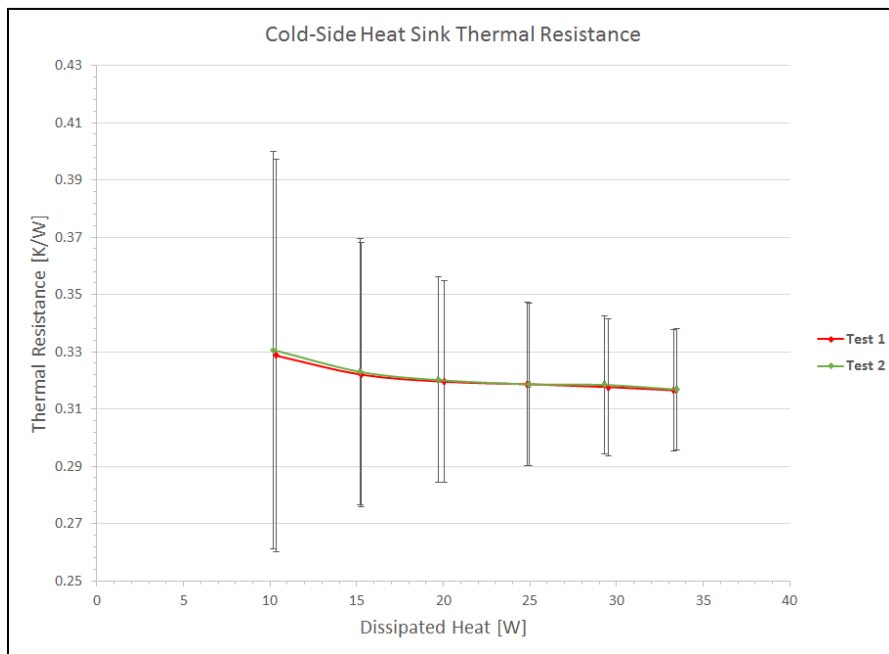


Figure 13. Cold-side heat sink thermal resistance using area-weighted temperatures

#### *4.4.1 Analytical Approximation of Thermal Resistance*

Using both Laird's "AZTEC" tool and Sandia's TE model, it is possible to estimate the heat sink thermal resistance value required to match the manufacturer's curve for cooling capacity. From these efforts it was determined that, based on the TE module performance specifications, the heat sink thermal resistances must be closer to 0.16K/W.

Using this thermal resistance value allows Sandia's software model to predict the maximum (0°C  $\Delta T$ ) cooling capacity of 58W specified by the manufacturer. However, this thermal resistance value over predicts the maximum pull down capacity. For this condition, the model predicts approximately 10W of cooling capacity at 42°C  $\Delta T$  where the manufacturer's specification indicates a 0W capacity.

It is expected that the true heat sink thermal resistances lie somewhere between the 0.16 and 0.3K/W. The discrepancy between the experimental testing and analytical assessment may be the result of:

- Dissimilar thermal spreading effects in the experimental heat sink testing; the heater used was smaller than the actual TE modules in use and a higher thermal spreading penalty was likely observed than would be seen in actual operation.
- Area-weighting of temperature measurements; heater and heat sink temperatures were highly non-uniform.
- High uncertainty measurement due to small temperature differences.
- Modeling challenges since both Laird and Sandia TE models generate a capacity vs temperature difference curve with a slope that is less steep than the manufacturer-specified curve provided for the assembled Laird cooler.

The Sandia Cooler heat exchangers were expected to have a thermal resistance of ~0.1 K/W at 2000 rpm, including the thermal spreading resistance due to concentrated heat loads. Despite the large uncertainty, these results suggest that the Sandia cooler at 2000rpm may reduce the thermal resistance by 38-71% and thus improve the overall system performance.

#### **4.5 Recommendation to Move Forward with Sandia Prototype**

After reviewing initial experimental and modeling efforts, it was determined that the use of Sandia impellers in the proposed prototype could offer significant improvement over the Laird device performance because of the reduced thermal resistance. Efforts proceeded, as described in the sections below, to design, build and test SCTD prototype.

## 5. MODELED PERFORMANCE AND PRELIMINARY PROTOTYPING

During the course of this project it was desired to have a system level model of the thermoelectric device to not only predict the potential performance of the Sandia Cooler device, but also to understand the experimental results from the baseline unit. Thus, Sandia developed an analytical model for a general thermoelectric cooling device.

### 5.1 Model Description

A thermal circuit model based on the model of Lineykin and Ben-Yaakov [9] was developed to describe the TE device. It was assumed that the device was used to cool an insulated enclosure. The model represents the TE phenomena in a thermal circuit as shown in Figure 14. The model was originally designed such that multiple different TE modules could be considered in the system design. Each module was then characterized by the module properties  $\alpha_m$ ,  $R_m$ , and  $\theta_m$  which are Seebeck coefficient, electrical resistance, and thermal resistance respectively. Additionally, the thermal interface resistance between the module hot and cold sides and the hot and cold side heat sinks was included. The model then represented the TE modules as parallel heat paths between the two heat sinks. The heat sinks were treated as simple thermal resistances to the ambient temperature on the hot side and the enclosure temperature on the cold side. On the cold side, heat gain through the enclosure walls was included in the model as well as heat input from a resistive heating element. In this way, the model represented the experimental apparatus that was used to characterize the commercial and custom devices.

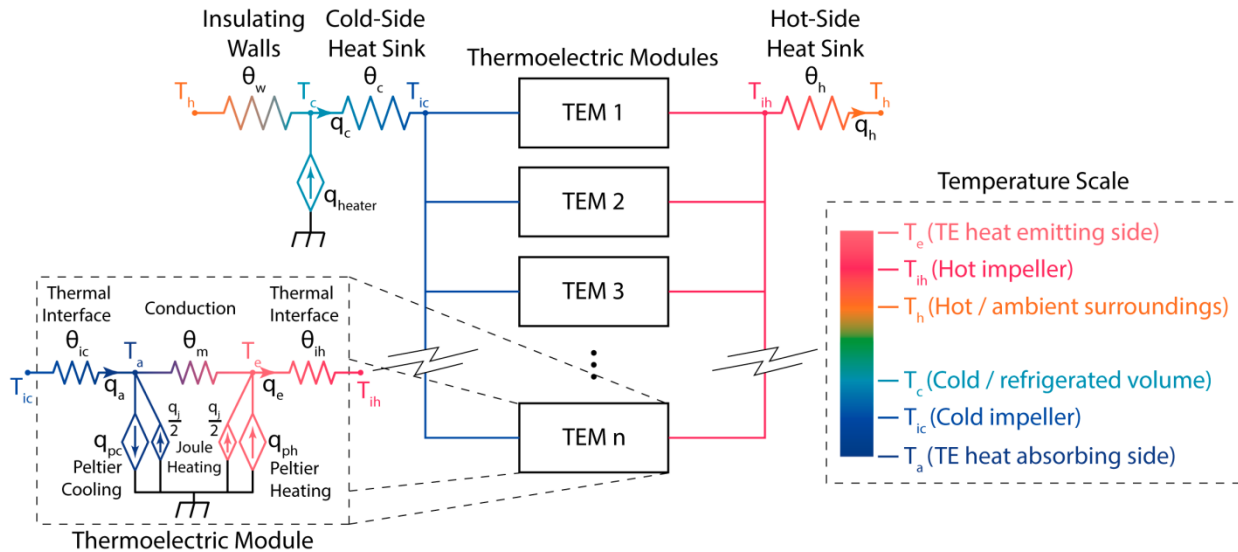


**Figure 14.** Thermoelectric module modeling approach

This thermal/thermoelectric model was originally developed using MATLAB<sup>®</sup> and was designed to estimate the system's operating point based on known inputs. These inputs were the TE current, the exterior ambient temperature, the properties of the TE modules, and the properties of the heat-sink-impellers (i.e. thermal resistance). The outputs of the model were the cold side cooling capacity, the temperature of the refrigerated enclosure, and the TE voltage and power

consumption. Later, this model was simplified to use a single TE module with a variable number of identical couples. The model was then converted to an Excel spreadsheet for ease of use.

The MATLAB<sup>®</sup> model solved the TE equations, energy balances, and heat transfer rate equations simultaneously. The TE equations are shown in Equations (5) – (7):

$$V = IR_m + \alpha_m(T_e - T_a) \quad \text{Eq. (5)}$$

$$q_e - \alpha_m T_e I = -\frac{T_e - T_a}{\theta_m} + \frac{I^2 R_m}{2} \quad \text{Eq. (6)}$$

$$q_a - \alpha_m T_a I = -\frac{T_e - T_a}{\theta_m} - \frac{I^2 R_m}{2} \quad \text{Eq. (7)}$$

In addition to  $\alpha_m$ ,  $R_m$ , and  $\theta_m$ , the variables in these equations are the voltage applied to the TE modules  $V$ , the current through the modules  $I$ , the hot side temperature  $T_e$ , the cold side temperature  $T_a$ , the hot side heat load  $q_e$ , and the cold side cooling capacity  $q_a$ . Equation (5) takes into account the Seebeck voltage produced by the temperature difference across the modules. Equations (6) and (7) include the Seebeck effect, Joule heating and heat conduction across the modules. Conduction reduces both the hot side heat load and the cold side cooling capacity. Joule heating adds to the hot side heat load while reducing the cold side cooling capacity. The energy balance and heat transfer rate equations are given in Equations (8) – (10):

$$q_h = q_e = \frac{T_e - T_{ih}}{\theta_{ih}} = \frac{T_{ih} - T_h}{\theta_h} \quad \text{Eq. (8)}$$

$$q_c = q_a = \frac{T_{ic} - T_a}{\theta_{ic}} = \frac{T_c - T_{ic}}{\theta_c} \quad \text{Eq. (9)}$$

$$q_c = q_{heater} + \frac{T_h - T_c}{\theta_w} \quad \text{Eq. (10)}$$

In Equation (8), the hot side heat load of the TE modules is set equal to the heat flow through the thermal interface to the heat sink and through the heat sink to the ambient air at  $T_h$ . The thermal interface resistance is  $\theta_{ih}$  and the heat sink thermal resistance is  $\theta_h$ . Similarly, in Equation (9) the cold side cooling capacity is equal to the heat flow from the enclosure at  $T_c$  through the heat sink and the thermal interface to the cold side of the TE modules. The cold side heat sink thermal resistance is  $\theta_c$  and the thermal interface resistance is  $\theta_{ic}$ . Finally, in the experimental setup the cooling capacity equals the sum of the heater power and the heat leak through the insulated walls as shown in Equation (10).

## 5.2 Model Inputs

As mentioned before, a number of input parameters are required for the system model. In addition to boundary conditions, such as ambient air temperature, and imposed conditions, such as the power supply voltage applied to the TE modules, properties of the modules, interfaces and heat sinks were required. For the heat sink thermal resistances, the values for the Laird device were inferred from the model based on the TE module properties and the performance curve

provided in the device specification. For the SCTD, the heat sink thermal resistance was based on impeller performance as a function of rotational speed. This dependence was captured in an analytical expression such that the speed was entered as an input to the model.

The thermal resistance of the interface between the TE modules and the heat sinks was taken into account with an interface resistance. This value was based on the data sheet for the Laird thermal grease that was used. An experiment was performed to verify that this thermal resistance was valid.

The properties of the TE modules needed for the model were calculated from the performance specifications provided by the Laird data sheets. These calculations were carried out according to the procedure in [9] using Equations (11) – (13):

$$\alpha_m = \frac{U_{\max}}{T_h} \quad \text{Eq. (11)}$$

$$R_m = \frac{U_{\max}(T_h - \Delta T_{\max})}{I_{\max} T_h} \quad \text{Eq. (12)}$$

$$\theta_m = \frac{2T_h \Delta T_{\max}}{I_{\max} U_{\max} (T_h - \Delta T_{\max})} \quad \text{Eq. (13)}$$

The equations show that the module Seebeck coefficient, electrical resistance, and thermal resistance can be calculated from the maximum voltage ( $U_{\max}$ ), the hot side temperature ( $T_h$ ), the maximum temperature difference ( $\Delta T_{\max}$ ), and the maximum current ( $I_{\max}$ ). As a check, these calculations were carried out for an example Laird TE module, CP14,71,10 shown in Figure 15. The datasheet for this module provided the  $U_{\max}$ ,  $I_{\max}$ , and  $\Delta T_{\max}$  shown in Table 6. The module properties  $\alpha_m$ ,  $R_m$ , and  $\theta_m$  were then calculated from Equations (11) – (13) with a  $T_h$  of 298K and are also shown in Table 6. Note that these are overall values for the module and include not only the properties of the TE couples, but the electrical and thermal contacts between the couples and the ceramic plates on either side.

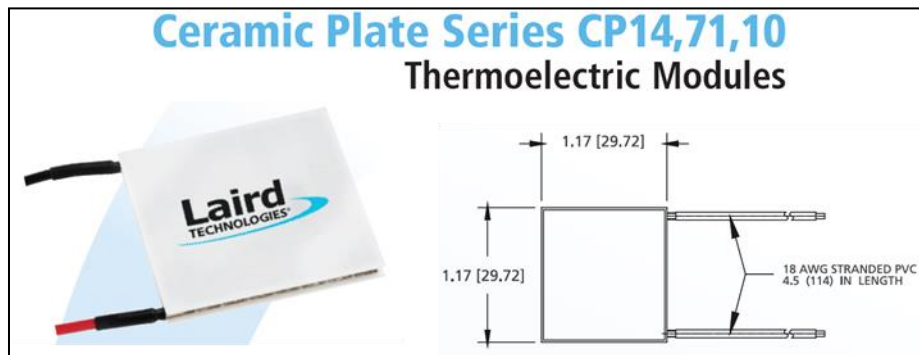


**Figure 15.** Example Laird thermoelectric module used for model validation

**Table 6. Example Laird thermoelectric module specified and calculated properties used for model validation**

Module Properties	From Datasheet			Calculated		
	$U_{max}$ (V)	$I_{max}$ (A)	$\Delta T_{max}$ (C)	$\alpha_m$ (mV/K)	$R_m$ ( $\Omega$ )	$\theta_m$ (K/W)
CP14,71,10	8.6	3.9	67	29	1.7	5.2

To verify the validity of these calculations, the module properties were then put into the system model and the performance curves for the module were reproduced. A comparison of the data sheet curves (solid lines) and the model predictions (dotted lines) is shown in Figure 16. The figure shows cooling capacity ( $Q_c$ ) as a function of the module temperature difference for a range of electrical currents from 0.8A to 3.9A. Although the model slightly over predicts cooling capacity for the higher currents, the overall agreement is quite good, indicating the validity of the TE module property estimation procedure (Eq. 7-9).

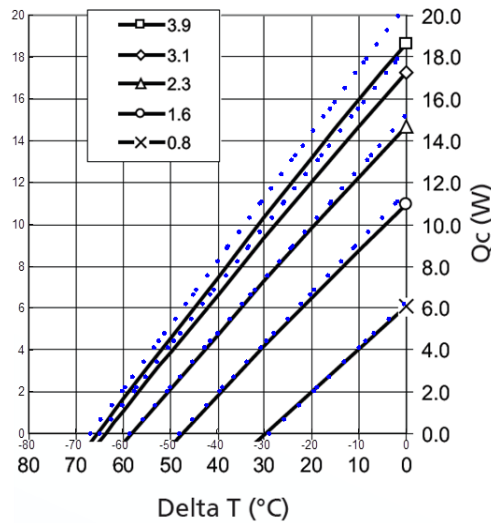


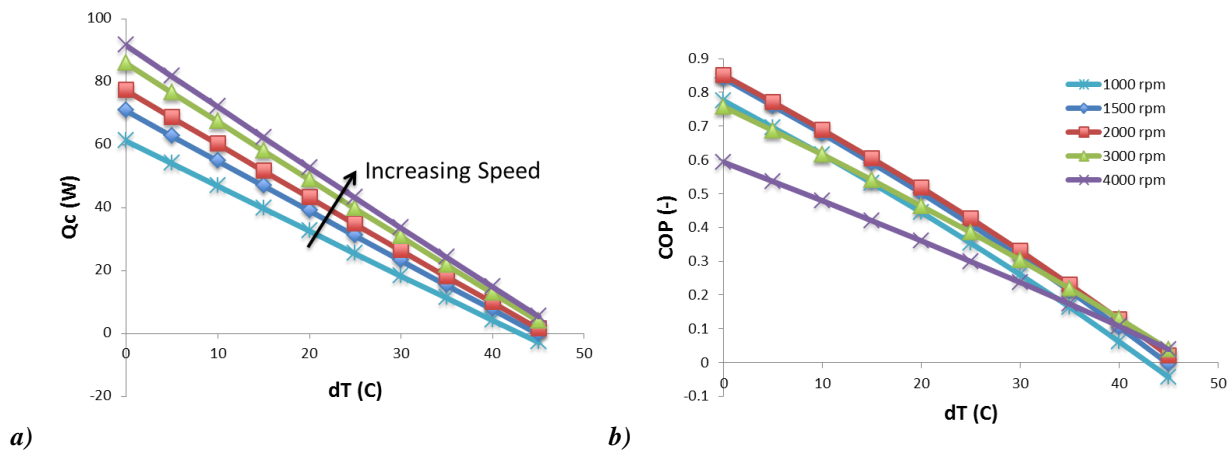
**Figure 16.** Laird Thermoelectric module manufacturer specified area and model predicted performance

With a method to determine module properties from data sheet values, it was necessary to identify the TE modules that were used in the Laird TE device. Initially, with only the size of the modules and the electrical resistance known, the system model was used to examine various Laird modules to estimate which one was used. The performance of the system was predicted using an estimate of the heat sink thermal resistances and the properties of Laird modules with a 40mm square footprint. The module that best matched the Laird device specifications was the CP14,199,06 module. This module has a calculated Seebeck coefficient of 0.076V/K, an electrical resistance of 2.93 ohms, and a thermal resistance of 1.27K/W. Two of these TE modules were used in the system model and the thermal resistance of the heat sinks was adjusted to get the best agreement between the model and the Laird device datasheet.

Later, through conversations with Laird engineers and after disassembling a Laird device, it was determined that the actual TE modules used in the device were instead CP12,161,055 modules. Based on the Laird datasheet, these modules have a calculated Seebeck coefficient of 0.061V/K, an electrical resistance of 2.78 ohms, and a thermal resistance of 1.85K/W. Note that these values are quite different than the CP14,199,06 module properties. The effect on system performance will be discussed in the next section.

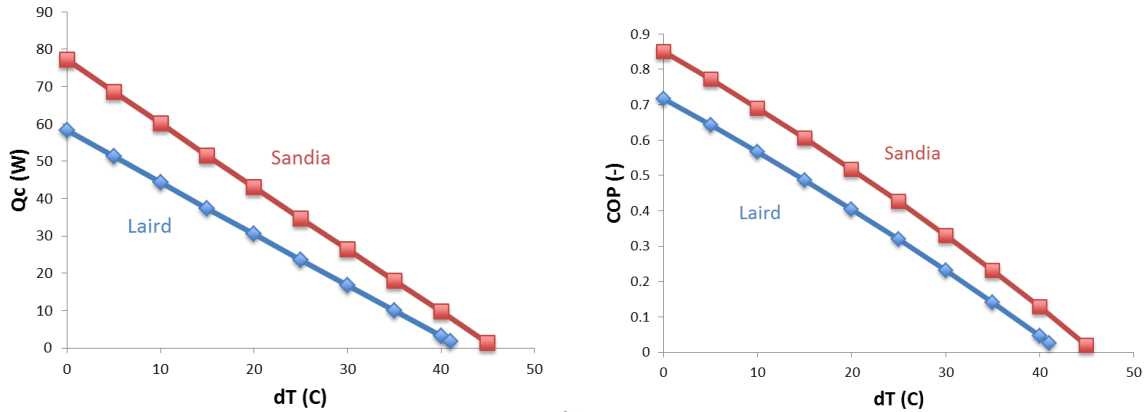
### 5.3 Model Results

With the input parameters defined, the system model was used to estimate the performance of the SCTD with two 40 mm square TE modules to directly compare to the Laird device. Initial predictions were made using the CP14,199,06 module properties. Figure 17 shows the predicted cooling capacity and COP as a function of system temperature difference for various speeds of the 5" diameter impellers. These calculations take into account the reduction of heat sink thermal resistance with impeller speed, reflected in the cooling capacity, as well as the increase in fan power, reflected in the COP. The indication from this early modeling result was that an impeller speed around 2000rpm might provide the best combination of cooling capacity and COP.



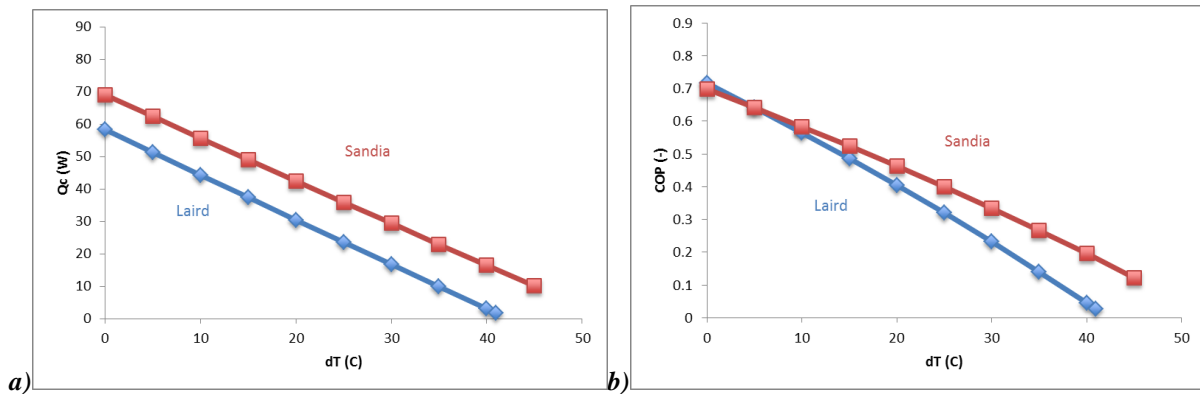
**Figure 17.** Model predicted a) capacity and b) COP of the Sandia Cooler Thermoelectric Device for a range of operating speeds with 5" impellers

Figure 18 shows the model prediction for the Sandia device at 2000rpm compared to the performance of the Laird device provided on the manufacturer's data sheet. The model predicts a cooling capacity of the Sandia design that is approximately 33% higher than the Laird spec with a 20% higher COP. These improvements are predicted for a device that has a 17% smaller footprint and 35% smaller volume.



**Figure 18.** a) Capacity and b) COP comparison between the Laird device and the modeled Sandia Cooler Thermoelectric Device with 5" impellers at 2000 rpm

Following disassembly of a Laird unit at Sandia, the actual TE modules were identified as Laird model number CP12,161,055. The TE properties of these modules were found to be significantly different than for the CP14,199,06 modules. As before, the properties were estimated based on the Laird data sheet and then used in the model to predict the device performance. Figure 19 shows the modified results using the correct TE module properties. Note that the predicted maximum cooling capacity dropped from 80W to 70W and the maximum COP, taking into account the higher motor power of the SCTD, dropped to about equal that of the Laird unit, at 0.7. The indication from this result was that the Sandia device would not provide as significant an improvement as initially thought. This will be discussed further in the context of the experimental results from the two devices.



**Figure 19.** a) Capacity and b) COP comparison between the Laird device and the modeled Sandia Cooler Thermoelectric Device with 5" impellers at 2000 rpm and the correct TE modules

In addition to the performance predictions just discussed, the system model was used to understand the performance of a more optimized device using the Sandia Cooler. As will be discussed in Section 6.2.1, with only two 40 mm square TE modules, the heating and cooling loads are not well distributed across the available footprint of the 127 mm diameter impellers. The result is that the impeller platens have to act as heat spreaders and the thermal spreading increases the impeller thermal resistance significantly. A more optimized design would cover the available impeller surface with evenly distributed TE couples. This would not only eliminate the

spreading resistance issue, but would allow the TE device to operate closer to the peak COP achievable with a given material and couple geometry by operating at lower current.

With this in mind, calculations were carried out assuming that the entire bottom surface of the impeller, except the motor cavity, could be populated with TE couples. These couples would be connected in series electrically and in parallel thermally, just like one large TE module. For these calculations, properties were need on a per couple basis. This was done by simply selecting the properties of a Laird module and calculating couple properties based on the number of couples that the module contained. Thus, Seebeck coefficient, electrical resistance, and thermal resistance per couple were calculated using Equations (14) – (16). The figure of merit,  $Z$ , was also calculated per Equation (17).

$$\alpha = \frac{\alpha_m}{N} \quad \text{Eq. (14)}$$

$$R = \frac{R_m}{N} \quad \text{Eq. (15)}$$

$$\theta = \theta_m N \quad \text{Eq. (16)}$$

$$Z = \frac{\theta \alpha^2}{R} \quad \text{Eq. (17)}$$

Table 7 shows these values calculated for couples based on the Laird ZT5,16,F1,4040 module. This module has a higher  $ZT$  than the CP12,161,055 module, achieved by using premium materials. The couple density of this module was used to determine the number of couples that could be used to cover the impeller surface. Note that even better performing TE modules are currently commercially available and advanced materials are being actively developed. Thus, the results to be described next should be reasonably achievable, if not conservative.

**Table 7. Calculated properties for Laird ZT5 16F1,4040 module**

$\alpha$ (mV/K)	$R$ (m $\Omega$ )	$\theta$ (K/W)	$Z$ (1/K)	$ZT$ at 25°C (-)
Seebeck Coefficient	Electrical Resistance	Thermal Resistance		Figure of Merit
0.416	18.7	317	$2.95 \cdot 10^{-3}$	0.88

The system model was exercised using the couple properties in the table above, the number of couples to cover the annular surface area on the bottom of a 5” impeller occupied by the fins, the thermal resistance of the 5” impeller at 2000rpm with no added spreading resistance, and the thermal interface resistance of the Laird thermal grease. The output of the model depends on the power supply voltage applied to the TE module. Lower voltage produces lower cooling power but high COP, while higher voltage produces higher cooling power but lower COP. Figure 20 shows the results from the model with several supply voltages compared to the Laird device performance specs. Depending on the desired temperature difference, a voltage can be chosen that provides cooling capacity and COP that are significantly higher than the Laird device. For example, at 48V the performance covers the same temperature difference span as the Laird unit

with more than double the cooling capacity and nearly double the COP. This is accomplished in a device that is smaller in volume than the Laird as well.

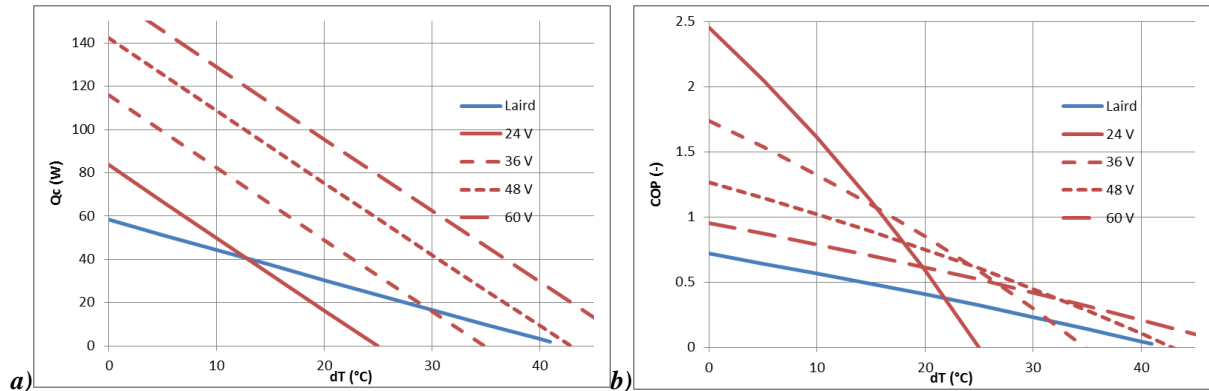


**Figure 20.** a) Capacity and b) COP comparison between the Laird device and the modeled Sandia Cooler Thermoelectric Device with 5" impellers at 2000 rpm with optimized couples for multiple voltages

Note that the above comparison is not quite fair in the sense that the Laird device could also be improved with higher ZT modules that covered more of the heat sink surface area. The area used in the improved SCTD is approximately three times larger than the area of the two 40 mm square modules used in the Laird device. An improved Laird device is not presented here since it would require detailed knowledge of the heat sink thermal resistance including spreading resistance effects. However, it is known that the SCTD heat exchanger thermal resistance is lower than the Laird heat exchangers and reasoned that a greater reduction in thermal resistance would result for the SCTD from eliminating the thermal spreading due to the geometry. The increased area covers the entire heat transfer surface for the SCTD but would still only cover a fraction of the Laird heat exchanger footprint.

## 6. PROTOTYPE DESIGN DEVELOPMENT

### 6.1 Conceptual Design

The general concept for the SCTD was to sandwich one or more TE modules between two Sandia Cooler impellers; one to act as the hot side heat exchanger and the other the cold side heat exchanger. In this configuration, the entire device would rotate as a unit and there would be no air gap and no air bearing required. The result would be a fairly simple device that just required one motor, a frame to mount it on, and a method to provide electrical power to the rotating TE module(s).

Concepts were initially envisaged that included customizing the number and design of the TE modules to match the performance of the impellers and the desired cooling capacity of the SCTD. However, the Sandia/OTS team decided to instead focus on a direct comparison to the chosen commercial unit from Laird. To make the comparison as direct as possible, the same TE modules would be used for the SCTD as the Laird unit. In addition, since the thermal interface resistance between the heat exchangers and the TE modules can have a non-negligible impact on performance, the same thermal interface material (Laird 1500 thermal grease) and clamping force would be used.

With these constraints, the remaining design issues included sizing and designing the impellers, selecting the appropriate motor, shaft, bearings and controller, designing a frame and shroud, and integrating these components into an overall system design that could be easily assembled. Figure 21 shows a cross-section of the final conceptual design. The cold-side impeller is on the left and the hot-side on the right. The motor stator is mounted on the stationary shaft on the hot side to minimize the transfer of motor waste heat to the cooled space. The motor rotor is integrated with the hot-side impeller. Both impellers rotate on the shaft on radial contact ball bearings. A rotary electric feed-through mounted on the left end of the shaft is used to provide power to the TE modules which are clamped between the two impellers. Space between the two impellers not occupied by TE modules is insulated. Overall, the design is compact and compared to other motor configurations has less potential for vibration and noise. The impellers and shaft are supported by a four-legged frame attached to a metal plate for mounting to the cooled enclosure. An insulated shroud fits closely over the impellers to minimize heat leak paths.

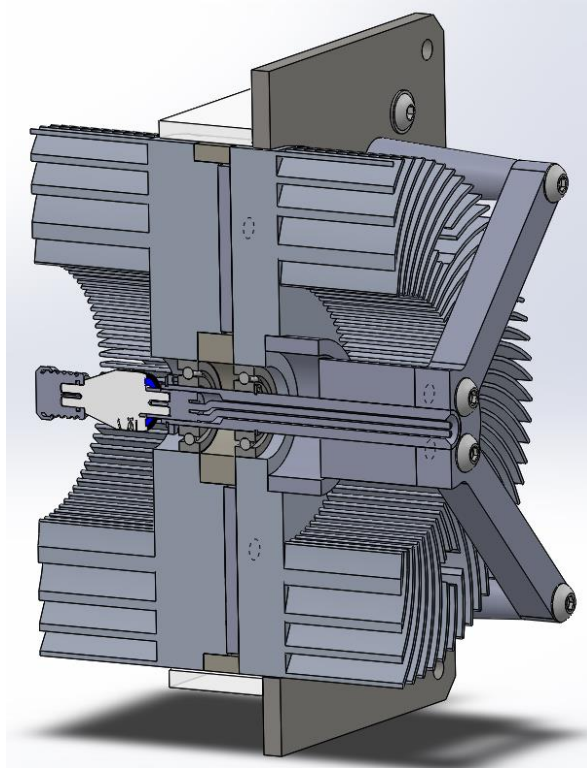


**Figure 21.** Cross-section of Sandia Cooler device concept

## 6.2 Impeller Design and Fabrication

The first step in the impeller design was to determine the size based on the requirements and constraints. One tradeoff would be impeller size versus performance. A lower thermal resistance could be achieved with a larger impeller, which would improve the system performance. However, the device had to be no larger than the Laird unit for comparison purposes. The Laird unit was 4.8" X 9" X 5.75" with an envelope volume of about 250in<sup>3</sup>. A Sandia Cooler-based device with 7" diameter impellers would approximately equal this volume. So, this served as an upper bound.

Another consideration was the size of the TE modules. The Laird unit used two CP12 modules (see Appendix C) that were each 40mm square. To clamp them between two impellers and leave room for a shaft and bearings required a minimum impeller diameter of 4.2".

Bounded by 7" and 4.2", the impeller diameter was chosen based on a compromise between performance and size. Also, since the two TE modules would not cover the entire surface of the heat sinks, heat spreading would need to be considered. A larger impeller would have an overall smaller thermal resistance for a distributed heat load. But, with the heat concentrated to two 40mm square areas, the effective thermal resistance would not be greatly improved at a larger diameter. Modeling results suggested that with 5" diameter impellers the device would offer improved performance over the Laird unit in a smaller volume. The fin geometry for the impellers would be a scaled version of the 4" V5 impeller that was developed by Sandia for

electronics cooling. This impeller had 80 fins that were 0.030” thick and 0.095” tall. Scaled, the fins would be 0.0375” thick and 1.19” tall.

### *6.2.1 Impeller Thermal Analysis*

Due to the heat spreading effect mentioned above, a thermal analysis was performed to determine the effective impeller thermal resistance that would be expected for the 5” impellers. Although two 40mm square TE modules was the intended design, several other configurations were investigated to understand the effect of distributing the heat load to 4 or 8 TE modules. Also, different impeller base thicknesses were investigated as well as the effect of using raised pads to mount the modules.

Comsol Multiphysics was used for these thermal analyses. Figure 22 shows the model geometry that was used on the left and an example output on the right. A quarter section of the impeller was used to take advantage of symmetry. For additional simplification the impeller fins were not included in the model; instead heat transfer through the fins to the air was modeled using a convective heat transfer coefficient on the top surface of the base. This heat transfer coefficient was defined such that it would produce the correct impeller thermal resistance when a uniform heat flux was applied to the base. This convective boundary condition is shown in the figure along with the symmetry and insulation boundary conditions on the other surfaces. A heat flux boundary condition was used to model the TE modules. The shape and location of this surface was changed depending on the configuration. The figure shows the configuration for two 40mm modules. The two other configurations examined were four 30mm modules and eight 20mm modules.

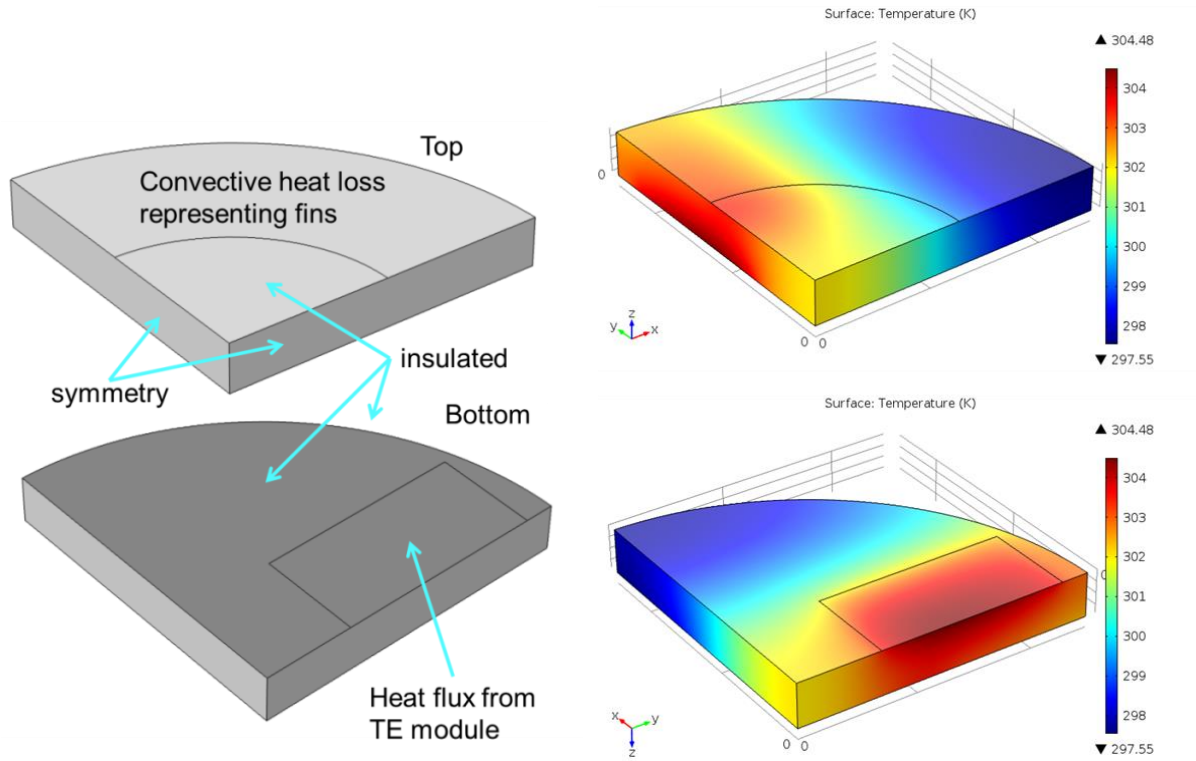


**Figure 22.** Comsol model of thermoelectric device showing geometry and boundary conditions (left) and example temperature distribution (right)

The Comsol model was used to calculate the steady-state temperature profile of the impeller platen given the boundary conditions and material properties. For the purpose of the model, a 6063 Al impeller was assumed with a thermal conductivity of 200W/m-K. The module heat flux was defined to give a total heat input of 120W to represent the hot side of the TE modules. For the convective boundary condition that simulated the impeller fins, an impeller speed of 2000rpm was assumed and an ambient temperature of 20°C was used. The effective thermal resistance was calculated as in Equation (18):

$$R_{\text{eff}} = (T_m - T_{\text{ambient}}) / Q \quad \text{Eq. (18)}$$

Where  $T_m$  is the average temperature of the surface representing the TE modules,  $T_{\text{ambient}}$  is the ambient temperature, and  $Q$  is the heat input. The example result on the right in Figure 22 shows that a noticeable temperature gradient develops in the case of the two 40mm modules. In contrast, Figure 23 shows the result for eight 20mm modules. The same temperature range is used as in the previous figure and a much reduced thermal gradient is observed.

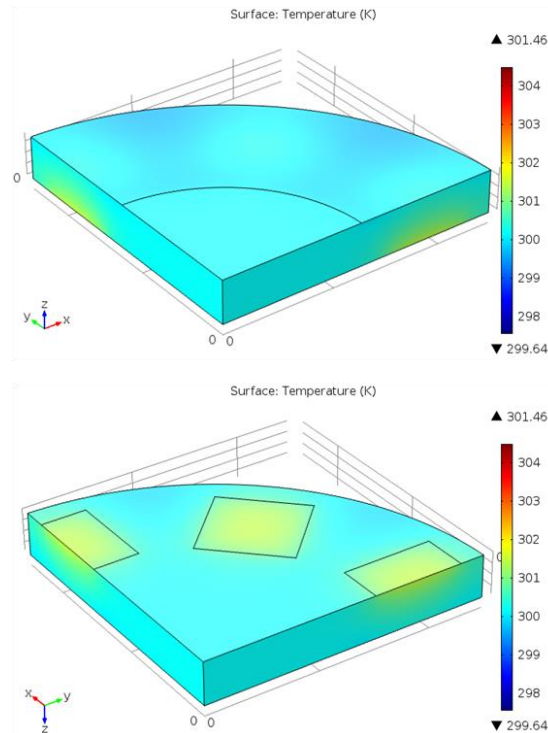


**Figure 23.** Temperature distribution for eight 20mm square thermoelectric modules

Table 8 shows the results of the simulation matrix. Four different platen thicknesses were evaluated along with the three module configurations and the effect of raised pads. With the two 40mm modules, a platen thickness of 0.5” gave the lowest effective thermal resistance of 0.084K/W. However, this was still 31% higher than if the heat load was uniformly spread across the platen surface. Thinner platens gave progressively higher thermal resistance values. Thus, 0.5” thick platens were chosen for the device impellers.

In order to provide space between the two platens for insulation to limit heat leakage, the effect of raised pads was also considered. Simulations were run with 0.25” thick pads for platen thicknesses of 0.375” and 0.5”. As the last two rows of the table show, the pads increased the thermal resistance further. However, this effect was considered acceptable compared to the heat leak effect. Because the cold side impeller would transfer less heat than the hot side, the thermal resistance penalty from the pads was best assigned to that impeller.

To compare the effect of different numbers of modules, a nominal platen thickness of 0.375” was used. The results show that spreading the heat to four 30mm modules lowers the effective thermal resistance substantially to within 11% of the baseline. Using eight 20mm modules brings the thermal resistance down to within 3% of the baseline value. Thus, a nearly optimal configuration would use eight 20mm square TE modules. However, to compare directly to the Laird unit, two 40mm modules were used.

**Table 8. Thermal model results for various platen thicknesses and module configurations**

<b>Platen thickness</b>	<b>TE modules</b>	<b>T<sub>max</sub> (K)</b>	<b>T<sub>min</sub> (K)</b>	<b>T<sub>mod</sub> (K)</b>	<b>R<sub>eff</sub> (K/W)</b>	<b>% over baseline</b>
0.375"	Baseline	302.4	299.8	300.8	0.064	0
0.375"	2X40mm	304.5	297.6	303.6	0.087	36%
0.5"	2X40mm	304.0	298.1	303.3	0.084	31%
0.25"	2X40mm	305.6	296.8	304.3	0.093	45%
0.05"	2X40mm	318.5	294.0	310.5	0.145	227%
0.375"	4X30mm	302.1	298.8	301.7	0.071	11%
0.375"	8X20mm	301.5	299.6	301.1	0.066	3%
0.375" w/ 0.25" pads	2X40mm	304.95	297.6	304.6	0.095	48%
0.5" w/ 0.25" pads	2X40mm	304.65	298.1	304.3	0.093	45%

### 6.2.2 Impeller Fabrication

The two 5" diameter impellers were fabricated at SNL using a Haas OM-2A CNC vertical 4-axis mill with a 30,000rpm spindle. As previously described, the fin geometry was scaled directly from the smaller V5 impeller that had been optimized for electronics cooling. Figure 24 shows pictures of the hot side impeller. The picture on the right shows the rotor magnets and flux ring embedded in the outer surface for the direct-drive motor, further described in Section 6.3. The bearing observed in both pictures was pressed into an interference fit in the platen. The figure also shows the eight screw holes for clamping the TE modules between the two impellers. Note that these holes created truncated fins in eight places.

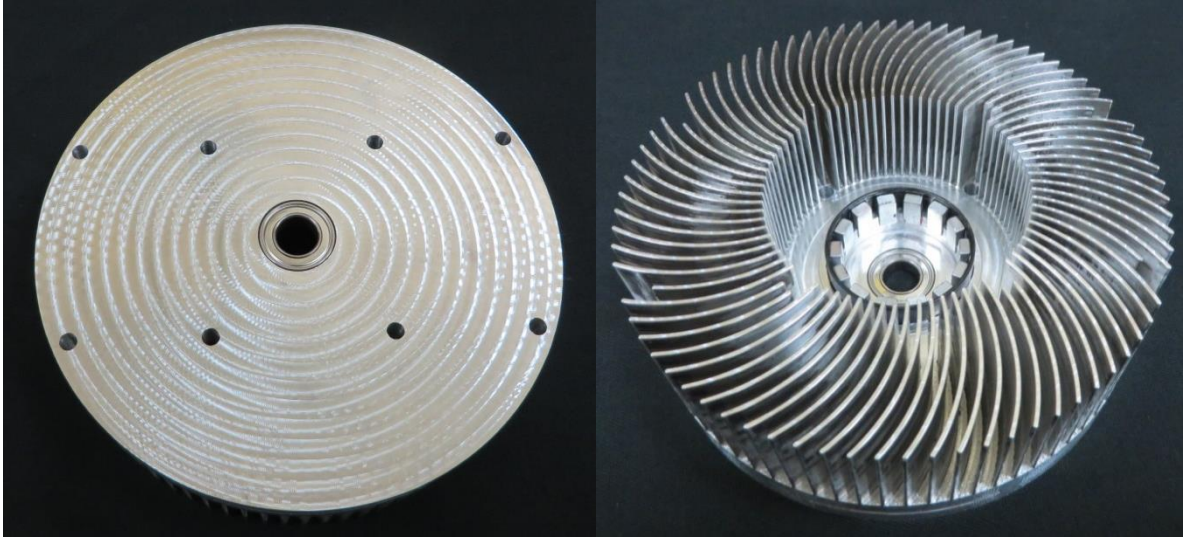


**Figure 24.** Hot side impeller assembly

The cold side impeller is shown in Figure 25. The picture on the right shows that the fins are mirror images of the hot side impeller. That is because the impellers are clamped together and rotate as one part. Thus, the hot side impeller rotates counter clockwise and the cold side impeller rotates clockwise. Rotating in the correct direction, the fins are backswept. Note also in the left hand picture that the cold side impeller includes 0.25" raised pads for the TE modules. As discussed previously, this is to allow for insulation between the impellers to minimize heat leakage. While difficult to see in the picture, small raised edges on the pads are used to precisely locate the TE modules for balance. An identical bearing is pressed into the cold side impeller platen. Threaded holes can be seen at the edges of the pads for clamping to the hot side impeller. The other threaded and through-holes near the bearing are for running wires and attaching the electrical feed-through.

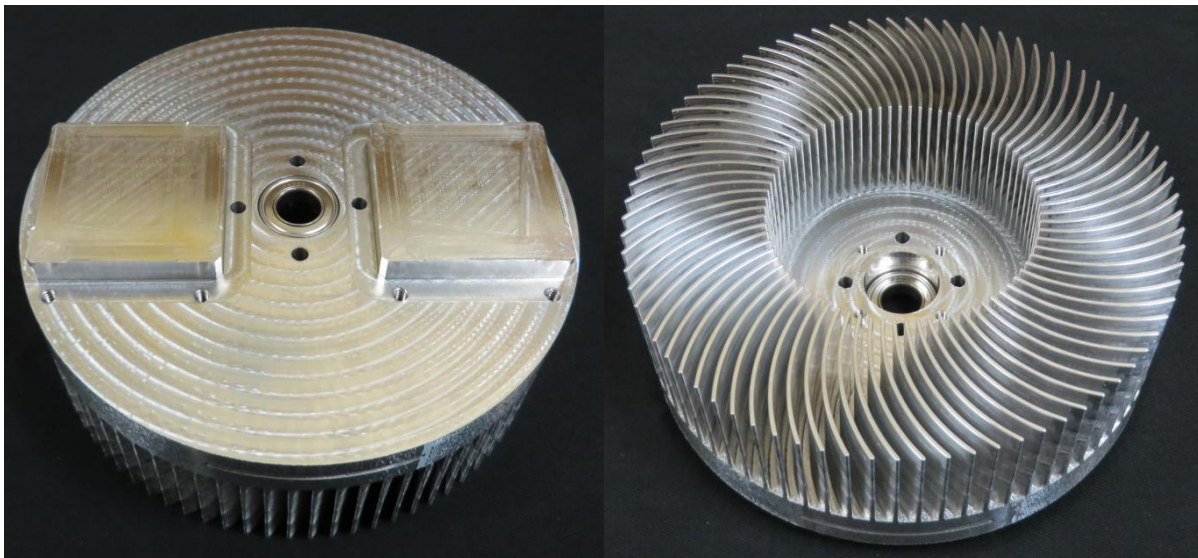


**Figure 25.** Cold side impeller assembly

## 6.3 Motor and Controller

### 6.3.1 Motor Selection

A Motrolfly DM-2810 three-phase brushless DC hobby motor was adapted to directly drive the two impellers. In this approach, the stator is held stationary on the shaft, while the rotor magnets and flux ring are embedded in the top surface of the hot side impeller. Motor sizing was influenced by several factors. The torque for each 5” diameter impeller was estimated as 20mN-m at 2000rpm based on previous impeller scaling studies. Peak motor efficiency should therefore occur near 40mN-m.

Another constraint was that the inner diameter of the stator fit over the shaft. Details on the shaft design constraints are given in Section 6.4.1. The smallest commercially available motor found to meet these design constraints was the Motrolfly DM-2810. The motor has 12 stator poles with an outer diameter of 30mm, an inner diameter of 10mm, and a thickness of 10mm. The rotor incorporates 14 NdFeB magnets with dimensions of 3mm x 5mm x 10mm. The stator was rewound in a distributed LRK configuration with 80 turns of 30AWG copper magnet wire per pole and connected in the wye configuration. This winding arrangement was chosen to obtain a top speed of around 2000rpm with a 30VDC bus.

### 6.3.2 Controller Selection

For simplicity, hobby brushless motor controllers using trapezoidal commutation were investigated to run the motor. Figure 26 shows efficiency versus torque at a constant speed of 2000rpm with the stock motor winding at different bus voltages. Lower bus voltages show better efficiency because the motor back EMF is better matched to the bus voltage and lower switching losses are incurred. In this case, the controller required a minimum of 8V to operate, though the motor could run on even lower bus voltage due to being wound for high speed operation. This trend shows the advantage of rewinding the motor to match the operating conditions.

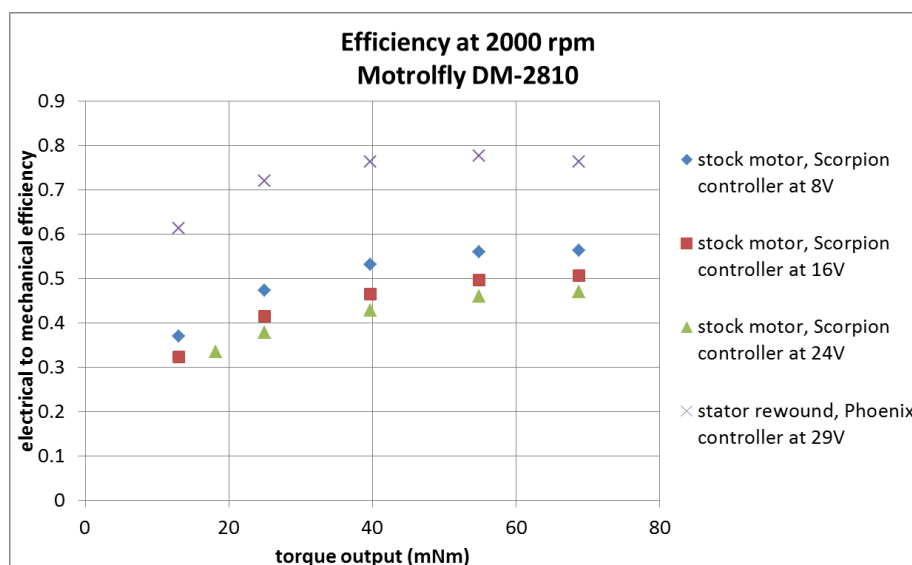


Figure 26. Motor/controller efficiency as a function of output torque

For operation with the 30AWG stator, a Phoenix Edge Lite HV 40 hobby controller was chosen. Testing of the controller on a hysteresis brake indicated that electrical to mechanical efficiency as high as 75% could be achieved with this controller and motor combination near the expected operating torque at 2000rpm. In this application, efficiency suffers at lower speeds both as a result of the lower speed itself and because of the lower impeller torque that accompanies it.

Electrical power consumption measurements on the device itself are shown in Table 9. Power consumption is higher than anticipated. The rotary electrical contact and impeller bearings account for a portion of the discrepancy, but the motor and controller efficiency are likely lower than brake measurements had indicated. The rotary electrical contact is specified with a typical rotation torque of 3.4mNm, but the manufacturer does not supply any information on the speed dependence. The rotation torque at operating speed may be higher. The bearings are 10mm inner diameter, 19mm outer diameter, and shielded on both sides. With 5N axial preload and 6.8N impeller mass per bearing, the frictional moment is estimated to be 0.5 to 1mN-m per bearing. The shaft power to run the impellers assuming 40mN-m torque at 2000rpm is 8.4W. The total accountable friction losses consume 4.9mN-m, which equates to 1.0W at 2000rpm. Thus, the total mechanical power for the system is estimated as 9.4W. Electrical power consumed at this operating condition was measured as 16.0W, implying around 59% electrical to mechanical efficiency for the controller and motor. The remaining 41% or 6.6 W is dissipated as heat. The effect of this heat dissipation will be discussed in a later section.

**Table 9. Motor power consumption for various impeller speeds**

5N bearing preload			
impeller speed	supply voltage (V)	supply current (A)	electrical power (W)
1408	30.29	0.245	7.42
1609	30.28	0.317	9.60
1809	30.27	0.419	12.7
1998	30.26	0.53	16.0

### 6.3.3 Control Module

Figure 27 shows the inside of the control box that was assembled to house the power supply, motor controller, and various power connections. A knob on the front panel adjusts the pulse-width modulation (PWM) signal applied to the motor, allowing for speed adjustment up to 2100rpm. Ports on the front panel, as seen in Figure 28, are provided for monitoring the voltage and current supplied to the motor controller using external multimeters. Additional ports allow integration of an external power supply for operating the TE modules. The two modules were run in series to reduce the current capacity required of the rotary electrical contact, so a 24VDC power supply is required. The two TE supply wires and three motor drive wires are integrated into a connector on the front panel and routed to the assembly on a single custom cable.

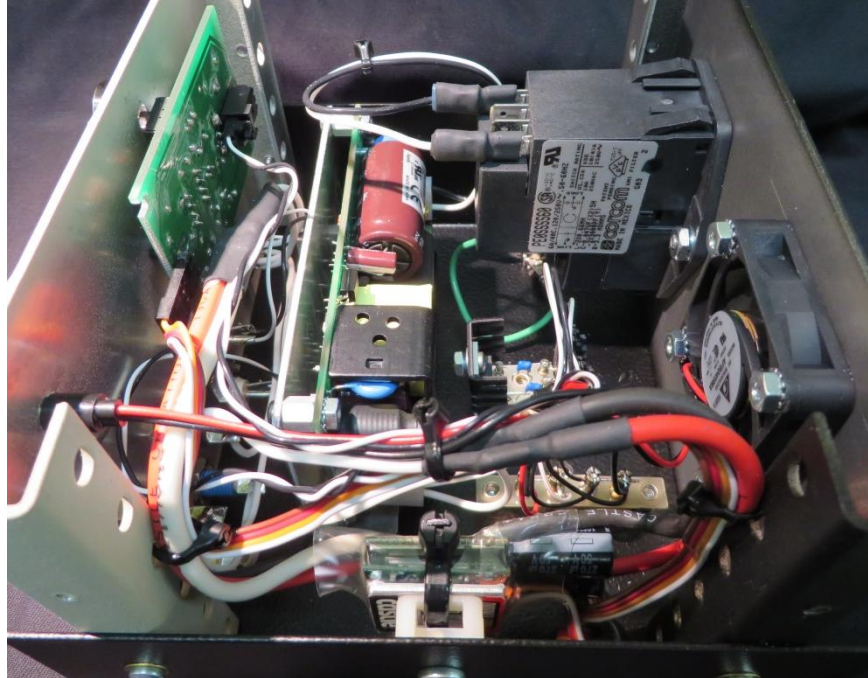


Figure 27. Control module includes power supply, controller, and diagnostics



Figure 28. Control module front panel

## 6.4 System Design and Assembly

### 6.4.1 Frame and Shaft Assembly

The shaft assembly consists of the shaft, a connector to interface with the rotary electrical contact, and the motor stator, as shown in Figure 29. The shaft diameter was driven partly by rigidity of the assembly, and partly by the diameter of the connector for the rotary electrical contact. With these considerations, a shaft size near 3/8" was deemed reasonable. Since the DM-

2810 motor stator had an inner diameter of 10mm, the shaft was made with a constant 10mm outer diameter for simplicity. The rotary contact was positioned on the cold side because the motor and framework did not allow space on the hot side. The interface connector is pressed into the shaft, and the remainder of the shaft is hollow to allow the wire leads to feed through to the hot side. The motor stator is a close slip fit over the shaft for radial alignment, and a roll pin keys the stator to the shaft to prevent rotation. Wicking Loctite was applied between the stator and shaft to ensure that it did not move axially. Snap rings locate the impellers on the shaft and provide a means for axial preloading of the bearings. For this, a wave spring and spacers were used.



**Figure 29. Motor stator and shaft**

The frame assembly is shown in Figure 30 and consists of a partition for mounting the assembly to an enclosure, a four-legged framework mounted on standoffs, and clamping block for securing the shaft to the frame. For the purposes of this prototype, the framework components were overdesigned for rigidity to ensure that resonances near the impeller operating frequency were avoided. An example structural simulation is shown in Figure 31. In this case, the full mass of both impellers (about 1.4kg) is applied to the end of the shaft. Assuming bonded contacts on both sides of the standoffs, a deflection of 0.001” is calculated. Rough estimations indicated a natural frequency near 100Hz, and later modifications increased this value to near 125Hz. With more detailed analysis, components could be made thinner to reduce material usage and assembly weight.

The partition is designed with a 0.025” radial clearance to the outer diameter of the impeller, allowing plenty of space for assembly tolerances and shaft deflection. This could likely be reduced to decrease the potential for gas movement between the hot and cold sides. The four-legged frame was designed to allow air flow into the center of the impeller and out around the full circumference. The shaft clamp bolts onto this framework, providing a rigid mount for the cantilevered shaft and a protected pathway for the motor wires. The TE and motor wires are guided through the shaft clamp, and the shaft is slip fit into the clamp. Two set screws in the clamp are tightened against flats on the shaft, securing it against rotation and wobble.

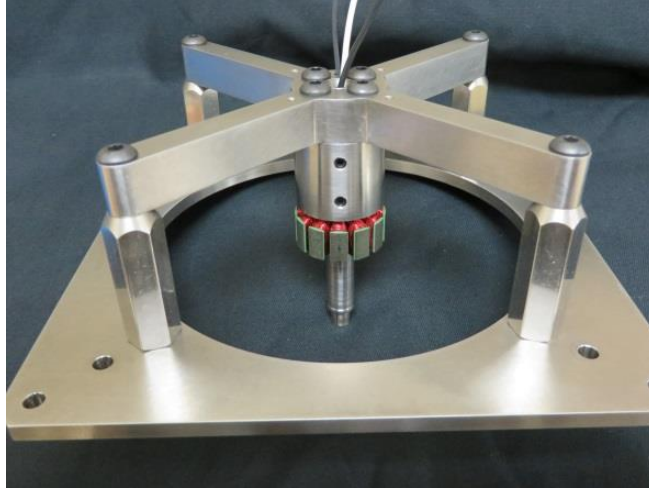


**Figure 30.** Frame and shaft subassembly

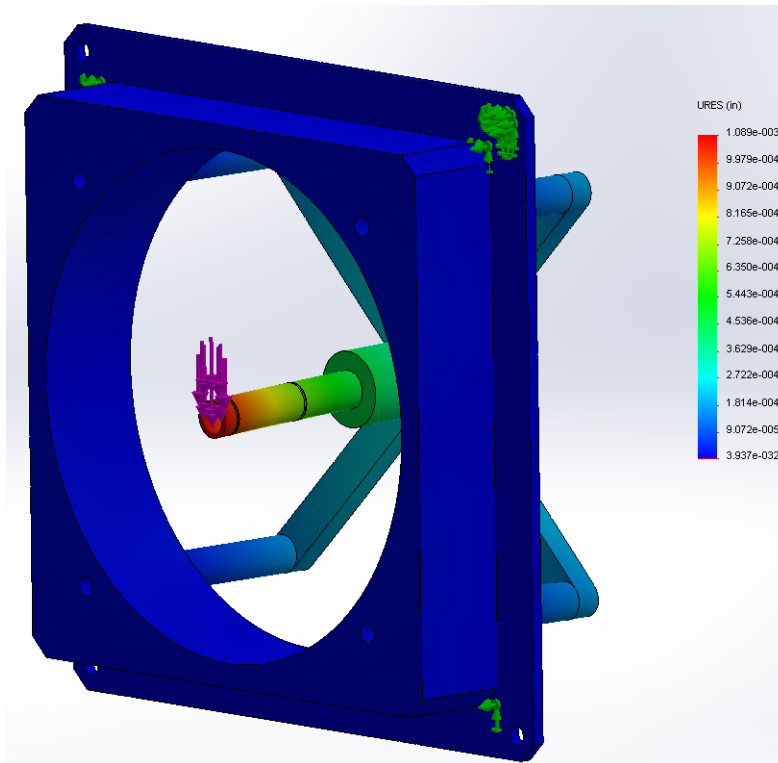
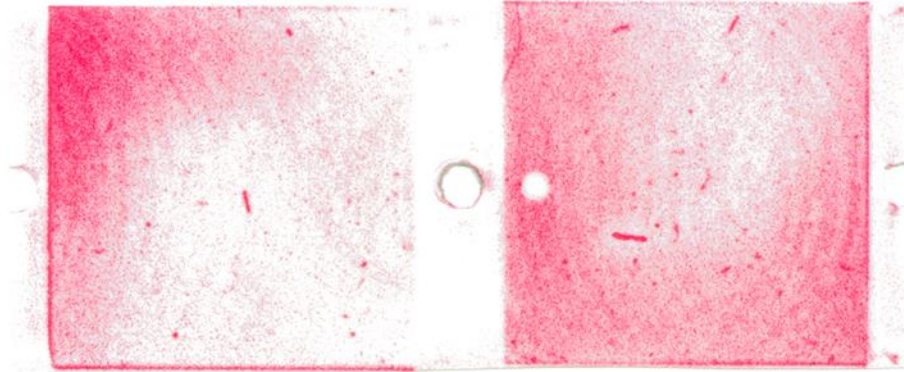


**Figure 31.** Structural model of frame

#### 6.4.2 Clamping Design

To obtain thermal interfaces similar to the baseline Laird commercial assembly, its clamping arrangement was evaluated. Two 40mm square TE modules are used with Laird 1500 grease at the heat sink interfaces. Three M5x0.8 screws at 50mm spacing are used to clamp the modules. Screw torque values were estimated upon removal. The screw between the two modules was estimated at 30in-lb, while the two outer screws were estimated at 15in-lb. Translating these torque values to clamping force, the clamping pressure was estimated to be 280 to 400psi, depending on friction assumptions. As another check, pressure indicating film was placed

between the modules and heat sink, and the unit was reassembled and torqued to the estimated specification. Film with a range of 71 to 355psi was used. An image of the film is shown in Figure 32. The magnitude of the clamping pressure appears somewhat lower than estimated with bolt force. Some uneven contact is seen, related to flatness tolerances on the heat sinks and a slight difference in thickness between the two modules. The bolts do not appear to cause any significant localized stresses.



Pressure distribution for Laird assembly  
(71-355 psi measuring range)

**Figure 32.** Pressure indicating film showing clamping pressure distribution for Laird device

The clamping arrangement for the SCTD was adapted from this baseline. Screw counter bores would be placed in the fin array of the hot side impeller and threaded holes in the bottom surface of the cold side impeller. Four smaller screws were positioned near the edges of each module instead of two larger ones at the center. This placed the screws near the inner and outer edges of the fins, and the interfering fins were simply shortened to accommodate the screws. Prior to final assembly, the TE modules were clamped between the impellers with pressure indicating film. As seen in Figure 33, with the baseline screw torque, contact at the outer edges is light. Upon measurement, the mounting pads on the cold side impeller were found to have a downward slope toward the outer radius of the impeller. The total difference from inner to outer edge was 0.0015". To accommodate, the outer two screws on each module were torqued to a higher value. A progression of torque values was tested until a uniform contact distribution was observed, as shown in Figure 33.

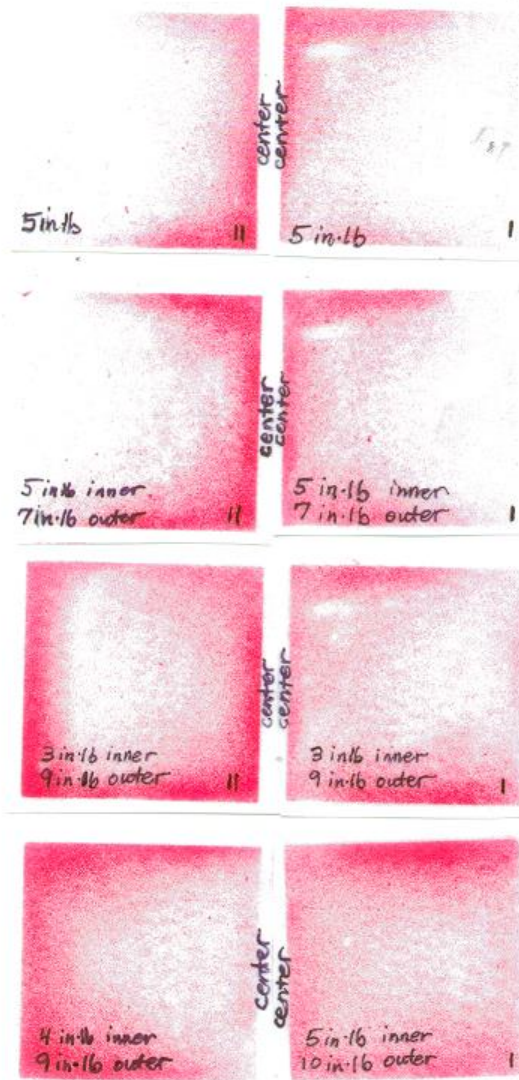


**Figure 33. Pressure indicating film showing effect of screw torque on clamping pressure distribution for the Sandia Cooler Thermoelectric Device**

### 6.4.3 Shroud Design

A rigid insulating shroud was designed to interface between the rotating impellers and the enclosure. The shroud is machined for a close 0.025" radial gap to the impellers, eliminating the need for close tolerances on the enclosure and simplifying installation. Glass-filled polycarbonate was chosen for rigidity, reasonable thermal resistance, and having a thermal expansion coefficient similar to aluminum. Pockets were created in the corners and filled with polyurethane foam for better insulation. The glass-filled polycarbonate structure has a face area of 4.68in<sup>2</sup>, thickness of 1.00", and a thermal conductivity of 0.25W/m-K, producing an estimated heat loss of 0.03W/°C. The polyurethane foam corners have a total area of 2.83in<sup>2</sup>, thickness of 1.00", and a thermal conductivity of 0.03W/m-K, giving an estimated heat loss of 0.002W/°C.

#### 6.4.4 Electrical Feed-Through

To reduce the current demand on the rotary electrical contact, the two TE modules were wired in series. A commercially-available Mercotac 205-H rotary electrical contact was chosen for this design. The contact is rated for 4A at 240VAC and has a contact resistance of  $1\text{m}\Omega$ . As discussed in Section 6.3.2, this contact introduces an undesirable drag torque of approximately  $3.4\text{mNm}$ . In a production device, a rotary transformer may provide a means of reducing drag torque and increasing longevity. For the purposes of this prototype, the chosen electrical contact was simple and functional.

#### 6.4.5 Final Assembly

Images of the impellers during assembly are shown in the figures below. The TE module wire leads were soldered together in series, leaving one wire from each module to connect with the rotary contact. As shown in Figure 34, polyurethane foam insulation was cut to fit around the raised pads on the cold side impeller, and glued in place with cyanoacrylate adhesive. The polyurethane foam has a face area of  $13.75\text{in}^2$ , an installed thickness of  $0.375''$ , and a thermal conductivity of  $0.03\text{W/m-K}$ , producing an estimated heat loss of  $0.028\text{W}/^\circ\text{C}$ . Laird thermal grease 1500 was applied to the raised pads, and the TE modules were installed, feeding the wires through the impeller face. Thermal grease was then applied to the exposed side of the modules.

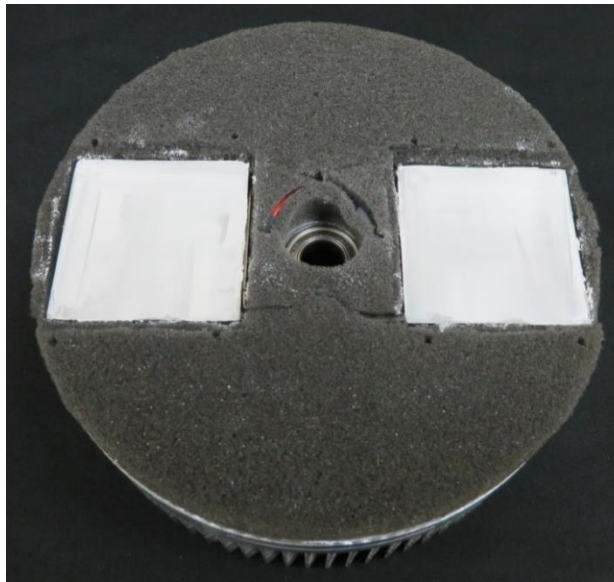


**Figure 34.** Cold side subassembly with foam insulation

The hot side impeller was then installed on top of the cold side impeller and TE modules. A spare 10mm shaft was inserted to keep the impellers concentric while clamping them together. The inner screws were torqued to 4-5in-lb, and the outer screws were torqued to 9-10in-lb. The impellers were removed from the spare shaft and installed on the frame and shaft assembly. A wave spring and spacers were installed to provide axial preload on the bearings, and a second snap ring was installed. The rotary electric contact was then installed in its connector, and a wire guide was installed to spin the contact without pulling on the wires. This can be seen in Figure 35 below. The cap was installed on the rotary contact, and the TE wires were soldered to the

leads. The glass-filled polycarbonate shroud was installed over the impellers and attached to the partition. Four #10 clearance holes in the corners of the partition are provided for mounting the device to an enclosure.



**Figure 35.** View of the cold side of the final assembly

To interface the TE wires and motor leads with the power supply and motor controller, a circular connector is installed on the frame by way of a delrin mounting cup, shown in Figure 36. Thus, a single cable is used to connect the device to the TE power supply and motor controller. The shaft clamp and this connector configuration fully enclose the small-diameter motor leads to prevent damage during handling, installation, and operation.

Two isometric views of the final SCTD assembly are shown in Figure 37. Once completely assembled, the device was operated using the control module and a 24V power supply. The bench top testing setup is shown in Figure 38. The startup and operation of the device was checked at a range of impeller speeds prior to packaging the device for shipment to OTS for evaluation.

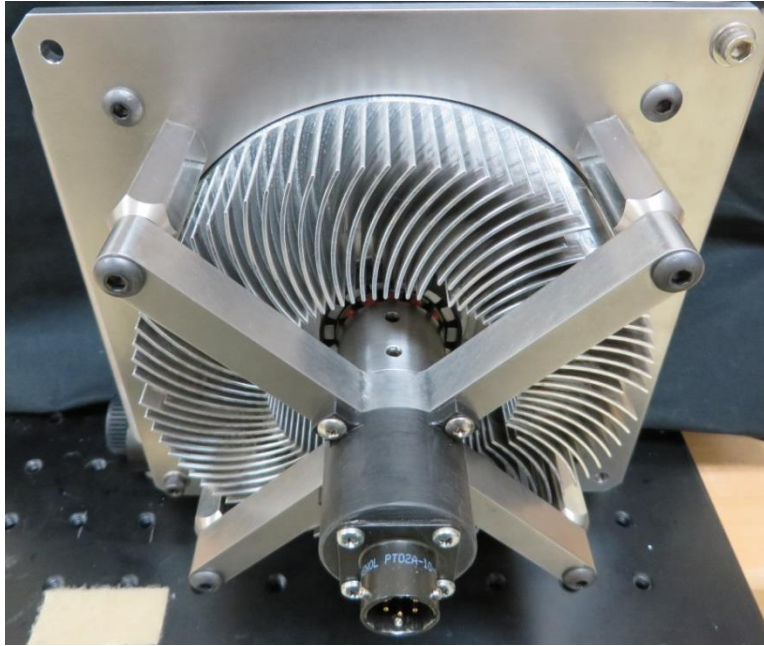


**Figure 36.** View of the hot side of the final assembly

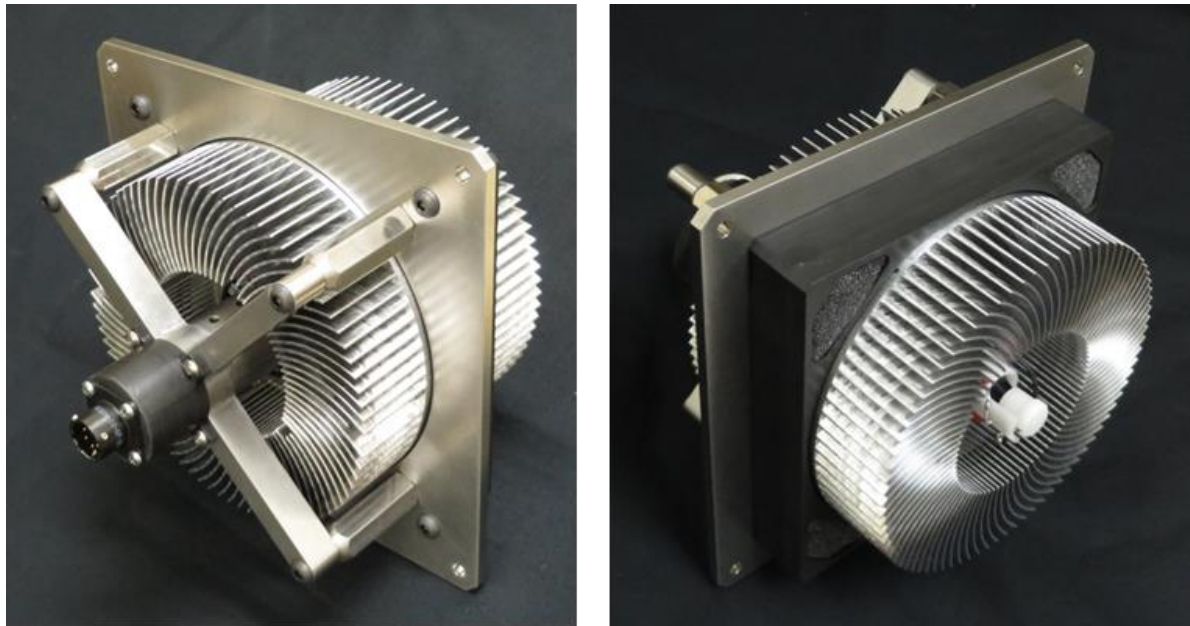


**Figure 37.** Isometric views of the final assembly

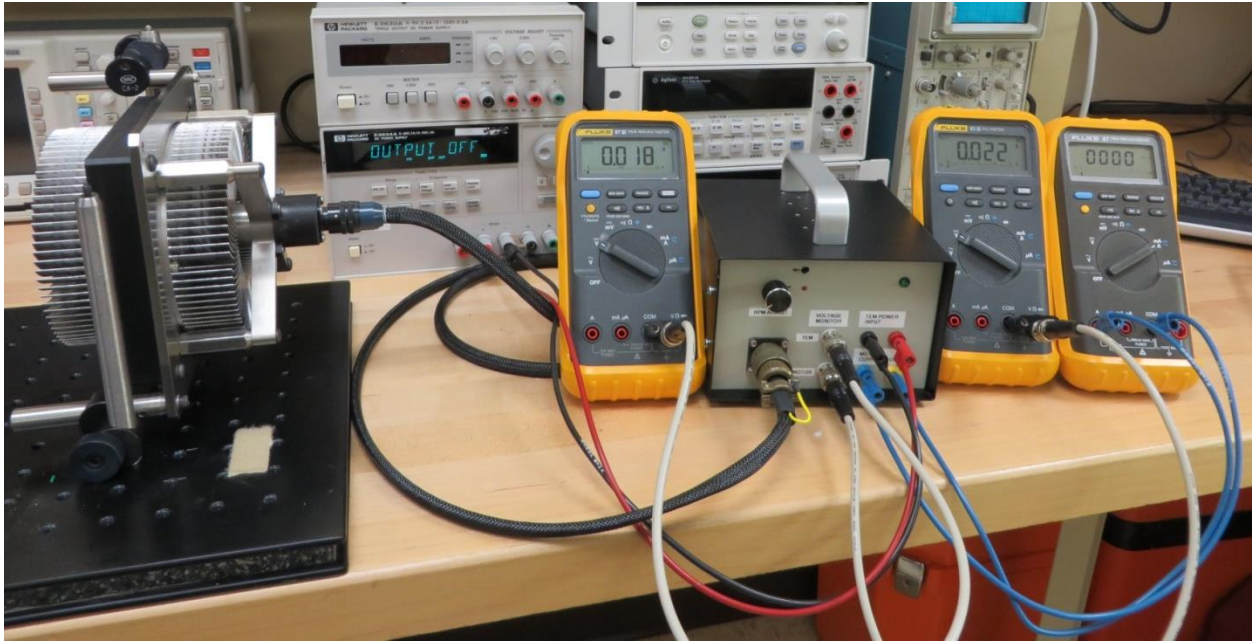


**Figure 38.** Bench top testing at Sandia prior to shipping to OTS

## 7. INITIAL PROTOTYPE TESTING

### 7.1 Experimental Set Up

Once the SCTD was constructed and received at OTS, prototype testing was initiated. As with the Laird baseline unit, the SCTD was installed on an insulated box, as depicted in Figure 39.

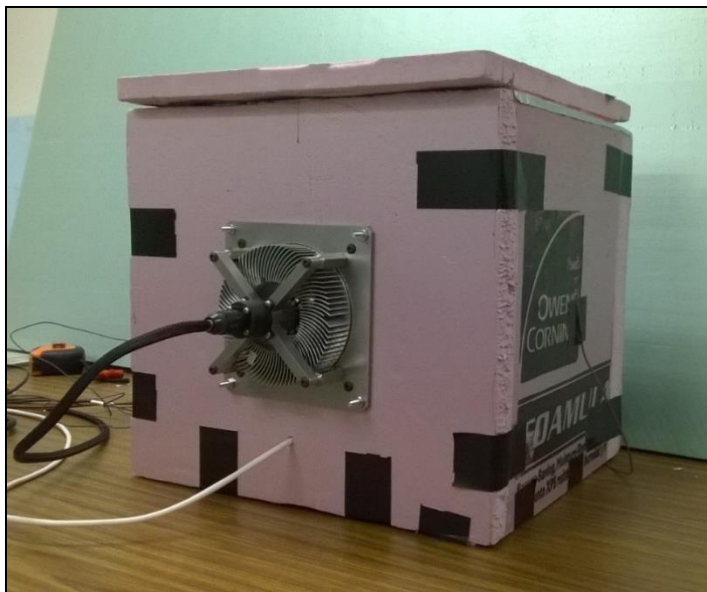


**Figure 39.** Sandia Cooler Thermoelectric Device preliminary prototype experimental setup

The light bulb was installed inside the box to serve as the heat source, with the same thermocouple arrangement as was used for the Laird unit. In addition to conducting testing at varying light bulb power levels, tests were also conducted for multiple rotational speeds, which were adjusted using the control assembly box constructed by Sandia. As initial tests were conducted, several challenges were identified and multiple system and experimental setup modifications were made before finalizing the test procedures and conditions.

### 7.2 Challenges Identified and Associated Modifications

After conducting initial tests with the prototype unit, several inadequacies in the test setup were identified. The following subsections detail the changes made to the experimental setup.

#### 7.2.1 Heat Source

Concerns arose regarding the effects of radiation heat transfer coming from light bulb used for heat input. Although radiation should ultimately be converted to convective heat transfer to the air, it is possible that the impeller was heated by radiation. Exploratory testing was conducted to evaluate the potential impact the light bulb and potential radiation effects had on the performance results. As can be seen in Figure 40, covering the light bulb with aluminum foil increased the maximum capacity of the SCTD by approximately 10%, suggesting that the heat source itself was negatively impacting test results.

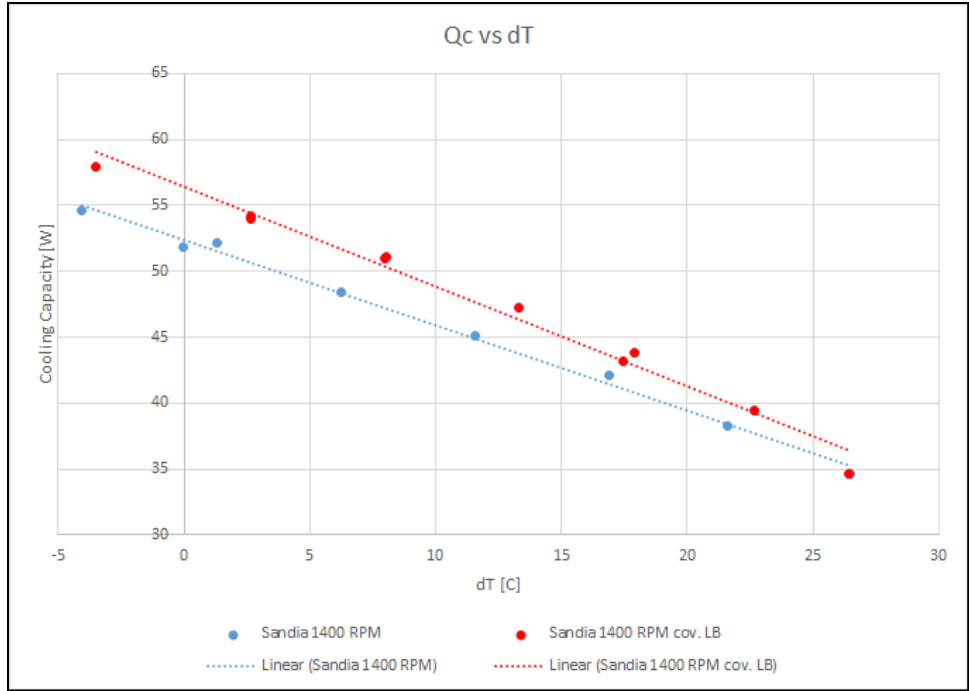


**Figure 40.** Capacity vs temperature difference for preliminary Sandia Cooler Thermoelectric Device prototype with and without covered light bulb

To mitigate these effects, the light bulb was replaced with an electric resistance heater and heat sink assembly. The large surface area and reflective surface are intended to minimize surface temperature and radiation heat transfer. The entire heater assembly is covered in aluminum foil ( $\epsilon < 0.1$ ) to further minimize the radiative emission. Figure 41 shows the resistive heating elements before being covered by aluminum foil. Two small heat sinks were installed under the resistors to minimize surface temperatures.

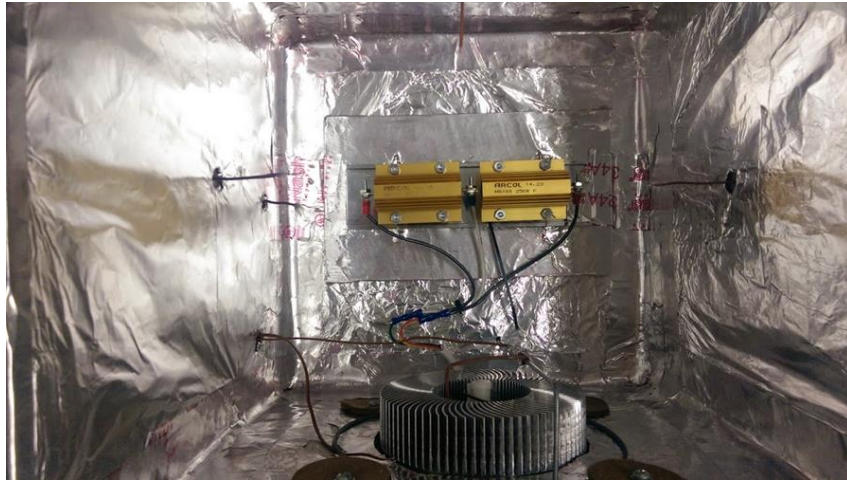


**Figure 41.** Uncovered heater assembly

### 7.2.2 Insulated Box Assembly

When testing the cooling devices in an enclosure, the quality of insulation determines the maximum temperature difference that can be tested before the heat leak into the enclosure equals the cooling capacity. Because the Sandia prototype has a very high air flow rate, the internal convection heat transfer coefficient is relatively large and the heat leak into the enclosure can be higher than that for the baseline Laird unit. To allow for a wider range of tests and investigation of larger temperature differences, the enclosure insulation was doubled, as shown in Figure 42. The figure also shows the layer of white corrugated plastic shielding, which was added to minimize heat transfer from the outside impeller exhaust air with the front surface of the enclosure.



**Figure 42.** Improved enclosure insulation

### 7.2.3 Motor Heat Contributions

Initial testing of the Sandia prototype suggested that the cooling capacity did not increase with motor speed. This was unexpected since the thermal resistance of the impellers drops with increasing speed. However, the motor power consumption was observed to increase significantly with speed and it was determined that some fraction of the electrical power to the motor entered the enclosure as heat. This heat leakage thus reduced the useful cooling capacity of the prototype. Because the effect may be mitigated in future prototypes, additional testing was performed in an attempt to isolate this heat source. Two additional UA heat leak tests were conducted to measure the temperature increase in the enclosure from running the motor and thus infer the motor heat entering the enclosure. Using this approach, the motor heat leak could be calculated by solving Equations 19 and 20 below for UA and  $Q_{motor}$ :

$$Q_{motor}(RPM) = UA(RPM) * \Delta T_{motortest} \quad \text{Eq. (19)}$$

$$UA(RPM) = \frac{Q_{bulb} + Q_{motor}(RPM)}{\Delta T_{UAtest}} \quad \text{Eq. (20)}$$

Exploratory testing for this phenomenon revealed that motor heat accounted for as much as 14% of the total cooling capacity of the Sandia cooler at the 2100rpm condition.

#### *7.2.4 Ambient Conditions*

Analytical models from Laird and Sandia suggest that TE performance changes as a function of ambient temperature, as well as a function of temperature difference across the unit. Final testing was conducted at an ambient temperature of 32°C. This temperature was selected since the Laird manufacturer specifications are derived at this ambient condition. Final tests were conducted in an environmental chamber capable of maintaining the temperature within  $<0.5^{\circ}\text{C}$ .

For the Laird unit, one test was performed at 20°C to understand the impact of the ambient temperature; the device had about 4% lower capacity at lower ambient temperature.

#### *7.2.5 Heat Leak Through the Thermoelectric Modules*

Initial testing of the enclosure heat leak was performed with the test unit (Laird or Sandia Prototype) installed. This was necessary because the heat leak must be measured with the internal fan/impeller spinning such that the enclosure heat leak value reflects the actual internal forced convection coefficient. Several factors eventually indicated that this approach was not appropriate for the measurement of the enclosure's heat leak.

When the reverse heat leak test is performed, the inside of the enclosure is heated to approximately 32°C, while the environmental chamber is regulated at 0, 15, or 32°C. This causes heat to flow out of the enclosure in the opposite direction it would flow while the TE cooler is operating. However, when this test is running, heat is able to transfer to the internal heat exchanger, through the TE modules, and out of the enclosure through the outer heat sink. Because the heat sinks have low thermal resistance and the TE modules are thermally conductive, a significant amount of heat was found to leave the enclosure in this manner (roughly 12-22W, depending on the conditions). During normal testing, current is applied through the TE modules and they are no longer thermally conductive, but instead pump heat out of the enclosure.

The result of this phenomenon was that all initial experiments for heat leak using the modified test setup produced extremely large values for UA. When actual performance tests were conducted, the real heat leak of the enclosure was much smaller (only heat transfer through the foam insulation). Using the large UA values from the erroneous heat leak testing resulted in very large calculated cooling capacities for both the Sandia and Laird unit, especially at large  $\Delta T$  conditions where the cooling capacity is calculated mostly, or entirely, from the estimated heat leaking into the enclosure.

To address this issue, only the inner half of the Laird unit was installed on the enclosure wall such that no heat could leak through the TE modules during testing. The Sandia prototype was modified to replace the TE modules with insulation. When these heat leak tests were performed, the UA values for the enclosure were much closer and results appeared to match the Laird-supplied performance curve more closely, as shown in Figure 43. Points calculated with the accurate UA value are within 10% of the manufacturer's specification.

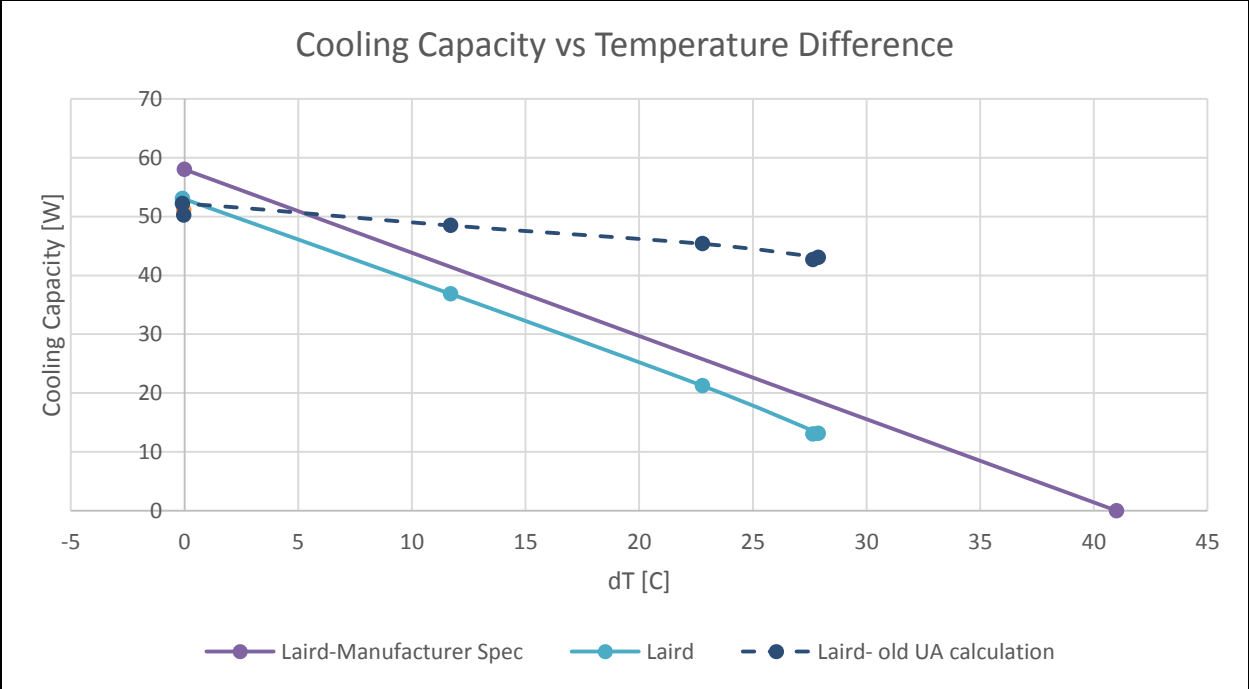


**Figure 43.** Cooling capacities calculated from erroneous heat leak test and corrected result for Laird

## 8. FINAL TESTING

### 8.1 Experimental Set Up

Given the challenges and issues identified during the initial baseline and prototype testing, several modifications were made to the experimental setup and test plan. These are outlined in detail above and summarized as follows:

- Both the Laird unit and the SCTD were installed on an insulated box, but the box insulation was increased over the original test setup configuration. The same box was used to test both units. Only the front panel was replaced between test conditions.
- The internal light bulb was replaced with an electric resistance heater to reduce potential radiation effects.
- The baseline Laird unit was modified such that the TE modules were wired in series, like the Sandia unit.
- Testing was conducted at a closely controlled ambient temperature of 32°C.
- Additional tests were conducted to evaluate motor heat leak into the box assembly.
- Additional tests were conducted to more accurately estimate the insulated box heat leak (UA) value.

In addition to the above setup modifications, the thermocouples used for temperature measurement were recalibrated and the screws on the SCTD were checked for the proper torque before conducting the final tests.

With the additional testing needs in mind, the completed test matrix included considerably more test points than originally planned. As with the initial approach, testing included some informational comparison or “background” tests to help calculate unit capacity and performance. These tests included the following:

1. Motor Leak: The ambient is maintained at 32°C. The unit fan/motor is operated, but the TE modules are not powered such that cooling is not provided. The internal box heater is turned off. Temperature increases inside the box are measured to determine the impact of the motor heat leak.
2. Heat Leak (UA) for Motor Leak: See Section 7.2.3 for additional details. The test is identical to the “Motor Leak” test, but 10W heat is added to the enclosure.
3. Heat Leak (UA) for Enclosure: Only the internal heat sink is installed. The insulated box assembly has no penetrations for the air conditioning unit. For the SCTD, the TE modules are replaced with insulation to eliminate heat leak through the modules. (See Section 7.2.5). The internal heater is turned on to maintain the temperature inside the box to 32°C. Two tests are conducted at an ambient temperature of 0°C and 15°C for each speed.

All above tests were performed for the Laird baseline unit and SCTD at three motor speeds (1400, 1700, 2000). Cooling performance tests were also conducted for the Laird unit and the SCTD at three motor speeds (1400, 1700, and 2000rpm). Tests were conducted at a temperature

difference of 32°C by adjusting the internal heater power, and for a heater power of 0W (maximum  $\Delta T$ ), 10W and 30W. A total of 16 performance tests were completed.

### 8.1.1 Measurement Accuracy and Uncertainty Analysis

Details of measurement equipment and their uncertainties are listed in Table 10. Thermocouples were individually calibrated in a thermal bath. Uncertainty propagation was carried out on all calculated values and error bars are shown on all results.

**Table 10. Measurement Equipment and Uncertainties**

Device	Make/Model	Uncertainty
Thermocouple wire	OMEGA/TT-T-24-SLE-100	$\pm 0.5^\circ\text{C}$
Thermocouple measurement block	National Instruments/9214	$\pm 0.37^\circ\text{C}$
Power Transducer (heater)	OhioSemitronics/GH-001E	$\pm 0.2\%$ of reading
Current Transducer (TE)	OhioSemitronics/CT7-015D	$\pm 25\text{mA}$
Voltage Transducer (TE)	OhioSemitronics/VT7-002D	$\pm 62.5\text{ mV}$
Current Transducer (Motor/Fan)	CRMagnetics/CR5220-10	$\pm 100\text{mA}$
Voltage Transducer (Motor/Fan)	CRMagnetics/CR5320-50	$\pm 500\text{mV}$

The greatest uncertainties exist in the measurement of motor and fan power consumption. These devices have a 1% full scale accuracy, but this is considered acceptable and the contribution of the value they measure is considerably less significant than the other powers that are measured more accurately. Additionally, tests to determine the heat gain to the enclosure due to the motor have greater uncertainty than the other tests because the measured temperature difference can be very small.

As shown in Table 11, for the SCTD, calculated values of UA are generally accurate within 3-6%. The cooling capacities calculated have varying uncertainties that increase with the temperature difference between the inside and outside of the enclosure. This occurs because the calculated cooling capacity has increasing dependence on the calculated UA. All calculated capacities for the prototype have uncertainties less than  $\pm 2.5\text{W}$ . For the Laird unit, uncertainties are greater because of a greater uncertainty in heat leak and fan power measurement.

**Table 11. Absolute and Relative Uncertainties for Calculated Parameters**

Calculated Value	Minimum Absolute (Relative Uncertainty)	Maximum Absolute (Relative Uncertainty)
Laird Motor Heat Gain	$\pm 1.2\text{ W} / (60\%)$	$\pm 1.2\text{ W} / (60\%)$
Laird UA	$\pm 0.04\text{ W/K} / (7\%)$	$\pm 0.32\text{ W/K} / (61\%)$
Laird Cooling Capacity	$\pm 1.5\text{ W} / (12\%)$	$\pm 3.3\text{ W} / (25\%)$
Sandia Motor Heat Gain	$\pm 0.63\text{ W} / (14\%)$	$\pm 0.86\text{ W} / (18\%)$
Sandia UA	$\pm 0.02\text{ W/K} / (3\%)$	$\pm 0.06\text{ W/K} / (6\%)$
Sandia Cooling Capacity	$\pm 1.2\text{ W} / (4\%)$	$\pm 2.5\text{ W} / (9\%)$

## 8.2 Results

The results of several heat leak tests for each system are plotted in Figure 44. The results agree with intuition that higher heat leak will occur due to greater forced convection heat transfer. The heat leak is the greatest with the Sandia unit operating at its maximum speed (2000rpm) and airflow rate. The Laird unit has the lowest heat leak due to its considerably lower air flow rate. The implication of this result is that although the cooling capacity of the SCTD is greater than the Laird unit, the SCTD cannot cool the enclosure to a lower temperature. This is because for a given  $\Delta T$  between the inside and outside of the enclosure, the higher air flow of the SCTD results in about twice the heat loss. This is partly a function of the enclosure itself. The convective effect would be lessened in a larger enclosure, for example. For small enclosures, though, lower air flow would be better. Sandia has developed new impeller geometries that have equally low thermal resistance with decreased air flow rate that could be an improvement in this regard on a future device.

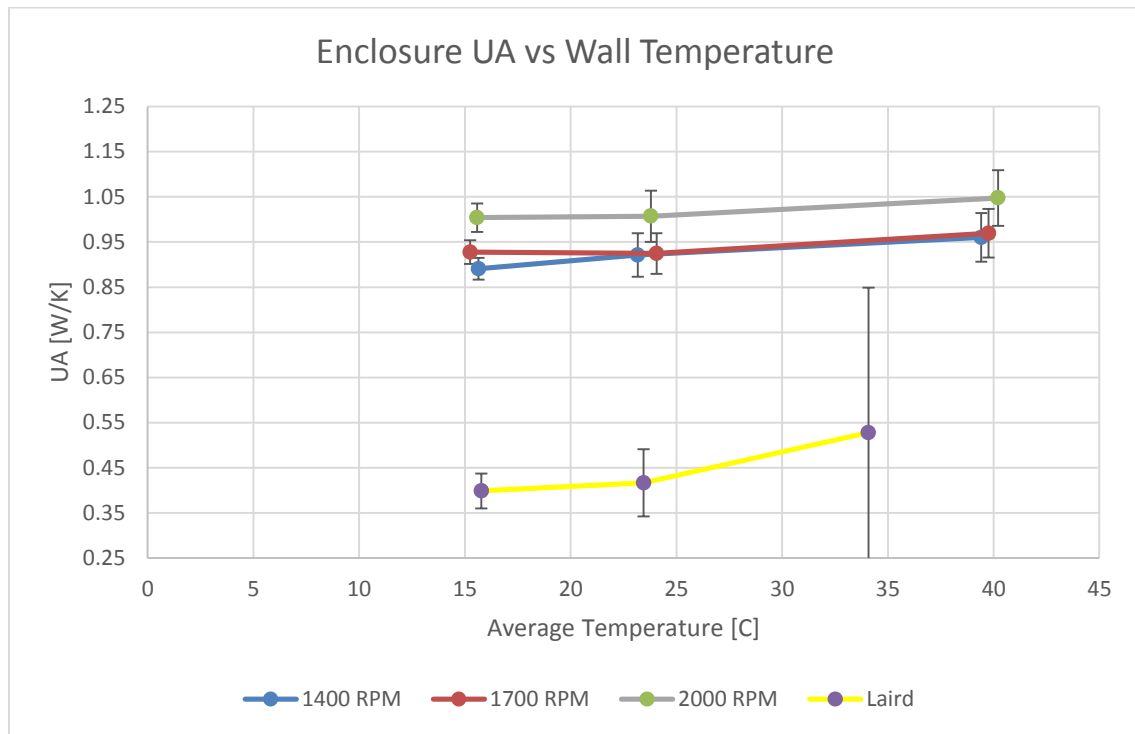


**Figure 44.** Enclosure heat leak for all systems/speeds

Figure 45 shows results from the cooling performance tests. Several conclusions can be made from these results:

- The Laird unit cooling capacity is marginally (4%) higher at 32°C ambient than 20°C ambient;
- The apparent capacity of the Sandia cooler does not increase as its motor speed increases. In fact, for larger DTs the lowest speed (1400rpm) produces greater cooling capacity than the highest speed.

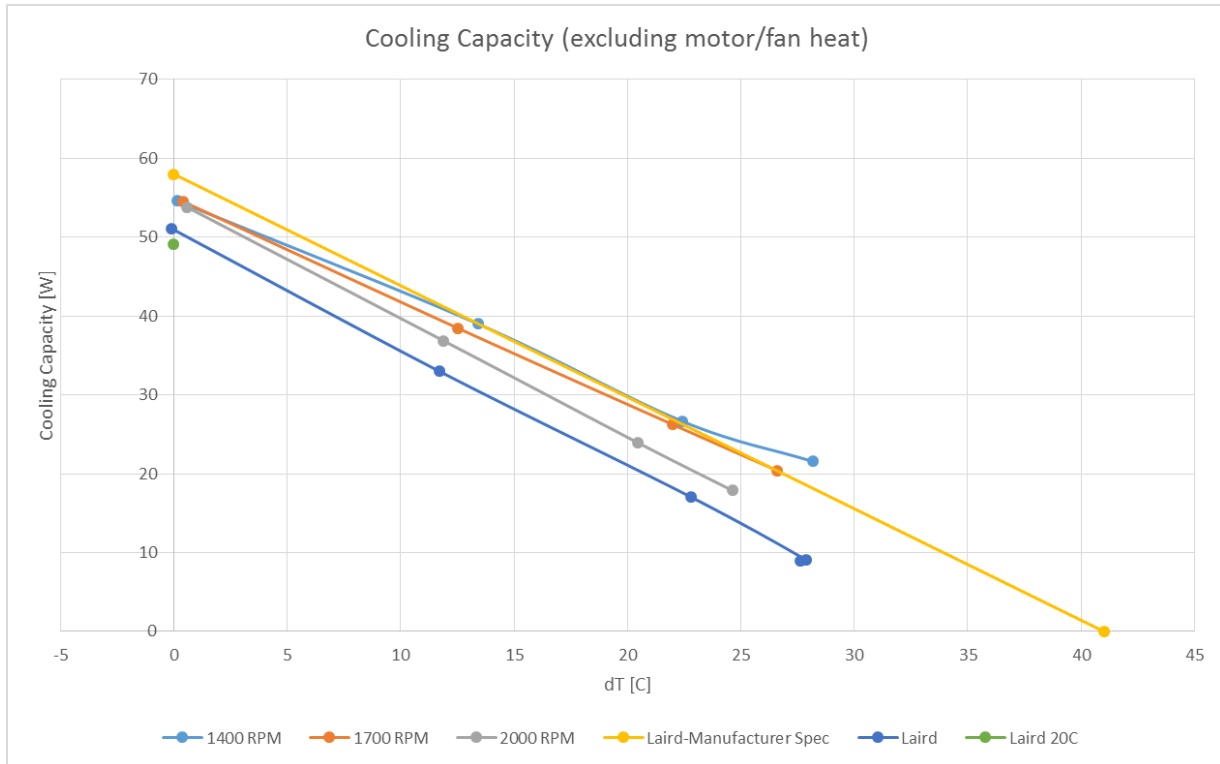


**Figure 45. Apparent cooling capacity (excluding effect of motor heat) vs. temperature difference**

Given the lack of capacity increase with motor speed, it is necessary to account for the motor heat entering the enclosure as described in Section 7.2.3 **Error! Reference source not found.** Figure 46 shows the estimated cooling capacities for the Laird and Sandia devices accounting for the heat entering the enclosure from the motor. This result confirms that the SCTD does have higher cooling capacity at higher impeller speeds, but the effect is overshadowed by the heat that enters the enclosure from the motor. Note that compared to Figure 7, the final set of Laird measurements indicate a higher cooling capacity than the baseline tests due to the inclusion of fan heat gain into the enclosure, the new low-radiation heating element, and more precisely controlled experimental conditions.

When motor heat leak is taken into account, the performance of the SCTD at 2000 rpm is slightly better than at 1400 rpm for  $\Delta T$  less than  $\sim 20$  °C. At 0 °C  $\Delta T$ , the 2000 rpm cooling capacity is about 7% higher than the 1400 rpm case. Modeling results would suggest that the improvement with impeller speed should be greater. This will be discussed in a later section. At 0  $\Delta T$  the improvement of the SCTD over the Laird device is 9-14% (5-7 W) depending on speed. At the largest  $\Delta T$  achieved the additional capacity results in more than double the Laird cooling capacity.

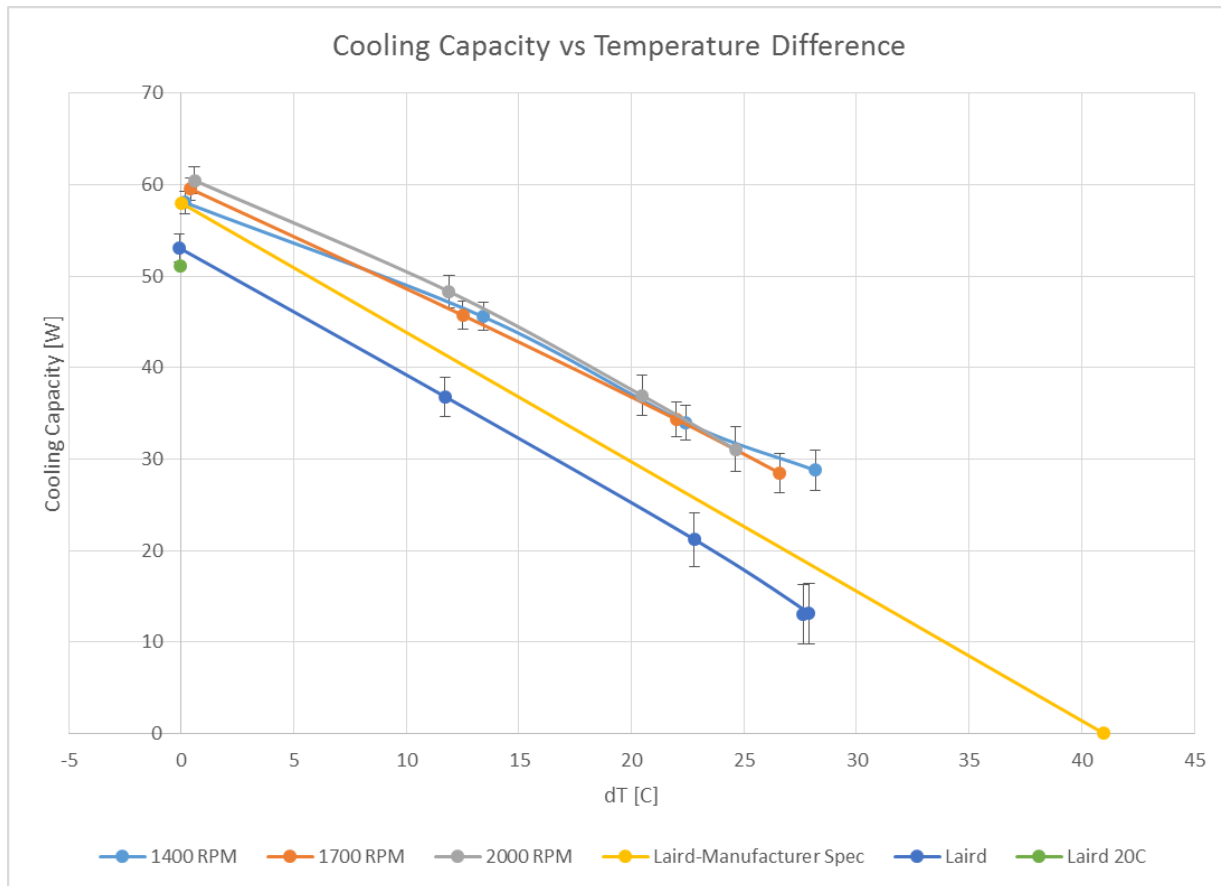


**Figure 46.** Capacities including motor heat

Based on the above results and measured power consumption, the COPs can be calculated as shown in Figure 47. Just as the measured cooling capacity of the Laird unit is below the manufacturer-specified performance, the COP is also lower than expected. The COP of the Sandia prototype exceeds the COP of the baseline Laird unit at all speeds, even with the use of a large and relatively inefficient motor. The COP of the SCTD at 1400 rpm is about 7% higher than the Laird device at 0 dT and increases to about double the COP of the Laird device at a dT of 27 °C. Further improvement of COP could be realized for the Sandia device with a higher efficiency motor/controller. This effect is seen in the fact that the COP for lower speed operation of the SCTD is highest. The improvement in cooling capacity due to increased rotation speed is overshadowed by the added motor power.

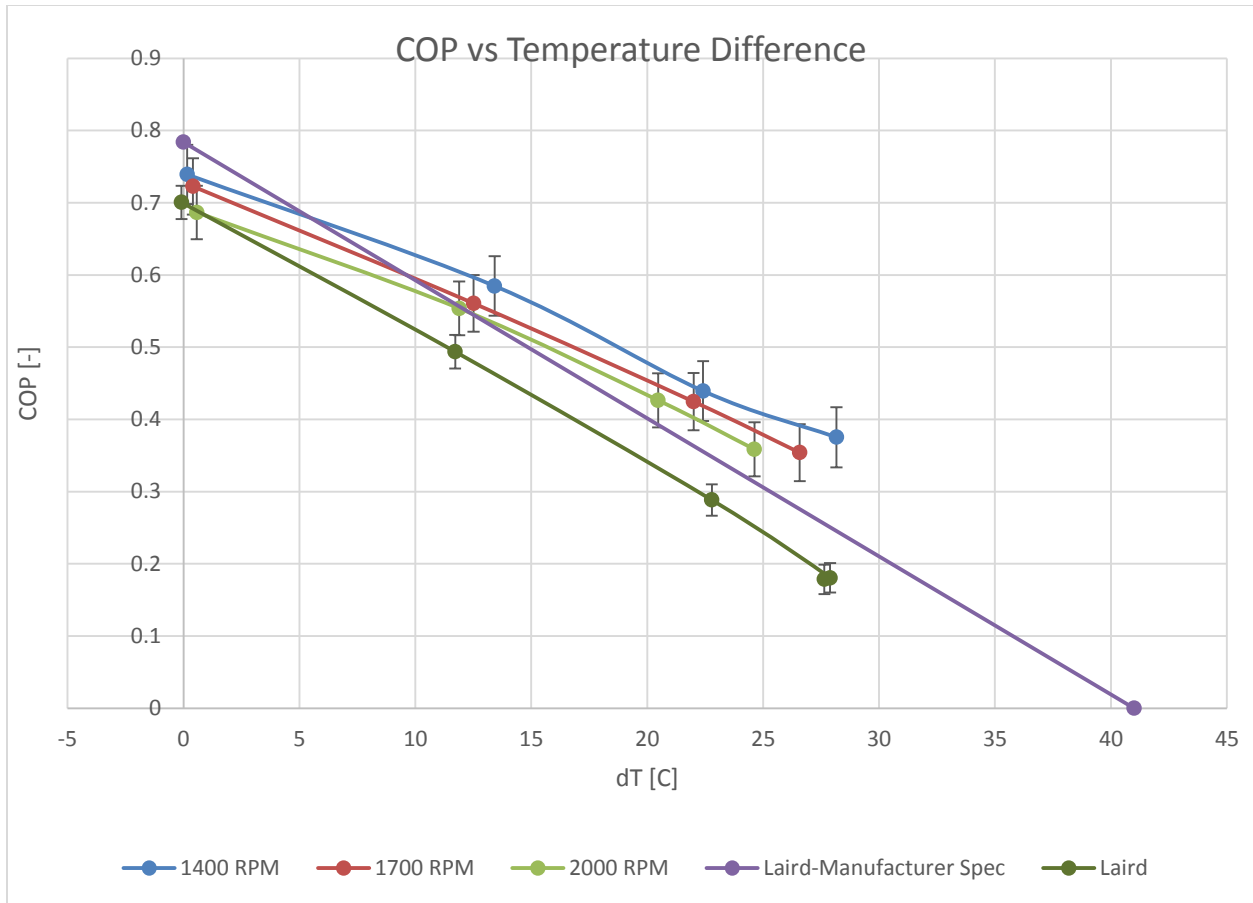


**Figure 47. COP vs temperature difference**

Figure 48 shows the measured COP values excluding the power consumed by fans and motors. Again, the SCTD has greater performance than the Laird unit at all speeds. The COP of the SCTD is similar to the theoretical COP given by Laird at low temperature differentials, but exceeds it at higher temperature differences.

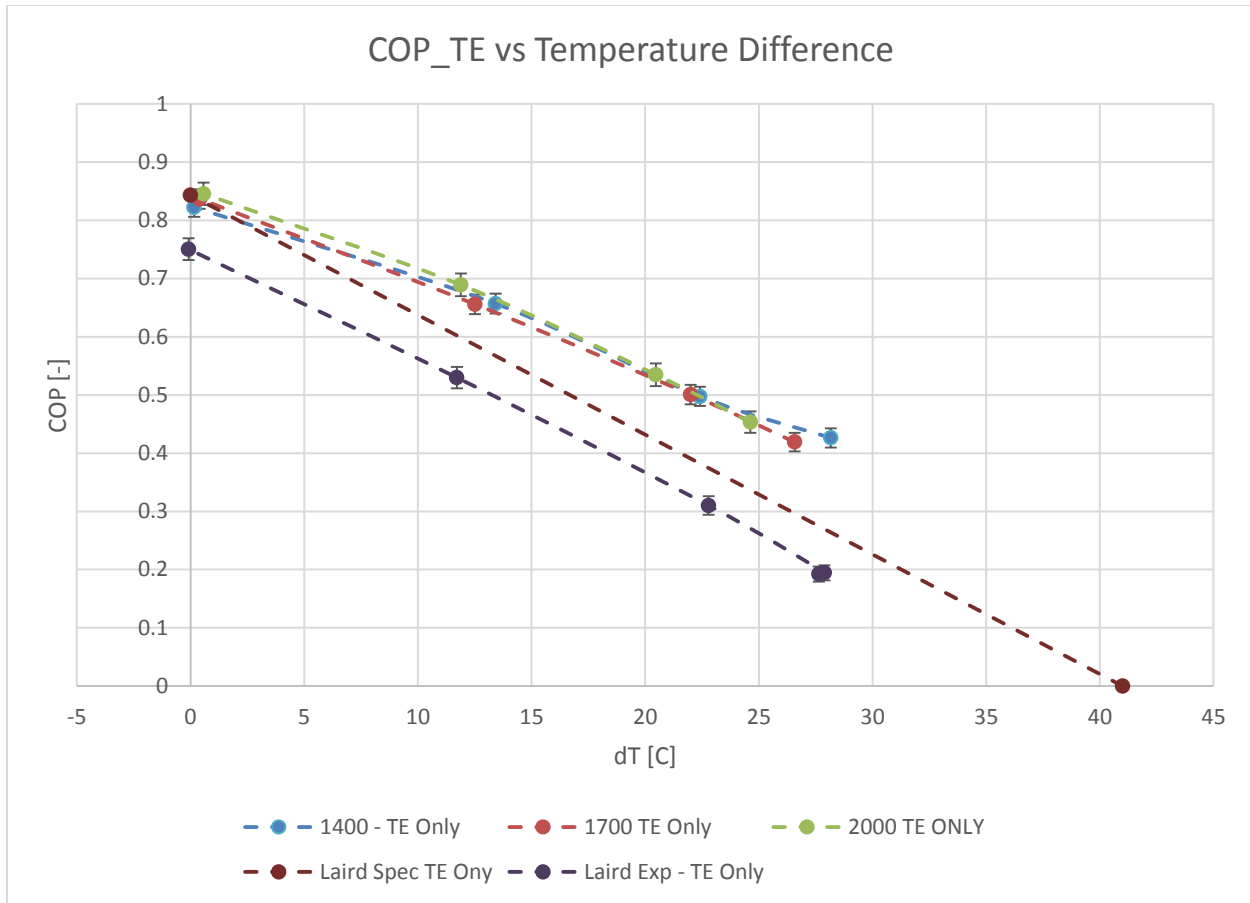


Figure 48. COP for thermoelectric performance only (excludes fan and motor power)

### 8.3 Comparison with Model Predictions

The final experimental results deviate somewhat from cooling capacities predicted by Sandia’s modeling. Figure 49 shows the cooling capacities predicted by the theoretical model. The experimentally measured cooling capacities are about 8-15% lower than predicted. It is important to note that the Laird device was also measured to perform approximately 9% lower than the manufacturer-predicted capacity. This may indicate that the TE modules, which are the same in both devices, are performing below the specifications in Laird’s data sheets.

The relative differences in cooling capacities are quite similar when comparing the experimental findings to the theoretical models. At 1400rpm, the model predicted the SCTD would provide 11.5% higher capacity than the Laird device; experimental results showed its capacity to be 12% higher.

The largest deviation from predicted performance occurs at 2000 rpm for the SCTD. The model predicts a 22% increase in capacity compared to the Laird device and only a 14% increase is observed. These results suggest that the actual heat transfer performance at 2000rpm is not significantly higher than at 1400rpm, as is predicted by the model. One possible explanation could be that recirculating airflow in the small enclosure volume affects the impeller thermal resistance in a manner not captured by the model used to determine the device’s thermal

resistance. In general, discrepancies between the model and experimental performance may be explained by uncertainties in the simulated predictions of thermal resistance and thermal spreading, which were computationally determined but not validated by physical experimental testing

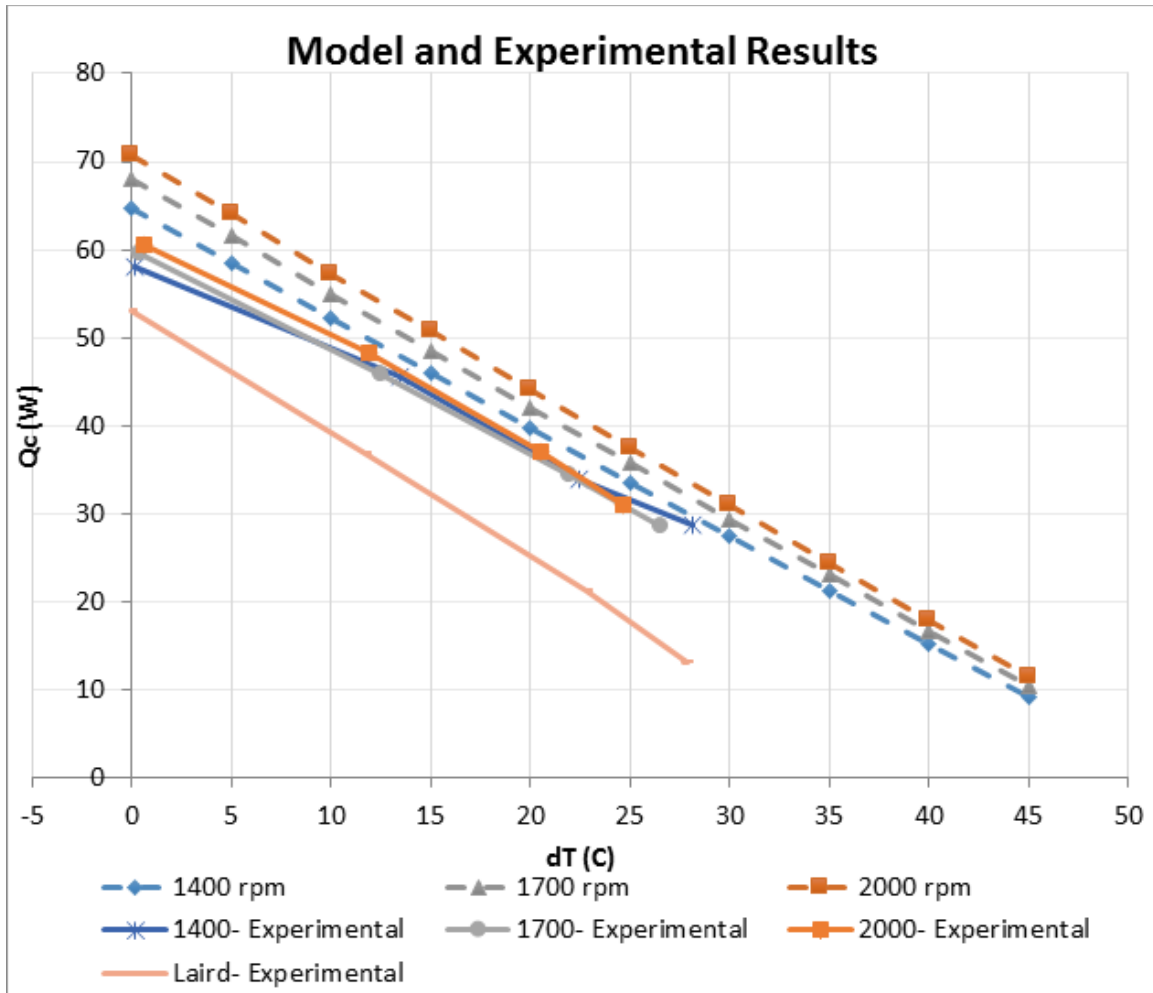


**Figure 49.** Predicted SCTD cooling capacities

## 9. CONCLUSIONS AND RECOMMENDATIONS

The OTS/Sandia team successfully met the project objectives which included a review of existing TE applications, performance measurement of a commercially available TE device as a baseline, and theoretical and physical investigation of a SCTD. A SCTD prototype was successfully designed, fabricated and tested. The prototype used the same thermoelectric modules, thermal interface material, and a similar clamping strategy as the commercially available TE device. Measured performance improvement over the commercial unit was 12 - 14%, depending on the motor speed. This result matches well with simulated results at low motor speeds, but did not support the improved performance predicted at higher motor speeds.

The measured performance of the SCTD was not a significant improvement over the baseline Laird device. The lack of improvement stemmed primarily from two issues related to the use of just two TE modules. Firstly, this created a concentrated thermal load that significantly increased the thermal resistance of the impellers. Secondly, the modules must be operated with relatively high current to achieve the desired cooling capacity which limits the COP. As identified during the modeling stage of the project, several modifications to the SCTD configuration could lead to nearly double the cooling capacity and system efficiency. Specific areas for improvement to explore include the following:

- Advanced impeller design to provide comparable thermal resistance, but with higher heat exchanger effectiveness and lower motor power consumption
- Improved motor and controller efficiency to reduce power consumption and minimize motor heat leak;
- Improved thermal interface between impellers and TE module(s)
- Custom TE module or modules designed to match the footprint of the impellers and to provide a high COP for the required cooling capacity and temperature difference.
- Conducting CFD analysis of the impeller in an enclosure to determine if this has a negative impact on heat transfer performance.

In addition to investigating improvements for the SCTD itself, a closer look at the experimental setup and approach is warranted. As noted in Section 8.1.1, the measurement uncertainty for some parameters is relatively high, largely due to the small temperature differences used for key portions of the capacity calculations. Methods and instrumentation that could be used to reduce measurement uncertainty would allow for more accurate representations of both the baseline and SCTD system performance.

Given the compromises made during prototype development to enable fair comparison with the selected Laird baseline, and lessons learned during performance measurement and verification, it is recommended to pursue a second generation prototype of the SCTD. The second generation prototype would incorporate the improvements noted above. In addition, a second generation prototype would also assess non-performance aspects that may have an impact on marketability and user experience, such as acoustical performance, fouling mitigation, safety concerns, and operational life. The development and testing of an improved unit would further validate modeling efforts and more clearly define the market potential for this technology.

In addition to developing a second generation prototype, it is recommended that additional concept analysis is conducted to assess market potential. Specifically, a cost analysis and risk assessment should be performed. This effort should include a review of material and component costs, labor/manufacturing implications, and operational and safety considerations.

## 10. REFERENCES

1. Koplow, J. P., *Heat Exchanger Device and Method for Heat Removal or Transfer*, US Patent Application #: 12/185,570. Filed August 4, 2008. ORD. (SD# 10948.1)
2. Koplow, J. P., *A Fundamentally New Approach to Air-cooled Heat Exchangers*, Sandia Technical Report SAND2010-0258, Sandia National Laboratories, Livermore CA, January 2010.
3. Koplow, J. P., *Exploration and Development of Air Bearing Heat Exchanger Technology*, Sandia Technical Report SAND2011-1986, Sandia National Laboratories, Livermore CA, March 2011.
4. W. L. Staats, N. D. Matthew, E. S. Hecht, T. A. Johnson, and J. Koplow, *Heat Transfer and Pressure Drop Performance of the Air Bearing Heat Exchanger*, Proceedings of the 2014 ASHRAE Winter Conference, New York, NY.
5. Johnson, T. J., et al, *Development of the Sandia Cooler*, Sandia Technical Report SAND2013-10712, Sandia National Laboratories, Livermore CA, December 2013.
6. Schlichting H., *Boundary Layer Theory*, McGraw-Hill, New York, 1979.
7. Cobb, E. C., Saunders, O. A., *Heat Transfer from a rotating disk*, Proceedings of the Royal Society of London. Series A, Mathematical and Physical Science, 1956.
8. William Goetzler, Richard Shandross, Daniel Weintrabu, and Jim Young, *Market Assessment and Commercialization Strategy for the Radial Sandia Cooler*, Navigant Consulting, Inc., Burlington, Mass., February 2014.
9. Lineykin, S. and Ben-Yaakov, S., *Modeling and Analysis of Thermoelectric Modules*, IEEE Transactions on Industry Applications, 43 2 505-512, New York, 2007.

## APPENDIX A: DETAILED MARKET RESEARCH RESULTS

**Table 12. Market Research Results for Portable Coolers**

Manufacturer	Model	Volume	Price	Power	Cools X below Ambient	Heats X Above Ambient	Outside Dimensions
<b>Recreational</b>							
Coleman	Powerchill 3000000540	16 qt.	\$ 79.99	12V DC, 4A	40°F	N/A	15" x 10.6" x 15"
Coleman	Powerchill 3000001497	40 qt.	\$ 119.99	12V DC or 110V	40°F	N/A	21.75" x 15" x 17.125"
Coleman	Powerchill 3000001495	40 qt.	\$ 129.99	12V DC or 110V	40°F	140°F	21.75" x 15" x 17.125"
Koolatron	P9 Traveller III; 5958650091	8 qt.	\$ 99.95	12V DC, 110V AC, 3A, 36W	40°F	up to 149°F (not above amb.)	11.9" x 14.6" x 10.4"
Koolatron	P20 Compact Cooler; 5958650020	18 qt.	\$ 139.95	12V DC, 110V AC, 4A, 48W	40°F	N/A	16.25" x 17.5" x 8.5"
Koolatron	P25 Fun-kool; 5958650900	26 qt.	\$ 109.95	12V DC, 110V AC, 4A, 48W	25°F	N/A	17.25" x 16" x 11.5"
Koolatron	D25 Portable Softsided Cooler	26 qt.	\$ 109.25	12V DC, 110V AC, 4.5A, 60W	30°F	N/A	15" x 17.5" x 9"
Koolatron	P-27 Voyager; 5958650270	29 qt.	\$ 149.95	12V DC, 110V AC, 4A, 48W		N/A	15.4" x 17.5" x 16"
Koolatron	P-65 Kargo Cooler; 5958650650	33 qt.	\$ 159.95	12V DC, 110V AC, 4.5A, 60W	40°F	minimal	16" x 19.25" x 13.5"
Koolatron	P-75 Kool Kaddy	36 qt.	\$ 179.95	12V DC, 110V AC, 4A, 48W	40°F	N/A	15" x 15.5" x 20.5"
Koolatron	W75 Kool Wheeler; 5958650758	36 qt.	\$ 199.95	12V DC, 110V AC, 4A, 48W	45-50°F	minimal	16.5" x 22.1" x 16.7"
Koolatron	P95 Travel Saver; 5958650820	45 qt.	\$ 189.95	12V DC, 110V AC, 4A, 48W	40°F	minimal	17.5" x 15.5" x 20.5"
Koolatron	P-85 Krusader; 5958650850	52 qt.	\$ 199.95	12V DC, 110V AC, 4A, 48W	40°F	minimal	20" x 20.5" x 15.5"
Igloo	Iceless 26	26 qt.	\$ 99.99	12V DC, 110V AC	36°F	N/A	17.875" x 13" x 16.163"
Igloo	Iceless 28	28 qt.	\$ 109.99	12V DC, 110V AC	36°F	N/A	18.215" x 12.75" x 17.188"
Igloo	Iceless 40	40 qt.	\$ 159.99	12V DC, 110V AC	38°F	N/A	21.75" x 15.31" x 16.63"
Igloo	Cool Chill 40 qt.	40 qt.	\$ 159.99	12V DC, 110V AC	35°F	N/A	21.75" x 15.31" x 16.63"
Kampa		16 qt. (18L)		12V DC, 230V AC, 48W	20°C	heats to 65°C	35cm x 47cm x 31cm
Kampa		22 qt. (25 L)		12V DC, 230V AC, 48W	20°C	N/A	44cm x 37cm x 26cm
Kampa		26 qt. (30L)		12V DC, 230V AC, 48W	20°C	N/A	46cm x 43cm x 30cm
Kampa		40 qt. (45L)		12V DC, 230V AC, 55-72W	20°C	heats to 65°C	39.5cm x 68cm x 41.5cm
Vinotemp	VT-BAGCOOLERSB	28 qt. (32L)	\$ 102.95	12V DC		N/A	14.5" x 15" x 16.25"
Espow	ECAIRPF34	3.5 qt. (4L)	\$ 138.00	36-68W	15-20°C	heats to 65°C +/-10°C	
<b>Medical</b>							
Koolatron	P-20 Precision Control; 5958650022	18 qt.	\$ 549.00	12V DC, 110V AC, 220 V AC	45-50°F	N/A	16" x 8.5" x 17.5"
Koolatron	P-75 Precision Control; 5958650801	36 qt.	\$ 599.00	12V DC, 4.5A	45-50°F	80-100°F	16" x 16" x 21"
<b>Other</b>							
Koolatron	Cosmetic Cooler; 5958650908	7.5 qt.	\$ 99.95	12V DC, 110V AC, 4.5A, 60W	cools to 54°F (not below amb.)	N/A	10.9" x 8.7" x 10"

**Table 13. Market research results for compact refrigerators**

Manufacturer	Model	Volume	Price	Power	Cools X below Ambient	Outside Dimensions
Koolatron		1.7 cu.ft.	\$ 259.95	110V AC, 12V DC, 6A	30°C / 54°F	20" x 18.5" x 17"
Koolatron	CR48W	1.7 cu.ft.	\$ 129.95		40°F	18.5" x 17" x 20.25"
Avanti	SHP1700W	1.7 cu.ft.		110V/60Hz	low, med, high	20.25" x 17" x 19"
Danby	Diplomat DAR0488W	1.7 cu.ft.	\$ 119.99			16.9" x 18.9" x 20.75"
Haier	HRT02WNCBB	1.7 cu.ft.				20.1" x 16.9" x 18.9"

**Table 14. Market research results for wine coolers – 1**

Manufacturer	Model	# Bottles	Price	Power	Temperature Ranges	Outside Dimensions	Notes
Avanti	EWC801-IS	8		110V/60Hz	47-64°F	18" x 10" x 20.25"	1-zone
Avanti	EWC1201	12		110V/60Hz	47-64°F	25.25" x 10" x 20.25"	1-zone
Avanti	EWC1601B	16		110V/60Hz	51-62°F	20.25" x 17" x 19"	1-zone
Avanti	EWC1802DZ	18		110V/60Hz	Upper Zone: 7-12°C Lower Zone: 12-18°C	26.25" x 13.75" x 19.5"	2-zone
Avanti	EWC2700DZ	27		110V/60Hz	Upper Zone: 7-18°C Lower Zone: 11-18°C	39.25" x 13.5" x 22.25"	2-zone
Cuisinart	CWC-800	8	\$ 159.00	120V/15A	39-68°F	17" x 10" x 17.25"	1-zone
Cuisinart	CWC-1200DZ	12	\$ 299.00	120V/15A	39-68°F	21" x 18.5" x 15"	2-zone
Cuisinart	CWC-1600	16	\$ 199.00	120V/15A	39-68°F	20.9" x 15.7" x 17.7"	1-zone
Cuisinart	CWC-3200	32	\$ 399.00	120V/15A	39-68°F	20.75" x 16.25" x 31.3"	1-zone
Edgestar	TWR215ESS	21	\$ 399.00	115V/60Hz/140W/2.0A	Upper Zone: 45-66°F Lower Zone: 55-66°F	32.5" x 13.4" x 20.25"	2-zone
Edgestar	TWR325ESS	32	\$ 699.00	115V/60Hz/210W/3.0A	45-65°F	32.5" x 20.66" x 20.25"	2-zone
Koldfront (Edgestar)	TWR121SS	12	\$ 249.00	115V/60Hz/70W/0.95A	52-64°F	20.75" x 6.875" x 13"	1-zone
Koldfront (Edgestar)	TWR160S	16	\$ 199.00	115V/60Hz/65W/0.95A	52-64°F	20.5" x 17.25" x 20.25"	1-zone
Koldfront (Edgestar)	TWR181EDS	18	\$ 299.00	115V/60Hz/130W	Upper Zone: 45-54°F Lower Zone: 54-64°F	21.5" x 10.5" x 12"	2-zone
Koldfront (Edgestar)	TWR187ESS	18	\$ 399.99	115V/60Hz/110W/1.0A	Upper Zone: 54-66°F Lower Zone: 46-66°F	25.33" x 14" x 22.25"	2-zone

**Table 15. Market research results for wine coolers – 2**

Manufacturer	Model	# Bottles	Price	Power	Temperature Ranges	Outside Dimensions	Notes
Koldfront (Edgestar)	TWR247ESS	24	\$ 499.99	115V/60Hz/100W/1.4A	Upper Zone: 54-66°F Lower Zone: 46-66°F	33.5" x 14" x 22.25"	2-zone
Koldfront (Edgestar)	TWR282S	28	\$ 379.00	115V/60Hz/65W	50-65°F	28.5" x 18" x 22.5"	1-zone
Koldfront (Edgestar)	TWR327ESS	32	\$ 649.99	115V/60Hz/140W/1.9A	Upper Zone: 54-66°F Lower Zone: 46-66°F	33.5" x 15.75" x 22.5"	2-zone
Koolatron	WC24	24	\$ 299.95	120V AC, 60 Hz, 130 W	Upper Zone: 7-12°C Lower Zone: 12-18°C	29.5" x 17.75" x 20.75"	2-zone
Sunpentown	WC-06	6	\$ 142.00	115V/60Hz/70W	44-66°F	10" x 20" x 14.5"	1-zone
Sunpentown	WC-0802H	8	\$ 180.00	110V/60Hz/70W	52-64°F	16.5" x 20.7" x 11"	1 zone; with heating capability
Sunpentown	WC-0888H	8	\$ 179.00	120V/60Hz/1A/70W	45-64°F	10" x 20.5" x 17.7"	1 zone; with heating capability
Sunpentown	WC-12	12	\$ 180.00	115V/60Hz/70W/0.8 kWh-24 hr	50-66°F	14" x 21" x 19"	1-zone
Sunpentown	WC-1271	12	\$ 189.00	110-120V/60Hz/70W/ 1.0 kWh-24hr	52-66°F	10.25" x 19.5" x 25.6"	1-zone
Sunpentown	WC-1272H	12	\$ 199.00	110V/60Hz/70W/0.6 kWh-24hr	51-64°F	10" x 20.5" x 24.5"	1 zone; with heating capability
Sunpentown	WC-1682	16	\$ 209.00	110-120V/60Hz/70W/ 1.0 kWh-24hr	52-65°F	16.5" x 19.7" x 20.5"	1-zone
Sunpentown	WC-1685H	16	\$ 229.00	110V/60Hz/70W/0.65 kWh-24hr	51-64°F	16.5" x 19.7" x 20.5"	1 zone; with heating capability
Sunpentown	WC-1857DH	18	\$ 242.00	110V/60Hz/1A/140W/1.0kWh-24hr	Upper: 45-64°F Lower: 51-64°F	13.58" x 20.28" x 28.43"	2-zone; with heating capability
Sunpentown	WC-20SD	20	\$ 219.00	115V/60Hz/70W/1.0 kWh-24 hr	54-66°F	15.75" x 20.2" x 21.6"	1-zone
Sunpentown	WC-20TL	20	\$ 219.00	115V/60Hz/70W/1.0 kWh-24 hr	54-66°F	15.75" x 20.2" x 21.6"	1-zone; touch sensitive controls
Sunpentown	WC-2192DH	21	\$ 285.00	110V/60Hz/1A/140W/1.1kWh-24hr	Upper: 45-64°F Lower: 51-64°F	13.58" x 20.28" x 31.7"	2-zone; with heating capability
Sunpentown	WC-2461H	24	\$ 316.00	120V/60Hz/1A/140W	45-64°F	20.3" x 20.5" x 24.5"	2-zone; with heating capability
Sunpentown	WC-30U	24	\$ 589.00	115V/60Hz/110W/0.97 kWh-24 hr	39-68°F	15" x 24.6" x 33.7"	1-zone
Vinotemp	VT-6TEDS	6	\$ 167.00		44-66°F	10.125" x 19.75" x 14.875"	1-zone
Vinotemp	VT-6TED-WB	6	\$ 261.00		48-68°F	16.75" x 7.75" x 30.25"	1-zone; wall mount
Vinotemp	VT-8TEDTS-ID	8	\$ 209.00		46-64°F	10.25" x 23.875" x 16.125"	1-zone
Vinotemp	VT-12TEDS	12	\$ 209.00		50-64°F	14" x 19.25" x 18.875"	1-zone
Vinotemp	VT-12TEDS-2Z	12	\$ 282.00		44-66°F	13.625 x 18.75" x 21.375"	2-zone
Vinotemp	VT-12TEDi	12	\$ 240.00		50-66°F	13.5" x 19.75" x 19"	1-zone
Vinotemp	VT-16TEDS	16	\$ 230.00		54-66°F	17.25" x 18.625" x 20.125"	1-zone
Vinotemp	VT-18TEDS	18	\$ 261.00		54-66°F	14" x 19.25" x 25.75"	1-zone
Vinotemp	VT-21TEDS-2Z	21	\$ 387.00		46-64°F	11.875" x 23.25" x 33.5"	2-zone
Vinotemp	VT-28TEDS	28	\$ 387.00		54-66°F	18.25" x 20.875" x 29.25"	1-zone
Vinotemp	VT-48TEDS-2Z	48	\$ 692.00		54-66°F	27.75" x 20.5" x 33.5"	2-zone
Wine Enthusiast	B2720201	6	\$ 129.95		46-66°F	14.75" x 10.25" x 20.25"	1-zone

**Table 16. Market research results for air conditioners**

Manufacturer	Model	Capacity (Btu)	COP	Power	Ambient Range	Dimensions	Notes
EIC Solutions	ThermoTEC 120	200		120/220V AC, 24-28V DC	up to 140°F (DC); 104°F (AC)	8.25" x 6"	heating capacity available
EIC Solutions	ThermoTEC140	400		24-28V DC	up to 140°F	7.25" x 7"	heating capacity available
EIC Solutions	ThermoTEC140B	400		120/220V AC	up to 140°F	12" x 6"	heating capacity available
EIC Solutions	ThermoTEC141	800		120V AC (others optional)	up to 140°F	13" x 13"	heating capacity available
EIC Solutions	ThermoTEC145	1500		120V AC (others optional)	up to 140°F	20.25" x 13"	heating capacity available
EIC Solutions	ThermoTEC151	2500		120V AC (others optional)	up to 140°F	23.5" x 19.5"	heating capacity available
EIC Solutions	ThermoTEC161	3200		220V AC	up to 140°F	23.5" x 19.5"	heating capacity available
EIC Solutions	ThermoTECHazardous	400, 800, 1500		120V AC (240V AC optional)	up to 140°F	varies	heating capacity available
EIC Solutions	ThermoTEC145Military	1500		120/220V AC, 24-28V DC	up to 160°F	12.625" x 19.5"	heating capacity available
EIC Solutions	ThermoTECCB	5000-20000		115, 230, 400, 480V	up to 140°F	varies	meant for enclosures; compressor based
TECA Corp.	AHP-6200	6060-7000		120/240V AC	up to 70°C		indoors cooling, through mounted
TECA Corp.	AHP-4200	3350-4760		120/240V AC	up to 70°C		indoors cooling, through mounted
TECA Corp.	AHP-3200	3130-3515		120/240V AC, 24V DC	up to 70°C		indoors cooling, through mounted
TECA Corp.	AHP-2200	1990-2680		120/240V AC, 24V DC	up to 70°C		indoors cooling, through mounted
TECA Corp.	AHP-1800	1420		120/240V AC, 24V DC	up to 70°C		indoors cooling, through mounted
TECA Corp.	AHP-1501	1300		120/240V AC, 24V DC	up to 70°C		indoors cooling, through mounted
TECA Corp.	AHP-1400	1090		120V AC	up to 70°C		indoors cooling, through mounted
TECA Corp.	AHP-1200	670		120/240V AC, 24V DC	up to 70°C		indoors cooling, through mounted
TECA Corp.	AHP-500	432, 593	0.85-1.25	24V DC	up to 70°C		indoors cooling, through mounted
TECA Corp.	AHP-401	486		120/240V AC	up to 70°C		indoors cooling, through mounted
TECA Corp.	AHP-400	297, 405	0.56 - 1.12	24V DC	up to 70°C		indoors cooling, through mounted
TECA Corp.	AHP-301FF	220		120/240V AC	up to 70°C		indoors cooling, through mounted
TECA Corp.	AHP-300FF	250	0.42	12/24/48V DC	up to 70°C		indoors cooling, through mounted
TECA Corp.	AHP-150FF	123	0.4	12/24V DC	up to 70°C		indoors cooling, through mounted
TECA Corp.	FHP-220	1770-2480		120/240V AC, 24V DC	up to 70°C		indoors cooling, flush mounted
TECA Corp.	FHP-2850	2200		120/240V AC	up to 70°C		indoors cooling, flush mounted
TECA Corp.	FHP-1501	1270		120/240V AC, 24V DC	up to 70°C		indoors cooling, flush mounted
TECA Corp.	FHP-750	560		120/240V AC, 24V DC	up to 70°C		indoors cooling, flush mounted
TECA Corp.	FHP-500	372, 536	0.72-1.0	24V DC	up to 70°C		indoors cooling, flush mounted
TECA Corp.	FHP-401	447		120/240V AC	up to 70°C		indoors cooling, flush mounted
TECA Corp.	FHP-400	280, 360	0.48-0.99	24V DC	up to 70°C		indoors cooling, flush mounted
TECA Corp.	LHP-1200XE	770		120V AC	up to 70°C		indoors cooling, liquid cooled
TECA Corp.	LHP-1200DP	770		120V AC	up to 70°C		indoors cooling, liquid cooled
Watronix, Inc.	INB 140-12-AA	140		12V DC	up to 140°F		
Watronix, Inc.	INB 180-12-AA	180		12V DC	up to 85°C		
Watronix, Inc.	INB 340-24-AA	340		24V DC	up to 65°C		
Watronix, Inc.	INB 500-24-AA	512		24V DC	up to 70°C		
Watronix, Inc.	INB 720-24/28-AA	720		24V DC	up to 65°C		
Advanced Thermoelectric	ElectraCOOL TAC-60	205		12V DC	up to 65°C; 40°C max delta T	4" x 4"	\$200 each
Advanced Thermoelectric	TACE 100W	341		12V DC	up to 70°C, 40°C max delta T		weather proof air conditioned enclosure; \$750
Align Sourcing (8 total models)		50 - 680		12-58V			air-to-air assembly
Laird (14 total models)		68 - 665		12V/24V DC			Air-to-air assembly; customizable

**Table 17. Market research results for dehumidifiers**

Manufacturer	Model	Tank Capacity	Price	Power	Moisture Removal Rate	Dimensions	Notes
Hoffman Pentair	H2OMIT		\$ 814.80				
Sunpentown	SD-652Ti	2.2 L	\$ 115.00	12V DC, 85 W	650ml / 24 hrs	8.05" x 5.5" x 14.17"	Has UV light to kill bacteria
Sunpentown	SD-350Ti	2 L	\$ 85.00	12V DC, 60 W	350ml / 24 hrs	8" x 4.9" d 13"	Has UV light to kill bacteria
Sunpentown	SD-350	2 L	\$ 79.00	12V DC, 60 W	350ml / 24 hrs	8" x 4.9" d 13"	

**Table 18. Market research results for other thermoelectric applications**

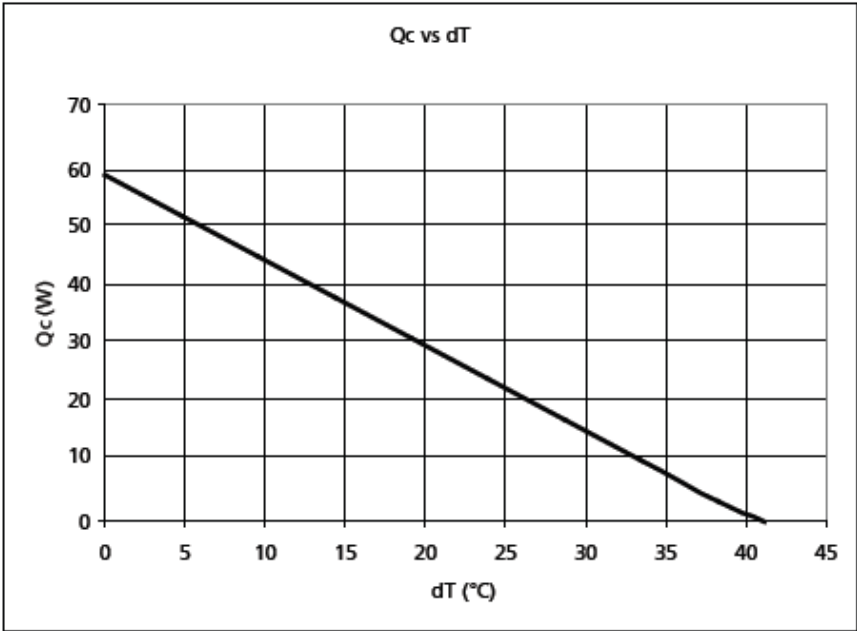
Product	Manufacturer	Model	Volume / Size	Price	Power	Outside Dimensions	Notes
Tabletop Water Cooler	Avanti	WD31EC	2, 3, or 5 gallons		110V/60Hz	15.75" x 12.25" x 12.75"	hot and cold
Tabletop Water Cooler	Avanti	WD29EC	3 or 5 gallons		110V/60Hz	15.25" x 12" x 11"	cold only
Mini Beer Keg	Koldfront (Edgewater)	KBC51SS	(1) 5L mini-keg	\$ 459.00	115V/60Hz	17.33" x 10.66" x 16.33"	36-50°F temperature range
Mini Beer Keg	Koolatron	59586611230	(1) 5L mini-keg	\$ 199.95	110V AC/12V DC	11.5" x 9" x 17.2"	cools to 45°F below ambient
Yogurt Maker	Cuisinart		50 oz.	\$ 129.95		9.75" x 7" x 10"	

# APPENDIX B: LAIRD THERMOELECTRIC AIR CONDITIONER SPECIFICATIONS

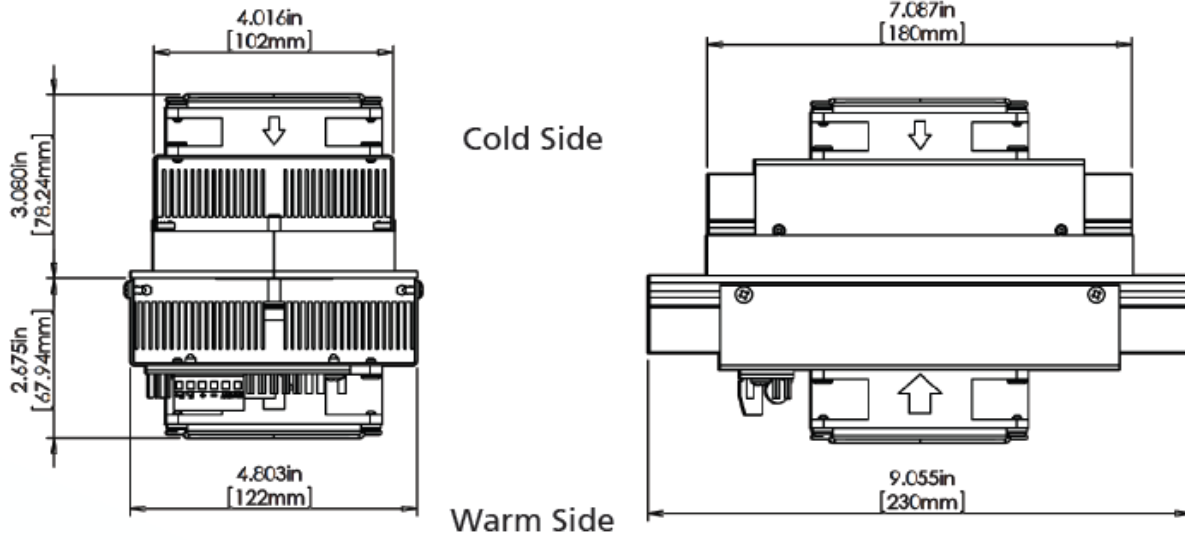
Laird AA PowerCool Series, Thermoelectric Assembly, Model AA-060-12-22

Specifications	
Cooling Power $Q_{cmax}$ (W)	58
Running Current (A)	5.7
Startup Current (A)	7.2
Nominal Voltage (V)	12
Max Voltage (V)	15
Power Input (W)	74
Operating Temperature (°C)	-10 to 51
Weight (kg)	2.5
MTBF (fans – hrs)	40,000
Performance Tolerance	10%

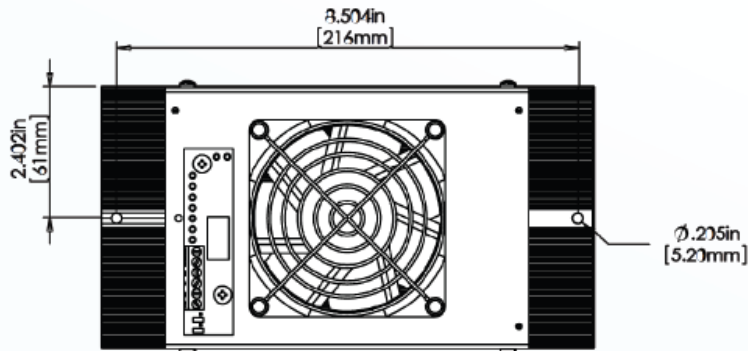
## PERFORMANCE CURVE



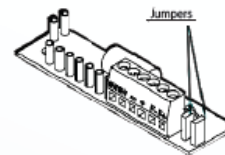
## ISOMETRIC DRAWINGS



## MOUNTING HOLE LOCATION



## WIRING SCHEMATIC



### Electrical connections

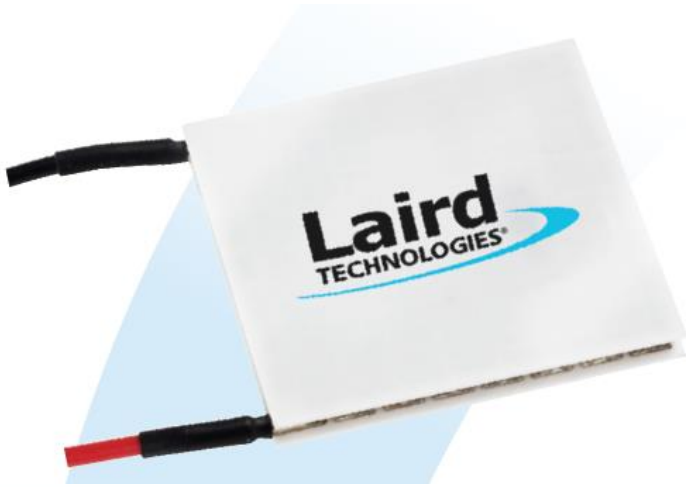
"+" :-+ TEM  
 "- " :- TEM  
 "F+" :-+ Fan(s)  
 "F-" :- Fan(s)

To use single supply:  
 Lift the jumpers and rotate 90° to short-cut the pin pairs.  
 Connect the unit to "+" & "-".

Warning: Single supply no applicable in heating mode or with PWM-regulation.

## APPENDIX C: THERMOELECTRIC MODULE SPECIFICATIONS

Laird Thermoelectric Modules, Ceramic Plate Series CP12, 161, 055



### PERFORMANCE SPECIFICATIONS

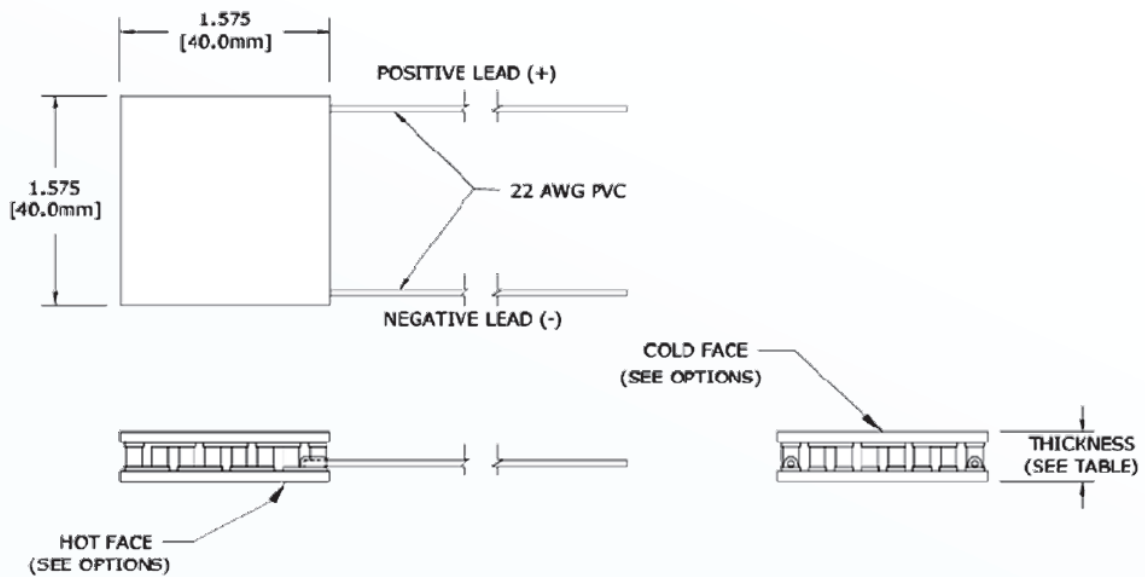
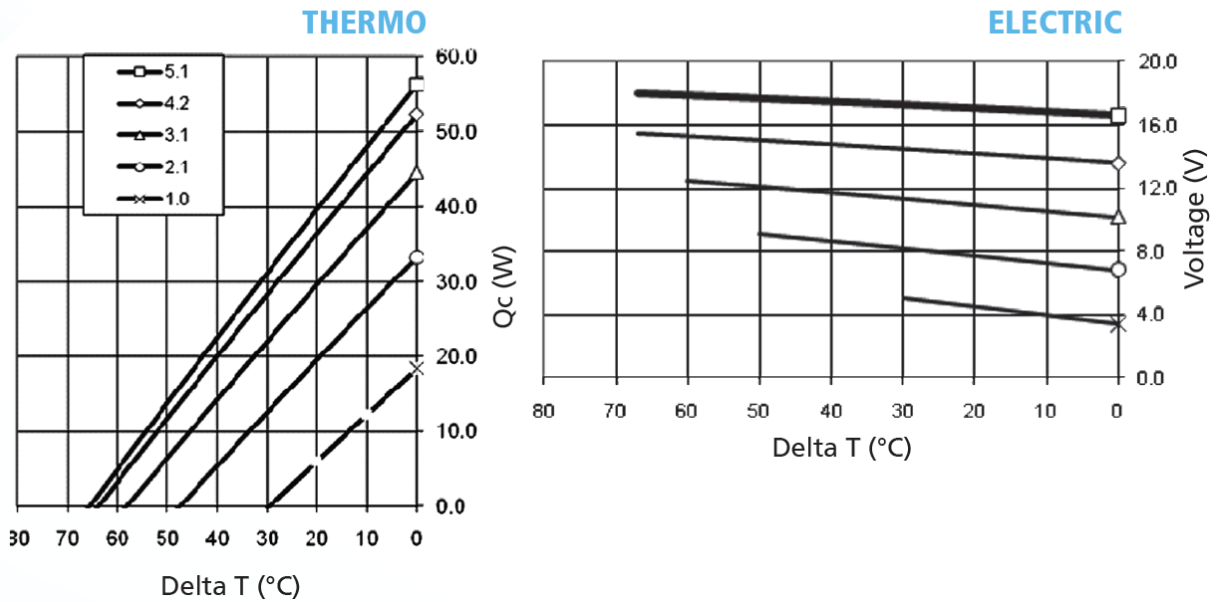
Hot Side Temperature (°C)	25°C	50°C
Qmax (Watts)	56.3	62.0
Delta Tmax (°C)	67	75
I <sub>max</sub> (Amps)	5.1	5.1
V <sub>max</sub> (Volts)	18.3	20.4
Module Resistance (Ohms)	3.21	3.68

SUFFIX	THICKNESS (PRIOR TO TINNING)	FLATNESS & PARALLELISM	HOT FACE	COLD FACE	Lead Length
L1	0.134" ± 0.001"	0.001" / 0.001"	Lapped	Lapped	10"
L2	0.134" ± 0.0005"	0.0005" / 0.0005"	Lapped	Lapped	10"

### SEALING OPTION

SUFFIX	SEALANT	COLOR	TEMP RANGE	DESCRIPTION
RT	RTV	White	-60 to 204 °C	Non-corrosive, silicone adhesive sealant
EP	Epoxy	Black	-55 to 150 °C	Low density syntactic foam epoxy encapsulant

## Performance Curves at $T_h = 25^\circ\text{C}$



Ceramic Material: Alumina ( $\text{Al}_2\text{O}_3$ )  
 Solder Construction:  $138^\circ\text{C}$ , Bismuth Tin (BiSn)

## DISTRIBUTION

1 MS0899 Technical Library 9536 (electronic copy)





**Sandia National Laboratories**